

Diss. ETH Nr. 13362

Investigation of Plume Opacity Formation at Cement Kiln Stacks

A dissertation submitted to the
Swiss Federal Institute of Technology Zurich

for the degree of
Doctor of Technical Sciences

Presented by
Laurent Seyler

Dipl. Chem. - Ing. ETH
born on September 06, 1971
citizen of Luxembourg

accepted on recommendation of
Prof. Dr. K. Hungerbühler, examiner
Prof. Dr. M. Morbidelli, co-examiner
PD. Dr. J. - P. Kunsch, co-examiner

Zurich, 1999

Acknowledgments

Many persons have been involved in this project. Without the support (moral, financial, professional, organizational, ...) of these persons, the present work could not have been realized. Therefore I owe them very much.

Zu allererst gebührt K. Hungerbühler ein besonderer Dank. Er hat mich sehr mit seiner offenen und speditiven Art mit Rat und Tat unterstützt. Neben den fachlichen Aspekten kamen die praxisbezogenen Aspekte nie zu kurz. Diese gab er mir auf meinen weiteren Weg mit und unterstützte damit meine persönliche Entwicklung.

E grouse Merci un den J. - P. Kunsch. Hien huet mer tatkräfteg während der ganzen Zäit de Réck gestäipt a mer geholléf wou en nëmme konnt. Merci fir déi vill gudd Diskussio'unen an d'Iwernalm vun dem Koreferat!

Desidero ringraziare sentitamente anche M. Morbidelli per il suo interesse per il mio lavoro, le stimolanti conversazioni e per aver accettato di essere il mio correlatore.

Ein RIESIGER Dank gebührt P. Kutschera. Er war viel mehr als "nur" die Industriekontaktperson. Mit seiner offenen und sehr angenehmen Art sorgte er für eine sehr gute Zusammenarbeit zwischen Industrie und ETH. Er war mir ein sehr wichtiger Berater, Lehrmeister und Vermittler. Er gab dem Projekt die wesentlichen Impulse und war mir mehr als einmal eine Stütze auf welche ich mich verlassen konnte. DANKE!!

Ebenso gebührt H. Nyffenegger ein grosser Dank für seine fachliche Unterstützung. Ohne sein Know-how sowie seine tollen Regler könnte meine Anlage immer noch nicht kontrolliert qualmen.

O. Kut sowie F. Mayer möchte ich speziell für ihre unkomplizierte und speditive Hilfe in allen Lebenslagen danken. Die täglichen Gespräche bedeuteten für mich eine unheimlich grosse moralische Unterstützung. Desweiteren halfen mir F. Mayer sehr bei der Analytik sowie bei apparativen Problemen und O. Kut mit seinen Korrekturen. U. Fischer möchte ich für seine Korrekturen und Tips danken.

M. Wohlwend hat meiner Anlage erst mit elektronischen Komponenten aus seiner Werkstatt Leben eingehaucht. Auch in der grössten Ausweglosigkeit konnte er immer wieder eine Lösung aus seinem Hut hervorzaubern. Danke!

Dem Werkstatt-Team und insbesondere U. Senn ein Danke für all die Arbeiten an dem Windkanal.

Special thanks to S. Myers and J. Epperson for their opacity readings. I really enjoyed working with them. The resulting correlation was a milestone in my project.

Many thanks to all the known and unknown persons from "Holderbank" Ltd., Holnam Inc. and St. Lawrence Cement who supported this project in any form.

U. Baltensperger danke ich recht herzlich für die Hilfe bei der Aerosolanalytik sowie

für die Ausleihe des Aerosolgenerators.

Merci à L. Cavin et N. Richard pour leurs relations amicales et les soirées inoubliables à Dietikon.

Merci dem P. Dimmer fir seng laangjäähreg Frëndschaft an déi vill schéin Momenter an der Schwäiz.

Thanks Michalien for initiating me into the world of Pantaloon and the world of good bad taste.

Das sehr offene und überaus gute Gruppenklima schätzte ich sehr. Schuld daran waren: A. Beck, Ch. Blickenstorfer, K. Fenner, S. Hellweg, V. Hoffmann, Ch. Jahn, G. Jödicke, Zellenkollege G. Koller, J. Ladner, A. Lalive d'Épinay (Danke für's Baden-Consulting), J. Michel (vielen Dank für all die Unterstützung in administrativen Fragen), J. Pastré (Danke für die Hessen-Kultur), M. Scheringer, E. Uerdingen, Th. Vögl, J. von Grote, F. Wegmann (Danke für die lustigen Diskussionen) sowie die alten Mitkämpfer A. Keller (vielen Dank für all die schönen Wanderungen in Graubünden), A. Sjöberg (Tack för die Einweihung in die Geheimnisse des Skifahrens), A. Weidenhaupt, M. Gleichauf, M. Meier sowie P. Flückiger.

Ein weiterer Dank gilt dem Chemiebar-Team: D. Carini, T. Hug, S. Lehnert und F. Lode.

Tack Tina för die Hilfe bei der Stressbewältigung im allerletzten Teil meiner Dissertation.

Schlussendlich nach e grouse Merci u méng Famill fir déi Ënnerstëtzung, déi se mer während ménger Zäit un der ETH zoukomme gelôos huet.

October, 1999

Laurent Seyler

Abstract

The formation and growth of aerosols, leading to the formation of a detached plume at the exit of industrial stacks, have been a subject of growing concern. One reason for this fact is the legislation limiting the maximum plume opacity in North America and Canada.

Some kilns experience increased plume opacity at the stack even if the emissions of single components are in compliance with the respective legislation limits. Often, plume opacity only appears at a considerable distance from the stack exit.

As the investigation of plume opacity phenomena in the field is rather difficult, a special purpose wind tunnel has been built in the laboratory for investigating these phenomena. Exhaust gases were synthesized and led into the wind tunnel whose 'atmosphere' was controlled by an air-conditioner. The opacity of the plume has been read with the help of a dispersion photometer that can be moved in three directions inside the wind tunnel. The dispersion photometer value has been converted to opacity values with the help of an empirical correlation. Moreover it was checked if the assumptions of the theoretical dispersion model (uniform wind flow profile, turbulent exhaust gas stream) could be reproduced in our equipment. Therefore the chloride concentrations of the different samples collected were compared to the concentrations predicted by the model described in Chapter 4.

The formation and dispersion of plumes has been studied in this wind tunnel in order to gain an understanding of opacity formation processes as well as information on precursor substances, as well atmospheric as exhaust gas conditions leading to plume opacity and chemical composition of the aerosols formed inside the plume.

A first variable screening has been done with the help of a fractional factorial design. Afterwards these variables have been studied in detail in several series of experiments. The results show that mainly ambient air temperature as well as the exhaust gas temperature reduce opacity significantly. Hydrogen chloride reacts readily with ammonia (two common constituents of exhaust gases in the stack) to form ammonium chloride aerosols which scatter light. Sulfates are only formed by oxidation of sulfur dioxide in presence of an aqueous phase as well as ammonia if the ambient air temperature is sufficiently low (below 6°C). In the experiments conducted, dust, the ambient relative humidity, the exhaust gas moisture content, the exhaust gas oxygen concentration, UV-radiation as well as the concentration of nitrogen oxides did not have any significant influence on plume opacity. The effect of hydrocarbons was not studied in the scope of this project.

The knowledge gained about plume opacity is important in order to develop efficient and at the same time economic measures against increased opacity in industrial stacks. Considering the fact that plume opacity is much more sensitive to a change in the hydrogen chloride concentration than to the equivalent change of the sulfur dioxide concentration, measures taken in order to meet plume opacity regulations should mainly concentrate on the elimination of hydrogen chloride. Moreover different design modifications (reduction of the stack diameter, increase of the flow rate of exhaust gases by adding hot air to the exhaust gas stream) could be taken in order to increase turbulence at the stack exit which increases the entrainment rate of the ambient air which for its part contributes to the reduction of opacity.

Zusammenfassung

Das Interesse an der Bildung und dem Wachstum von Aerosolen, welche am Austritt von Industrieschornsteinen zur Bildung von sekundären, abgelösten Abgasfahnen führen, hat in letzter Zeit stark zugenommen. Ein Grund hierfür liegt sicherlich in der Tatsache, daß spezielle Gesetzgebungen die maximale Opazität von Abgasfahnen in Nordamerika und Kanada einschränken.

Bei einigen Fabriken werden dieser Grenzwert für Opazität manchmal leicht überschritten, obwohl die Grenzwerte der einzelnen Komponenten im Abgas eingehalten wurden. Oft ist diese erhöhte Opazität erst in einem beträchtlichen Abstand vom Kaminaustritt zu beobachten.

Da sich die Untersuchung der Opazitätsphänomene im Feld jedoch als ziemlich schwierig erweist, wurde in unserem Labor eine spezielle Anlage für entsprechende Untersuchungen entwickelt und gebaut. Das Abgas wurde synthetisiert und anschliessend in den Windkanal, dessen "Atmosphäre" mit Hilfe einer Klimaanlage geregelt wird, eingeleitet. Die Opazität der Abgasfahne wurde mit Hilfe eines Streulichtphotometers bestimmt, welches in drei Richtungen im Windkanal bewegt werden kann. Die Streulichtwerte wurden mittels empirischer Korrelationen in Opazitätswerte umgewandelt. Daneben wurde überprüft, ob die Annahmen eines theoretischen Dispersionsmodelles (uniforme Verteilung der Strömung der Umgebung, turbulente Abgasströmung) in unserer Anlage reproduziert werden konnten. Dazu wurden verschiedene Abgasproben entnommen, deren Ammoniumchloridkonzentration ermittelt und mit den Werten verglichen, welche mit dem in Kapitel 4 beschriebenen Modell berechnet wurden.

Die Bildung sowie die Ausbreitung von Abgasfahnen wurde in dem

Windkanal untersucht, um den Opazitätsbildungsprozess besser zu verstehen. Dabei sollen auch Informationen erhalten werden bezüglich: i) der Vorläufersubstanzen, ii) der opazitätsfördernden atmosphärischen sowie abgasseitigen Bedingungen sowie iii) der chemischen Zusammensetzung der Aerosole in der Abgasfahne.

Die Identifikation der einflußreichsten Variablen erfolgte mittels eines unvollständigen Versuchsentwurfes. Anschliessend wurden diese Variablen in verschiedenen experimentellen Serien genauer untersucht. Die Resultate zeigen, daß hauptsächlich die Umgebungstemperatur sowie die Abgastemperatur einen stark inversen Einfluß auf die Opazität ausüben. Salzsäure reagiert augenblicklich mit Ammoniak (beide Komponenten sind häufig in Abgasen anzutreffen) um Ammoniumchlorid zu bilden, welches das Sonnenlicht streut. Sulfate konnten nur in Anwesenheit einer aquatischen Phase und bei tiefen Umgebungstemperaturen (tiefer als 6°C) durch Oxidation von Schwefeldioxid gebildet werden. In den von uns durchgeführten Experimenten hatten weder Staub noch die Umgebungsfeuchte, die Abgasfeuchte, die Abgassauerstoffkonzentration, die UV-Strahlung oder die Stickstoffoxidkonzentration einen wesentlichen Einfluß auf die Opazität. Die Effekte von Kohlenwasserstoffen wurden im Rahmen dieser Arbeit nicht untersucht.

Das erlangte Wissen bezüglich Abgasfahnenopazität ist wichtig, um effiziente und kostengünstige Maßnahmen treffen zu können, um die Opazität zu senken. Unter dem Blickpunkt einer größeren Sensitivität der Opazität bezüglich Änderungen in der Salzsäurekonzentration als der entsprechenden Änderungen in der Schwefeldioxidkonzentration, sollten sich diese Maßnahmen auf die Elimination von Salzsäure konzentrieren. Daneben könnten verschiedene konstruktive Änderungen (Reduktion des Kamindurchmessers, Erhöhung der Abgasgeschwindigkeit indem heiße Luft dem Abgasstrom beigemischt würde) ergriffen werden, um die Turbulenz am Kaminaustritt zu erhöhen. Diese Maßnahme würde die Einmischungsrate der Umgebungsluft erhöhen und somit die Opazität erniedrigen.

Résumé

La formation et la croissance d'aérosols, qui sont responsables pour la formation de fumées détachées à la sortie des cheminées industrielles, ont fait l'objet de nombreuses études. Ceci est dû entre autre au fait que des législations limitant l'opacité maximale de fumées industrielles aux Etats Unis d'Amérique et au Canada ont été introduites au début des années soixante-dix.

Pour certaines usines, ces législations ont parfois été violées malgré le fait que les limites d'émissions pour les composants des gaz respectifs furent respectées. Souvent cette opacité ne peut être observée qu'à une certaine distance de la sortie de la cheminée.

Cependant comme l'étude de ces phénomènes en grandeur nature s'est montrée très difficile, nous nous sommes décidés à développer et à construire un équipement destiné à l'étude des phénomènes d'opacité au laboratoire à l'échelle réduite. Les gaz sont synthétisés puis introduits dans un tunnel dont l'atmosphère est contrôlée par une climatisation. L'opacité de la fumée a été déterminée à l'aide d'un photomètre de dispersion qui peut être dirigé dans trois directions. Les valeurs indiquées par le photomètre de dispersion ont été converties en valeurs d'opacité à l'aide d'une corrélation empirique. On démontre que les hypothèses de travail du modèle théorique de dispersion (profil du courant d'air uniforme, turbulences des gaz à la sortie de la cheminée) peuvent être reproduites dans notre équipement. Pour cela, des échantillons de fumées furent prises dont les concentrations de chlorure d'ammonium furent déterminées. Ces concentrations expérimentales ont été comparées à celles prédites par le modèle qui est présenté au Chapitre 4.

La formation et la dispersion de fumées ont été étudiées dans le tunnel

afin d'obtenir de plus amples connaissances sur la formation d'opacité: les substances préliminaires, les conditions météorologiques, les gaz qui sont responsables pour une augmentation de l'opacité, et sur la composition chimique des aerosols formés à l'intérieur de la fumée. Un premier screening des variables a été fait à l'aide d'un plan d'expérience factoriel. Ensuite les variables les plus importantes ont été étudiées plus en détail à l'aide de séries expérimentales supplémentaires.

Les résultats nous montrent principalement que la température ambiante ainsi que celle des gaz d'échappement exercent une influence inversement proportionnelle sur l'opacité. L'acide chlorhydrique et l'ammoniaque (qui sont présents dans les gaz) reagissent instantanément pour former des aerosols de chlorure d'ammonium qui dispersent la lumière. Les sulfates ne sont formés à partir de dioxyde de soufre qu'en présence d'une phase aqueuse et d'ammoniaque, et seulement si les températures ambiantes sont assez basses (en dessous de 6°C). Dans nos expériences, ni la poussière, ni l'humidité ambiante, ni la teneur en eau des gaz, ni la concentration en oxygène des gaz, ni la lumière UV, ni les NO_x n'ont exercé une influence significative sur l'opacité. Les effets qu'exercent les hydrocarbures sur l'opacité n'ont pas été étudiés dans ce projet.

Les connaissances acquises sur l'opacité des fumées sont importantes si l'on veut prendre des mesures à la fois efficaces et économiques en vue de la réduction de l'opacité. Par exemple l'influence de la teneur en acide chlorhydrique étant plus importante que celle en dioxyde de soufre, les mesures à prendre en vue d'une réduction de l'opacité devraient se concentrer sur l'élimination de l'acide chlorhydrique. De même plusieurs modifications au niveau du design (réduction du diamètre de la cheminée, augmentation de la vitesse du courant de gaz en injectant de l'air chaud) pourraient être prises en vue d'augmenter les turbulences à la sortie de la cheminée. Ceci augmenterait l'entraînement de l'air ambiant ce qui aurait pour conséquence la réduction de l'opacité.

Contents

1	Introduction	1
1.1	Growing concern for plume opacity	1
1.2	Scope	4
1.3	Objectives	5
2	Opacity	7
2.1	What is opacity?	7
2.1.1	Definition	7
2.1.2	Types of opacity	9
2.2	Main factors influencing plume opacity	12
2.3	Opacity reading according to EPA Method 9	15
2.4	Accuracy in estimating plume opacity	15
3	Hypotheses for opacity formation	17
3.1	Ammonia	18
3.2	Chlorides	19
3.3	Sulfates	21
3.4	Water	23
3.5	Dust	24
3.6	Nitrogen dioxide	24
3.7	Hydrocarbons	24

3.8	UV-radiation	26
4	Plume dispersion model	29
5	Experimental equipment	35
5.1	Concept	35
5.2	Equipment design	36
5.3	Description of the experimental equipment	39
5.3.1	Preparation of simulated exhaust gases	39
5.3.2	Wind tunnel	43
5.3.3	Dispersion photometer	47
5.3.4	Chemical analysis of aerosol particles	52
5.3.5	Controlling	53
5.4	Experimental procedure	55
5.4.1	Starting-up of the equipment	56
5.4.2	Reference measurements	56
5.4.3	Measurements	57
5.4.4	Shut-down of the equipment	58
6	Experiments	59
6.1	Fractional factorial design at two levels	62
6.2	Night experiments	65
6.2.1	Experimental conditions	65
6.2.2	Results of the night experiments	68
6.2.3	Chemical analysis	73
6.3	Day experiments	76
6.3.1	Experimental conditions	76
6.3.2	Results of the day experiments	77

6.4	Summary of the fractional factorial design series	82
6.4.1	Consequences for further experiments	84
6.5	Hydrogen chloride series	85
6.6	Sulfur dioxide series	87
6.6.1	Influence of the sulfur dioxide concentration on opacity	87
6.6.2	Influence of the sulfur dioxide concentration in combination with the ambient relative humidity on opacity	90
6.6.3	Comparison between the influence of the sulfur dioxide concentration and hydrogen chloride concentration on opacity	93
6.6.4	Moisture content of the exhaust gas series	94
6.6.5	Dust series	96
6.6.6	Influence of the ambient air temperature	98
6.7	Exhaust gas temperature series	100
6.8	Validation of the wind tunnel's fluid dynamics	102
7	Discussion and conclusions	109
7.1	Influence of temperature	110
7.2	Formation of ammonium chloride	111
7.3	Sulfate formation and its influence on opacity	113
7.4	Hydrocarbons/UV - light/ NO_x	114
7.5	Influence of oxygen	115
7.6	Influence of ambient as well as exhaust gas humidity	115
7.7	Influence of dust	115
7.8	Relevance for industry	116
8	Outlook	119

8.1	Abbreviations	121
8.2	Symbols	122
	8.2.1 Latin symbols	122
	8.2.2 Greek symbols	123
8.3	Subscripts	123
A	Opacity reading according to EPA Method 9	133
A.1	Certification and training of observers	133
A.2	Preobservation operations	134
A.3	On-site field observations	134
	A.3.1 Opacity observations	135
	A.3.2 Field data: the "Visible Emission Observation Form"	136
A.4	Postobservation operations	136
A.5	Calculations	136
A.6	Auditing procedures	136
B	Solving of fluid dynamical problems	137
B.1	Initial wind tunnel	137
B.2	Situation after the first modifications	140
	B.2.1 Wind tunnel	140
	B.2.2 Mixing problem	143
	B.2.3 Controller problem	143
C	LabView programs	147

List of Tables

2.1	Summary of the main factors influencing plume opacity (Weir et al.,1976)	13
3.1	List of main secondary aerosols influencing possibly plume opacity	18
3.2	List of main possible gas-phase reactions and constants: * F-P refers to Finlayson-Pitts and Pitts jr., (1986); S refers to Seinfeld (1986); D refers to Dahlin, Su and Pe- ters (1981); WS refers to Wexler and Seinfeld, (1986) .	28
5.1	Results of the equipment design by the way of scale-down considerations	39
6.1	2^{3-1} Fractional Factorial Design	63
6.2	Main normalized variables for the night plume experiment	66
6.3	2^{9-5} Fractional Factorial Design of the night experiments	67
6.4	Night plume experiments results	69
6.5	Fractional factorial design coefficients for the night plume simulation according to three different methods: mean values of y_i , maximum values of y_i and the values of y_i of each sampling location	70
6.6	Main normalized variables for the day plume experiment	76
6.7	2^{10-6} Fractional Factorial Design	78
6.8	Day plume simulation results	79

6.9	Fractional factorial design coefficients for the day plume simulation according to three different methods: mean values of y_i , maximum values of y_i and for y_i of each sampling location A to O	80
6.10	List of influences that have been studied in different series as well as sections where the results can be found .	85
6.11	Experimental conditions for the hydrogen chlorides series	86
6.12	Experimental conditions for the sulfur dioxide series . .	89
6.13	Experimental conditions for the sulfur dioxide and moisture content of the ambient air series	92
6.14	Experimental conditions for the exhaust gas moisture content series	96
6.15	Experimental conditions for the dust series	99
6.16	Experimental conditions for the ambient air temperature series	102
6.17	Experimental conditions for the exhaust gas temperature series	104
B.1	Accuracy of the old and new control system for the modified wind tunnel (outlet cone)	144

List of Figures

2.1	Example of plume opacity	8
2.2	Classification of plumes	10
2.3	Opacity reading for attached plumes	11
2.4	Opacity reading for detached plumes	12
3.1	Graphical representation of the influence of the exhaust gas on the equilibrium constant of the ammonium chloride formation	20
3.2	The ozone formation process "Photosmog" (Hoigné, 1992)	25
3.3	The "PAN" formation process (Hoigné, 1992)	26
4.1	Scheme of the dispersion of plumes after the stack exit	30
5.1	Main studied variables within this project	36
5.2	View of the equipment for synthesizing the exhaust gas: furnace, steam generator, aerosol generator	40
5.3	View of the air-conditioner and wind tunnel	41
5.4	Gas bottles with mass flow controllers	42
5.5	Double walled evacuated silvered glass stack	43
5.6	Inside view of the wind tunnel with the stack, dispersion photometer and UV-tubes	44
5.7	Wind tunnel entry in order to improve mixing (dimensions in mm)	45

5.8	Spectrum of the Eversun sunbed tubes: Relative radiation intensity (%) plotted against the wavelength λ (nm)	46
5.9	Scheme of the dispersion photometer RM210, Sick (1996)	48
5.10	Reference measurement of the photometer, Sick (1996)	48
5.11	Opacities read during one experiment plotted versus the corresponding photometer values	49
5.12	Top and side view of the crane for moving the photometer	50
5.13	Picture of the crane moving the dispersion photometer in three directions	51
5.14	Sample train for chemical analysis of the aerosols formed, Oberholzer (1992)	52
5.15	Scheme of the sampling locations (photometer as well as chemical analysis) inside the wind tunnel (dimensions in mm)	57
6.1	Main variables studied within this project	60
6.2	Surface plot of the one-factor-at-a-time method	61
6.3	Surface plot of the factorial design method	61
6.4	Relative chloride and sulfate concentrations along the wind tunnel at stack height	74
6.5	Relative chloride and sulfate concentrations along the wind tunnel at 50 to 70 cm above stack height	75
6.6	Influences of different variables during the 'night' and 'day' experiments on opacity: 0 no influence;+ proportional influence; ++ very strong proportional influence; - inversely proportional influence; - very strong inversely proportional influence; ? influence not known yet	83
6.7	Opacity readings (maximum values) of the hydrogen chloride series at two different ammonia concentration levels 75 resp. 240 mg/m ³ _{n,dry} ; T _a =9°C, T _g =150°C	87

- 6.8 Ammonium chloride concentration results of the hydrogen chloride series at two different ammonia concentration levels 75 resp. 240 mg/m³_{n,dry}; T_a=9°C, T_g=150°C . 88
- 6.9 Opacity readings (maximum values) of the sulfur dioxide series; T_a=9°C, T_g=200°C, C_{NH₃}=75 mg/m³_{n,dry} for all three series 90
- 6.10 Results of the chemical analysis of the sulfur dioxide series; T_a=9°C, T_g=200°C, C_{NH₃}=75 mg/m³_{n,dry} for all three series 91
- 6.11 Opacity readings (maximum values) of the sulfur dioxide and ambient humidity series at T_a=9°C and M_a=60% resp. at T_a=3.5°C and M_a=82%; T_g=200°C, C_{NH₃}=75 mg/m³_{n,dry} 93
- 6.12 Results of the chemical analysis of the sulfur dioxide and ambient humidity series at T_a=9°C and M_a=60% resp. at T_a=3.5°C and M_a=82%; T_g=200°C, C_{NH₃}=75 mg/m³_{n,dry} 94
- 6.13 Comparison between the influence of the sulfur dioxide concentration and hydrogen chloride concentration on opacity at T_a=9°C and M_a=60% resp. at T_a=3.5°C and M_a=82%; T_g=200°C, C_{NH₃}=75 mg/m³_{n,dry} 95
- 6.14 Opacity values of the exhaust gas moisture content series at T_a=8.5°C and M_a=80% (r. h. relative humidity); T_g=200°C, C_{NH₃}=75 mg/m³_{n,dry}, C_{HCl}=60mg/m³_{n,dry} . 97
- 6.15 Results of the chemical analysis of the exhaust gas moisture content series at T_a=8.5°C and M_a=80% (r. h. relative humidity); T_g=200°C, C_{NH₃}=75 mg/m³_{n,dry}, C_{HCl}=60mg/m³_{n,dry} 98
- 6.16 Opacity readings of the dust series at T_a=9°C and M_a=60%; T_g=200°C, C_{NH₃}=75 mg/m³_{n,dry} 100
- 6.17 Results of the chemical analysis of the dust series at T_a=9°C and M_a=60%; T_g=200°C, C_{NH₃}=75 mg/m³_{n,dry} 101

6.18	Opacity values and sulfate concentrations of the ambient air temperature series at $M_a=60\%$, $T_g=150^\circ\text{C}$, $C_{NH_3}=75\text{ mg}/m_{n,dry}^3$, $C_{SO_2}=2500\text{ mg}/m_{n,dry}^3$	103
6.19	Opacity readings of the exhaust gas temperature series at $T_a=9^\circ\text{C}$ and $M_a=60\%$; $C_{NH_3}=75\text{ mg}/m_{n,dry}^3$, $C_{HCl}=60\text{ mg}/m_{n,dry}^3$	105
6.20	Results of the chemical analysis of the exhaust gas temperature series at $T_a=9^\circ\text{C}$ and $M_a=60\%$; $C_{NH_3}=75\text{ mg}/m_{n,dry}^3$, $C_{HCl}=60\text{ mg}/m_{n,dry}^3$	106
6.21	Experimental and predicted (model) ammonium chloride concentrations along the wind tunnel at stack height vs. time after leaving the stack; $T_g = 150^\circ\text{C}$, $T_a = 18^\circ\text{C}$, $M_a = 85\%$, $v_a = 0.35\text{ m/s}$	106
6.22	Experimental and predicted (model) ammonium chloride concentrations along the wind tunnel at stack height vs. time after leaving the stack; $T_g = 150^\circ\text{C}$, $T_a = 9^\circ\text{C}$, $M_a = 60\%$, $v_a = 0.35\text{ m/s}$	107
7.1	Influence of different variables on opacity formation: 0 no influence; + proportional influence; ++ big proportional influence; - inversely proportional influence; -- big inversely proportional influence	109
A.1	Source layout sketch	135
B.1	Initial lay-out scheme of the wind tunnel before modifications	137
B.2	Distribution of the air flow velocity (indicated in m/s) over the entire tunnel cross section at 1m and 3m after the tunnel's entrance; $T_{Lab} = 26^\circ\text{C}$, $T_{a,setting} = 20^\circ\text{C}$, $velocity_{setting} = 0.25\text{ m/s}$	138

B.3	Distribution of the air flow velocity (indicated in m/s) over the entire tunnel cross section at 3.9 m after the tunnel's entrance; $T_{Lab} = 26^{\circ}C$, $T_{a,setting} = 20^{\circ}C$, $velocity_{setting} = 0.25$ m/s	139
B.4	Scheme of the wind tunnel after the modifications	140
B.5	Distribution of the air flow velocities (indicated in m/s) over the tunnel cross section at 3m after the tunnel entrance; $T_{Lab} = 12^{\circ}C$, $T_{a,setting} = 8^{\circ}C$, $velocity_{setting} = 0.30$ m/s	141
B.6	Record of the tunnel temperature $T_{Tunnel}(^{\circ}C)$, the tunnel relative humidity $MoistureT$ (%) and the flow velocity V_a (m/s) after tunnel outlet modifications; $T_{Lab} = 12^{\circ}C$, $T_{a,setting} = 9^{\circ}C$, $M_{a,setting} = 56\%$, $velocity_{setting} = 0.30$ m/s	142
B.7	Record of the tunnel temperature $T_{Tunnel}(^{\circ}C)$, the tunnel relative humidity $MoistureT$ (%) and the flow velocity V_a (m/s) after controller and tunnel inlet modifications; $T_{Lab} = 12^{\circ}C$, $T_{a,setting} = 9^{\circ}C$, $M_{a,setting} = 85\%$, $velocity_{setting} = 0.35$ m/s	144
B.8	Distribution of the air flow velocity over the entire tunnel cross section at 3m after the tunnel's entrance after all the modifications have been made; $T_{Lab} = 12^{\circ}C$, $T_{a,setting} = 9^{\circ}C$, $velocity_{setting} = 0.30$ m/s	146
C.1	Example of the LabView program for controlling the moving of the photometer (part 1)	148
C.2	Example of the LabView program for controlling the moving of the photometer (part 2)	149
C.3	Example of the LabView program for controlling the moving of the photometer (part 3)	150
C.4	Example of the LabView program for controlling the moving of the photometer (part 4)	151

Chapter 1

Introduction

1.1 Growing concern for plume opacity

During the last century industry developed very quickly as a result of the introduction of the steam machine built by James Watt in 1785 (Dickinson and Jenkins, 1981). However in parallel to the growing industrialization air pollution became an obvious problem as is illustrated by the following example from Britain. Exactly 100 years ago, a London artist was unable to paint because the thick smog blanketing the city obscured his view of the Thames (Environment Agency, 1999). The need for remedy was obvious. Sir William Richmond wrote to The Times to complain, setting in train the formation of the Coal Smoke Abatement Society (1899), which evolved into the National Society for Clean Air and Environmental Protection (Environment Agency, 1999). At the end of the nineteenth century, Maximilian Ringelmann, a French engineer, developed the Ringelmann charts (Ringelmann, 1898). These charts which consist of black grids on white paper were used to evaluate the smoke density of plumes and thereby the burning efficiency of coal fired furnaces. The standard charts had 20, 40, 60 or 80 % of the white area covered with the black ink grid lines and were compared to the plume colours. These charts were introduced in the United States by W. Kent in 1897 (Kent, 1897). In 1910 the charts were officially recognized by the Massachusetts Legislature in the smoke ordinance for Boston (Pilat, 1984). In 1947 the state of California adopted the

Health and Safety Code Section 24242 which allowed also the evaluation of nonblack plumes using the Ringelmann chart. This regulation was the so called 'Equivalent Opacity' which was an enlargement of the Ringelmann regulation. The Los Angeles Air Pollution Control District developed a method for training air pollution inspectors to read plume opacity. This method compared plume opacity readings with light transmissometer measurements.

In the early 70's EPA specified the visual determination of opacity of emissions from stationary sources in the EPA Method 9 (Federal Register, 1971; Federal Register, 1974).

The formation of plume opacity phenomena is a subject of growing concern. Opacity standards are already part of the emission control regulations in the United States (Clean Air Act, 42 U. S. C. §7413 (a)(1)) as well as Canada (Ontario Government, Ministry of Environment, Regulation 308): " . . . no person shall cause or permit to be caused a visible emission that obstructs the passage of light to a degree greater than 20 % at the point of emission . . .".

Unfortunately some cement kiln stacks experience increased plume opacity even if the emissions are below the legislation limits (Chadbourne et al., 1980; Dellinger et al., 1980; MacIver et al., 1988; Güemez-Garcia et al., 1994, Dubois and Flores, 1996). Often increased plume opacity only appears after a considerable distance from the stack exit.

In recent years the Environmental Protection Agency applied the opacity regulations of the Clean Air Act (CAA) very strictly. In fact several companies (and even universities and hospitals) were fined or cited in the last few years by EPA for Clean Air Act violations (EPA, 1997A; EPA, 1997B; EPA, 1998A; EPA, 1998B; EPA, 1998C). This is why many efforts were made in order to understand and reduce opacity from cement kilns (Güemez - Garcia et al., 1994; Hawks and Rose, 1995).

On the other hand even in countries where such a legislation does not exist, plume opacity is not always accepted in the neighbourhood of industrial plants. This as well as other problems of social acceptance have become a concern in the last few years for instance by different chem-

ical industrial associations. This is why these associations initiated on their own the "Responsible Care" policy statement (Hungerbühler, 1999). The aim of this voluntary development program is the improvement of safety and ecology on one hand and a better public information on the other.

The need for a better communication with the public also becomes obvious when analyzing the results of reports commissioned by the Washington, D. C. -based Foundation for Clean Air Progress (Raber, 1997). An emission study revealed that since 1970 in the US, all pollutants emitted into the air have dropped by 69 million tons annually. Nevertheless, 58 % of the adults in a random nationwide telephone survey said they believe air quality has got worse over the past 10 years.

Beside these psychological aspects of air pollution aerosols also have an impact on our climate system. Anthropogenic aerosols act as part of the global eco-system by influencing the solar and terrestrial radiation. Again the extend of the effects of the anthropogenic aerosols on radiative transfer is determined by their effects on visibility and turbidity in the atmosphere (Pueschel, 1993). In urban centers visibility is up to 60% less than in sparsely populated regions. In the last years research indicates that anthropogenic aerosols can possibly cause local-scale warming of the atmosphere, however the global-scale effects are still not well understood.

As opacity is the most common method used in the United States to evaluate the emission of any air pollutant from a stationary source (neither access to a plant nor complex stack sampling methods are required (Pilat, 1984)), the facts mentioned above show the importance of all the measures taken in order to reduce opacity. On one side the Clean Air Act standards should be respected, on the other hand measures for reducing opacity should be taken and should be communicated to the public in order to improve the image of industry and hence increase the social acceptance.

1.2 Scope

Like any other industry the cement industry too has to respect the Clean Air Act regulations. However some cement kilns experience increased opacity. Once plume opacity appears, it can disperse several kilometres downwind. So far plume opacity phenomena are not well understood and there is no coherent information about plume opacity. Some hypotheses upon opacity formation exist (Hawks and Rose, 1995), however these hypotheses have so far not been verified systematically. In order to develop efficient and at the same time economic measures against increased opacity, more knowledge about plume opacity formation phenomena should be gained. However the study of plume opacity in a plant is rather difficult for different reasons (Kutschera, 1999):

- First of all the cement manufacturing process never takes place under stable conditions. The values of different parameters (e. g. furnace temperature, exhaust gas composition, ...) are not constant in time but oscillate around a certain value.
- Moreover there exist more than 8000 parameters in a cement plant complex that should kept constant (which is not possible) and that should be evaluated. In case opacity increases or decreases, it would be impossible to find out which one of the 8000 parameters was responsible for this variation in opacity.
- The parameters in a cement plant can be divided in control parameters and design parameters. The latter ones (for instance exhaust gas temperature, exhaust gas velocity) can also be changed unintentionally during the cement manufacturing process due to several phenomena (for instance accumulation phenomena, cycles, etc.).
- Finally there have been different approaches in industry to study plume opacity formation mechanisms. Process data were analyzed carefully and it was tried to find correlations between some process variables and increased plume opacity, unfortunately without

success.

Another problem related to field tests is the in-plume sampling technique. Samples are collected inside the plume with balloons and radio controlled aircraft. However, the samples are small, which limits the analysis of the particle size. In addition the sample may change between collection and analysis (Hawks and Rose, 1995). Moreover balloon sampling is expensive and difficult. It is quite problematic to hold the balloon inside the plume due to dispersion and turbulence effects. As the balloon is battery powered the sampling time is rather short and the samples quite small.

All these problems cited above lead to the conclusion that a lab scale experimental equipment should be designed and constructed in order to study plume opacity formation with more flexibility and greater ease.

1.3 Objectives

The present work should be a contribution to a systematical study of plume opacity formation phenomena. One objective of this work is the design and installation of an experimental equipment on lab scale that allows the simulation of plume formation as a function of different parameters (exhaust gas as well as meteorological conditions). Using this equipment a detailed investigation on plume opacity formation is carried out. This research involves the determination of:

- the precursor substances which play a role during opacity formation. This is done with the help of a chemical composition analysis of the aerosols.
- the exhaust gas- as well as the atmospheric conditions under which plume opacity increases.
- the factors responsible for the oxidation of sulfur dioxide and hence the formation of aerosols (exhaust gas moisture content, dust concentration, ambient relative humidity, ambient air temperature).

Moreover in order to reproduce large emissions (up to 400'000 m³/hr) in our lab-scale equipment, important scale-down considerations had to be made. Another goal of this work is the checking of these scale-down calculations. Therefore a theoretical model is used which describes the dispersion of a plume. This model has been used in many studies (Briggs, 1965; Damle, 1984; Damle, 1987; Fay et al., 1970; Hoult et al., 1969; Hoult et al., 1972; Ooms, 1972) and it has been shown that besides its simplicity the model predicts very well the dispersion of a plume (both in the field and under laboratory conditions). This is why the results of the theoretical estimations obtained with the help of the model cited above can be compared to measurements in order to check the validity of the experiments and hence the fluid dynamics inside the wind tunnel. The use of the model for interpreting the experimental results is justified by the firm foundation of the model including many validation exercises.

Chapter 2

Opacity

2.1 What is opacity?

2.1.1 Definition

Opacity can be defined in several ways, e. g. :

Opacity is defined as the percent obscuration of light transmission and is the difference between 100% light transmission and the percent transmission through the stack gases. It is a scientific and objective parameter but is mostly measured somewhat subjectively by regular calibration of human eyes (Toro, 1984).

An example of the application of this definition can be seen in Figure 2.1.

According to this definition, opacity can be defined as:

$$\text{opacity (\%)} = 100 - \text{transmission (\%)} \quad (2.1)$$

This equation can also be expressed by the Lambert - Beer law:

$$\text{opacity (\%)} = [1 - e^{AC_m L}] \cdot 100 \quad (2.2)$$

where L is the path length (m), A is an attenuation coefficient (m^2/g) and C_m is the mass concentration of the dust (g/m^3).

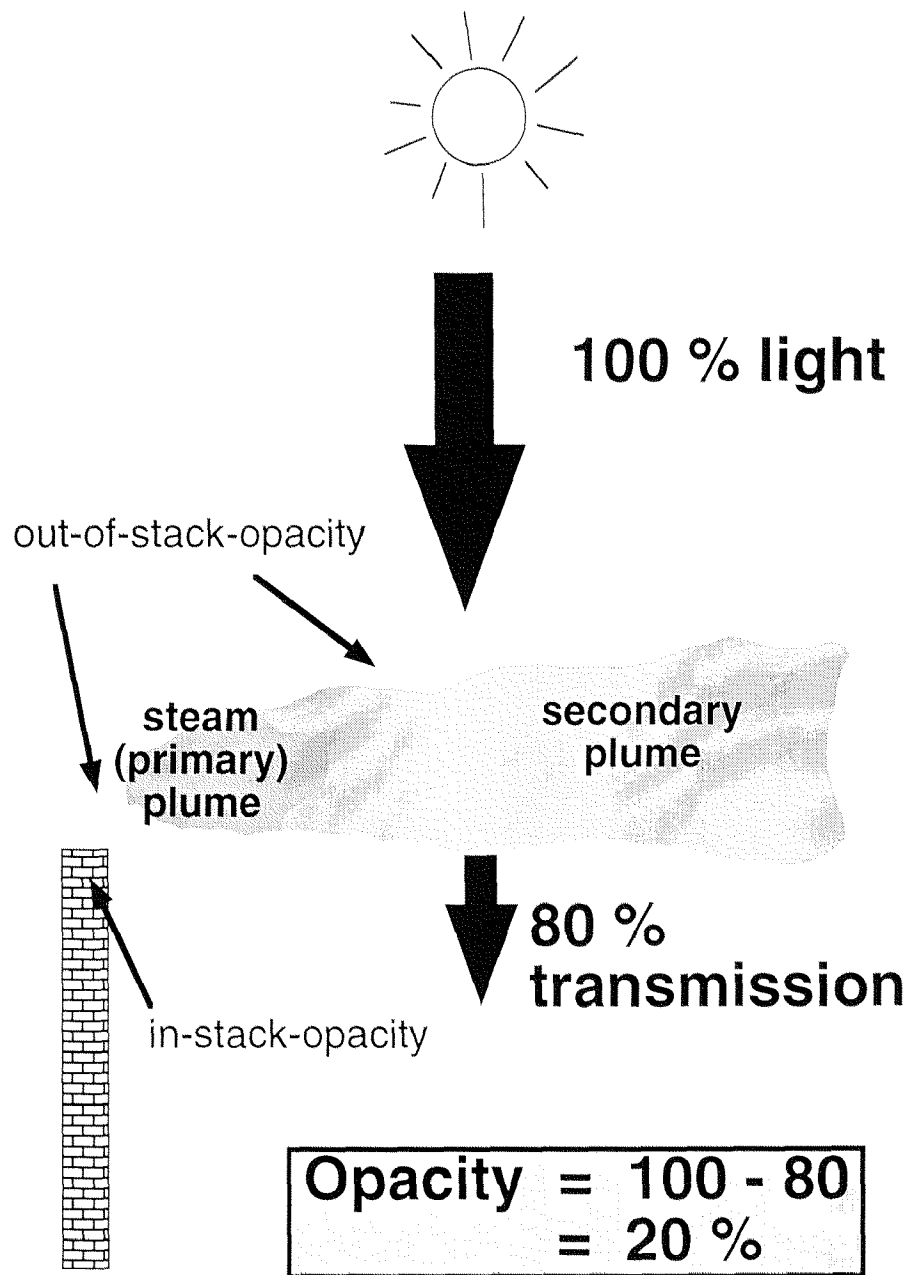


Figure 2.1: Example of plume opacity

The definition of opacity however must not be limited to optical radiations only, as shows the following definition:

The capacity of matter to block the passage of light or radiant energy such as heat. A measure of opacity might be the percentage of light transmission through a plume. Opacity is the opposite of transparency and an object with a high degree of opacity is said to be opaque (WQA, 1997).

2.1.2 Types of opacity

In-stack and out-of-stack opacity

Two types of opacity can be considered (see Figure 2.1):

- in-stack-opacity, which is mostly due to emitted dust, gases (e. g. NO_2) and aerosols
- out-of-stack opacity, which is the plume opacity formed after leaving the stack.

Types of plumes

Different types of plumes have to be considered (see Figure 2.2):

- *Primary plume*: the primary plume (steam plume) mainly consists of steam. In case the steam plume is followed by a secondary plume it is called primary plume. Otherwise it is called steam plume. The opacity of this primary steam plume is defined as being 100%. For this plume a distinction must be made again. This primary plume can be :
 - attached: The water condensation has occurred before the stack outlet or right at the stack outlet.

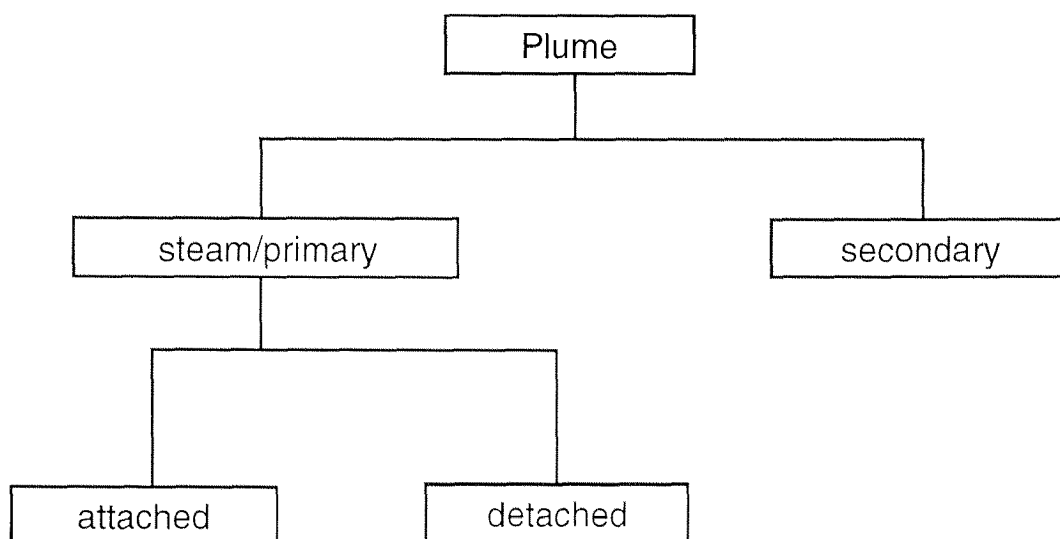


Figure 2.2: Classification of plumes

- detached: In this case, the water condensation occurs at a certain distance downwind after the stack exit. The plume has very little or no visible emissions at the stack.
- *Secondary plume*: In case the emissions are not visible at the stack exit but are still visible after the dissipation of the steam plume (primary plume), one speaks of a secondary plume formation (VA-Datenbank-Blatt, 1991). Its colour (bluish, grey, brownish, etc.) normally differs from the steam plume colour (white).

Where has opacity to be read?

Depending on the type of plume in question, opacity has to be read at different locations. The in-stack opacity can normally be determined by special in-stack (in-situ) light transmissometers (Chadbourne et al., 1980). This is normally done continuously (CEMS Continuous Emission Monitoring System) (Parker, 1995). However in case this in-stack opacity is lower than the out-of-stack opacity this latter one has to be read.

The question where the out-of-stack opacity has to be read is regulated by EPA Method 9. Method 9 states in general (Rose and Egsegian,

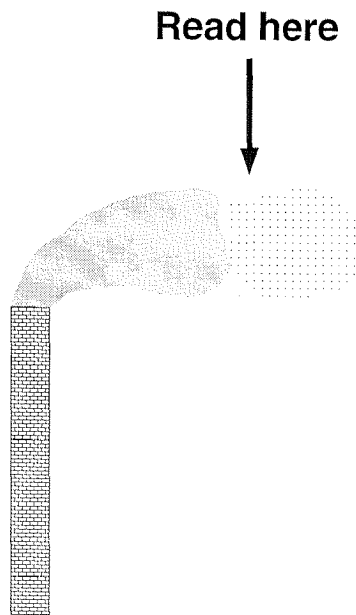


Figure 2.3: Opacity reading for attached plumes

1991):

Opacity observations shall be made at the point of greatest opacity in that portion of the plume where condensed water vapor is not present.

For wet plumes where the condensation of the water vapour has already occurred before exiting the stack (attached plumes) plume opacity can only be read downwind at a location where the water has evaporated (Pilat, 1984) (see Figure 2.3). EPA Method 9 states (Rose and Egsegian, 1991):

When condensed water vapor is present within the plume as it emerges from the emission outlet, opacity observations shall be made beyond the point in the plume at which condensed water vapor is no longer visible. The observer shall record the approximate distance from the emission outlet to the point in the plume at which the observations are made.

In case of detached plumes, opacity can be read before the water condensation occurs. Method 9 states (Rose and Egsegian, 1991):

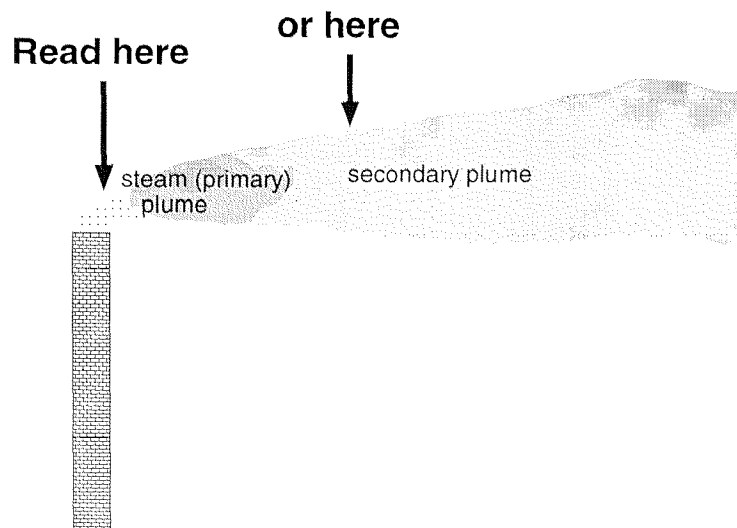


Figure 2.4: Opacity reading for detached plumes

When water vapor in the plume condenses and becomes visible at a distinct distance from the emission outlet, the opacity of the emissions should be evaluated at the emission outlet prior to the condensation of water vapor and the formation of the steam plume.

However if the opacity of the secondary plume is greater than that of the emissions at the stack exit, the opacity of the secondary plume must be read according to the Method 9 general rule (see above) (see Figure 2.4).

2.2 Main factors influencing plume opacity

Two very important factors influencing plume opacity are the mass of particles emitted with the exhaust gas as well as the particles diameter. In fact particles in the 0.2-1.0 μm range are particularly effective in obscuring visible light on a unit mass basis with a relatively sharp peak obscuration at 0.5 μm (blue light) (Damle et al., 1987).

Besides these variables there are other variables that influence plume opacity. These variables can be divided into two categories (Weir et al,

1976):

- *Controllable variables*: those variables that are a function of the control equipment and can be controlled by the operator of the (cement) plant or the designer
- *Uncontrollable variables*: those variables beyond the control of the operator

Table 2.1: Summary of the main factors influencing plume opacity (Weir et al.,1976)

Controllable factors influencing plume opacity	
mass emission of particulate matter	mean particle size
deviation from the mean size	stack diameter
stack gas temperature	stack gas velocity
Uncontrollable factors influencing plume opacity	
particle density	distance of observer from stack
particle index of refraction	non-level terrain
water vapor	observer offset angle
color of plume	time of day
wind speed	day of year
wind direction	longitude of stack
wind turbulence	latitude of stack
ambient air temperature and moisture	sun angle
color of the sky	human error

A summary of the main variables influencing plume opacity can be found in Table 2.1.

As far as the controllable factors are concerned the following statements can be made:

- the higher the mass concentration of particulate emissions the higher the opacity;
- the larger the diameter of the stack, the greater the path length over which light scatters and hence the greater the apparent opacity;

- for small particles ($0.5 \mu\text{m}$) opacity decreases as the deviation from the mean particle size is increased (particles of $0.5 \mu\text{m}$ are particularly effective in obscuring visible light) while for large particles (above $2 \mu\text{m}$) the converse is true;
- as the gas temperature influences the relationship between standard ($\text{m}_{n,dry}^3$) and actual volume, the lower the exhaust gas temperature, the higher the particle concentration and hence the higher the opacity.

As far as the uncontrollable factors are concerned the following can be said:

- the lower the density of the particles emitted at a given mass loading, the larger the number of particles and hence the higher opacity;
- different color contrast ratios between the plume and the sky lead to different opacities;
- the water content of the flue gas depends on the type of process used (wet, semi-wet, semi-dry or dry process) or on the fact if a scrubber or cooling tower is used or not;
- the higher the wind speed or the turbulences, the lower the opacity;
- the position of the sun influences the scattering angle through which incident light is reflected and refracted from the particles;
- the variation in opacity with changes in the elevation of the observer are more pronounced at low sun angles in winter than at high sun angles in summer;
- in the northern hemisphere, the opacity for plants in the south will always be higher than those seen by the same observer under identical conditions at an identical plant in the north due to higher sun angles in the southern latitudes.

2.3 Opacity reading according to EPA Method 9

Out-of-stack opacity is read by trained certified smoke inspectors according to EPA Method 9. A short description of this EPA Method 9 can be found in Appendix A.

2.4 Accuracy in estimating plume opacity

There are many factors influencing plume opacity (see Section 2.2). However studies of accuracy (Heinsohn et al., 1992) showed that EPA Method 9 for reading plume opacity is technically sound. The authors claim that individuals blessed with a keen ability to make visual differentiations are selected and trained according to EPA Method 9 guidelines in order to refine their talent. This training emphasizes unshakable mental impressions of 25, 50 and 75 percent opacity. At the end, individuals that have been certified are able to read opacity with demonstrably acceptable accuracy throughout the six-month period they are certified.

Moreover it could even be proven that the accuracy achieved by individuals during their initial recertification attempt is virtually the same as the accuracy six month earlier when they passed the certification test. This shows that the reader's ability to read accurate opacities does not deteriorate with time.

Chapter 3

Hypotheses for opacity formation

Light scatter makes plumes visible. Aerosols (colloidal systems of gases (air) with dispersed fine solid or liquid particles (1 nm to $0.1\mu\text{m}$ diameter)) (Römpp, 1996) are responsible for this light scattering. These aerosols may include (Rose and Hawks, 1995):

- primary particulate (raw material, dust)
- secondary particulate (formed by condensation reaction between gases)
- pseudo particulate (ammonium chloride)
- wet particulate
- water droplets
- condensing hydrocarbons

At the beginning of this work, a literature study concerning plume opacity phenomena was carried out that has been continued during the whole project. Unfortunately it could be noticed that the information about plume opacity formation was not always coherent as far as for instance precursor substances or the formation of secondary aerosols are concerned.

Table 3.1 shows that the opacity phenomena may be due to ammonium salts and/or condensable hydrocarbons. In this case ammonia would be one of the main precursor substances leading to increased opacity.

Table 3.1: List of main secondary aerosols influencing possibly plume opacity

NH_4Cl	ammonium chloride	(Cheney and Knapp, 1986)
$(\text{NH}_4)_2\text{SO}_4$	ammonium sulfate	(Dellinger, 1980)
NH_4HSO_3	ammonium bisulfate	(Dellinger, 1980)
NH_3SO_3	sulfamic acid	(Chadbourne, 1994)
$\text{NH}_4\text{SO}_3\text{NH}_3$	ammonium sulfamate	(Chadbourne, 1994)
$(\text{NH}_4)_2\text{S}_2\text{O}_6$	ammonium dithionate	(Chadbourne, 1994)
$(\text{NH}_4)_2\text{S}_2\text{O}_8$	ammonium persulfate	(Chadbourne, 1994)
$(\text{NH}_4)_2\text{SO}_3$	ammonium sulfite	(Chadbourne, 1994)
HC	condensable hydrocarbons	(McMurry, 1985)

3.1 Ammonia

In every study concerning plume opacity of cement kiln stacks, ammonium could be identified as being the main cation of the sampled aerosols. In each sample, taken at different plants under different atmospheric as well as exhaust gas conditions, ammonium could be identified (Cheney et al., 1983; Cheney and Knapp, 1986; Cheney and Knapp, 1987; Güemez-Garcia et al., 1994; Hess, 1993; Hung and Liaw, 1981; Richner, 1995; Chadbourne et al., 1980).

The precursor substance of this ammonium cation is most probably ammonia introduced into the kiln by:

- the raw materials (100-200 g NH_3 /t; mainly by shale as well as by limestone and coal). Ammonia can desorb at relatively low temperatures from the raw meal in the first and second stage of the heat exchanger (Richner, 1995).
- an ammonia slip during the NO_x reduction in the kiln where high temperatures and adequate catalysts exist (SCNR) (Richner, 1995; Hess, 1993; Cheney and Knapp, 1987).

Ammonia is present in the exhaust gases in gaseous form so that it can not be removed before the stack exit by bagfilters or electrostatic precipitators (ESP's).

Moreover ammonia reacts with several components (HCl , SO_4^{2-} , etc.) to form ammonium salts. These salts are very hygroscopic. They absorb the moisture of ambient air or of the exhaust gases and can form small droplets in the atmosphere. This effect can lead to an increase of opacity phenomena. Wet aerosols scatter light to a much higher degree than do dry particles.

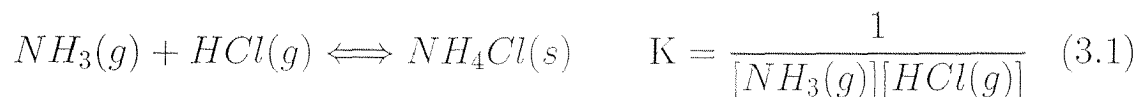
These ammonium salts formed tend to accumulate in a size range of 0.1 - 0.6 μm which is the wavelength of visible and UV - light (Richner, 1995).

As far as the anions of the aerosols are concerned, such coherent information unfortunately does not exist in literature as for the cations.

3.2 Chlorides

Chlorine which is also present in the exhaust gases as gaseous hydrogen chloride (Cheney and Knapp, 1983; Cheney and Knapp, 1986; Cheney, 1987) can react readily in the gas phase with ammonia to ammonium chloride.

Ammonium chloride (s) is directly in equilibrium with gaseous hydrogen chloride and ammonia as given by:



The equilibrium constant K is extremely sensitive to temperature T (K). This is shown in Equation 3.1 (Seinfeld, 1986):

$$K = \exp\left(-34.266 + \frac{21196}{T}\right) \quad (3.2)$$

Figure 3.1 shows a graphical representation of Equation 3.2. It may be seen that at 345°C the equilibrium constant is equal to 1. This means that the forward reaction (formation of ammonium chloride) is in equilibrium with the reverse reaction (sublimation of ammonium chlo-

ride) (see Equation 3.1). Above 345°C the reverse reaction is favoured whereas below 345°C the formation of ammonium chloride is favoured.

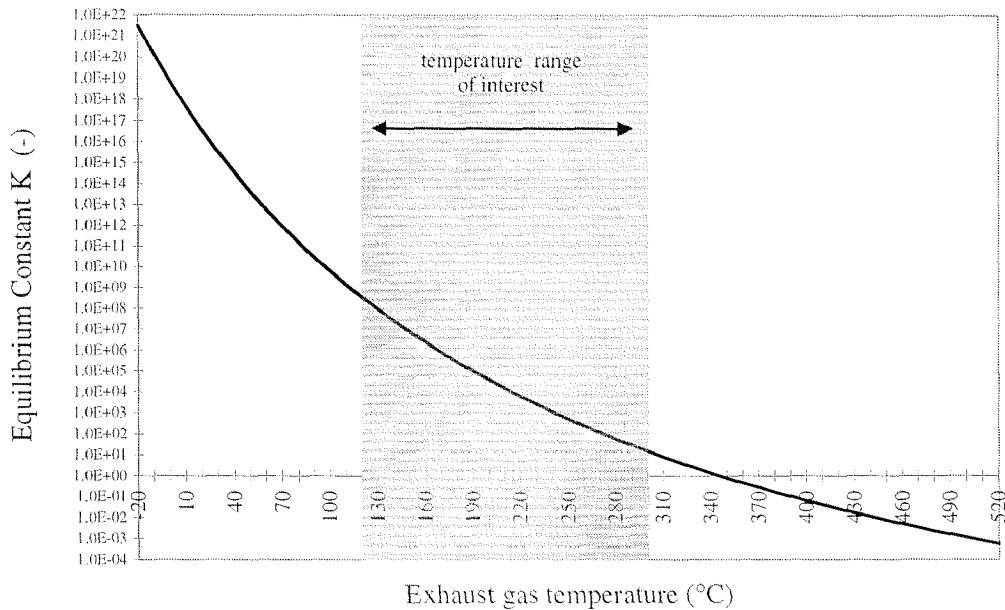


Figure 3.1: Graphical representation of the influence of the exhaust gas on the equilibrium constant of the ammonium chloride formation

As the gases leave the stack, they are diluted with ambient air. This entrainment of ambient air does not only dilute the gases but also cools them down. Although dilution decreases the concentrations of HCl and NH₃ (which inhibits the formation of ammonium chloride) a temperature drop favours the forward reaction to a much greater extent. Equation 3.2 shows that a temperature drop increases the equilibrium constant and hence moves the equilibrium towards the formation of ammonium chloride. An increase in temperature from 140°C to 300°C decreases the equilibrium constant of the formation of ammonium chloride by 2×10^7 .

At the stack exit, exhaust gases have to be cooled down before the reaction of ammonium chloride formation can start (see Figure 3.1). This could explain the detached character of the plume. Although there exists a certain dilution of the exhaust gases with ambient air, opacity of the plume increases due to an increased formation of NH₄Cl,

to pass through a maximum. After a certain distance, the quantity of entrained ambient air is so important, (which means that on one side ammonium chloride is dissipated and on the other side the reactants ammonia and hydrogen chloride are diluted to such an extent that the formation reaction of NH_4Cl stops) that plume opacity decreases to complete dissipation of the plume.

Visible limits for NH_4Cl are usually above 50 mg/m^3 . Moisture can increase opacity, as NH_4Cl is very hygroscopic (Richner, 1995; Chadbourne et al., 1994).

It has been shown in a study that there was approximately 12 times more HCl present than is required to tie-up the NH_3 (MacIver et al., 1988).

Chlorine can be introduced by (Richner, 1995):

- the raw materials (limestone)
- the fuel
- by the addition of chlorine to the kiln as calcium chloride for low alkali klinker production.

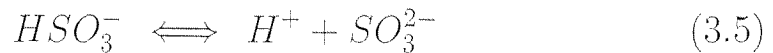
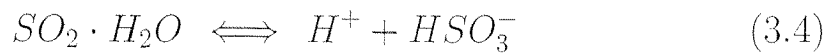
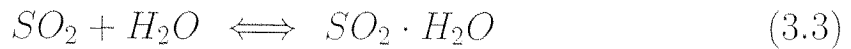
In many studies, ammonium chloride could be found as main component in the impingers (Cheney et al., 1983; Cheney and Knapp, 1986; Cheney and Knapp, 1987; CTL, 1995; Güemez-Garcia et al., 1994; Hawks and Rose, 1995; MacIver et al., 1988; Richner, 1995).

3.3 Sulfates

Ammonia can also react with sulfur oxides to form different ammonium sulfoxide components like (Chadbourne, 1980; Chadbourne, 1994):

$(\text{NH}_4)_2\text{SO}_4$	ammonium sulfate
NH_4HSO_3	ammonium bisulfate
NH_3SO_3	sulfamic acid
$\text{NH}_4\text{SO}_3\text{NH}_3$	ammonium sulfamate
$(\text{NH}_4)_2\text{S}_2\text{O}_8$	ammonium persulfate

SO₂ can be oxidized to SO₄²⁻ in the presence of moisture (Chadbourne et al., 1980; Chadbourne, 1994; Dellinger et al., 1980; Haury, 1976; Haury 1979; Mamane and Gottlieb, 1989; Richner, 1995). This seems to be a very fast reaction. Dellinger showed in laboratory experiments that the present SO₂ in exhaust gases can be oxidized to SO₄²⁻ within 15 seconds (Dellinger, 1980).



Ammonia increases the reaction rate of the oxidation up to 500 times. This is due to the fact that ammonia increases the pH. At basic conditions, sulfur oxides are mostly present as anions. According to Equations 3.4 to 3.6, the forward reaction is favoured in presence of ammonia.

As in the exhaust gases of cement plants, ammonia as well as oxygene, sulfur dioxide and moisture are present, this oxidation of SO₂ is likely to happen. Moreover it seems that a conversion of 4% of SO₂ present in exhaust gases (170 ppm ammonia and 200 ppm SO₂) is sufficient to cause opacity phenomena (Dellinger, 1980).

An increase of the ambient temperature would slow down the condensation of moisture in the atmosphere. This would also slow down the oxidation of SO₂, as the presence of an aqueous phase is necessary for this reaction. As a consequence the plume would dissipated before opacity occurs.

The detached plume can be explained by the time delay needed for sufficient temperature decrease so that moisture can condense. After the dissipation of the steam plume, a secondary plume appears, which could consist of ammonium sulfates. Sulfur dioxide would have been oxidized before in the steam plume.

It could be observed that without a steam plume, there existed only a smaller secondary plume (Ervin, 1996). This could be an argument for the formation of ammonium sulfates.

Moreover it has also been reported that opacity occurred, when the raw mill was shut down (Caluori, 1995). In this case, exhaust gases do not pass the raw meal whereas certain compounds (ammonia as well as components containing sulfur) can absorb to the raw meal in a compound operation mode.

Another possibility for the oxidation of SO_2 (as well as NO_x) is a heterogeneous reaction between mineral particles (for instance cement, mineral particles of soil origin), sulfur and nitrogen oxides. The formed salts containing sulfates and nitrates would scatter light and hence increase plume opacity. However these oxidation reactions are very slow. In case of reaction with cement (Mamane and Gottlieb, 1989):

- formation of 25 - 125 mg sulfates/g mineral ($[\text{SO}_2]$ was 0.86 ppm, relative humidity = 85%, exposure time 1 - 5 days)
- formation of 0.9 - 4.5 mg nitrates/g mineral ($[\text{NO}_x]$ was 0.18 ppm, relative humidity = 60%, exposure time 1 - 5 days)

This slow reaction rate excludes this oxidation mechanism as being responsible for high plume opacity formation.

3.4 Water

The influence of water (steam formation) on plume opacity phenomena is so far not well understood, however it can be excluded as a direct cause for opacity. In fact in case of a secondary plume, opacity persists after the steam plume has already been dissipated. Moreover opacity must be read after the steam has evaporated (see Section 2.1.2).

On the other hand, water possibly contributes to the formation of precursor substances causing plume opacity phenomena (Dellinger et al., 1980; Frankhauser, 1995; VA-Datenblatt, 1991, Richner, 1995):

- due to hygroscopy of ammonium salts, moisture increases the scattering of the light and hence plume opacity.
- the oxidation of sulfur dioxide can only take place in presence of an aqueous phase.

3.5 Dust

Like water, dust seems not to be a primary reason for increased plume opacity. If dust that could not be filtered off was responsible for increased opacity, detached plumes could not be observed. However the emissions right at the stack exit are not visible. Moreover the out-of-stack opacity is normally much higher than the in-stack opacity.

Of course dust can contribute in some indirect way to the formation of aerosols, for instance as condensation nuclei.

Moreover even if the dust emissions are not visible, they could however increase opacity of formed aerosols. Aerosols and dust would cause a low opacity, taken each emission alone. But taken together, the concentration of the particles could be above the visible limits.

3.6 Nitrogen dioxide

NO_2 has absorption bands in the visible region (it is of a brownish colour) and can therefore contribute to plume opacity (Lindau, 1991). However NO has to be oxidized to NO_2 after leaving the stack as 98 % of the NO_x in the exhaust gas are present as NO .

3.7 Hydrocarbons

Other substances that may cause opacity phenomena are condensable hydrocarbons which can form aerosols or small droplets. (McMurry, 1985; Richner, 1995). Hydrocarbons can be introduced by raw mate-

rial such as limestone and clay. Hydrocarbons are present in from of Kerogen.

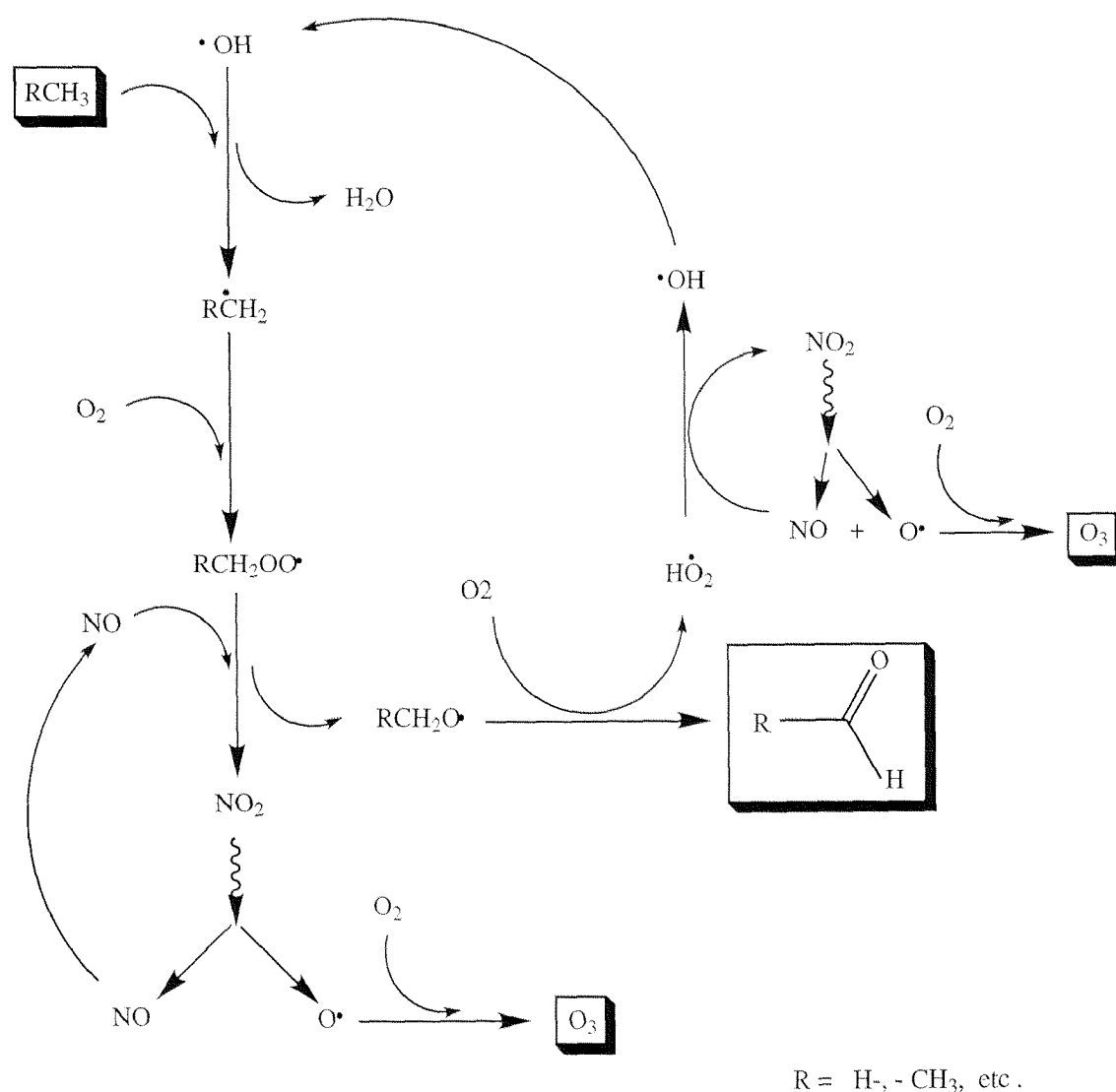


Figure 3.2: The ozone formation process "Photosmog" (Hoigné, 1992)

Moreover in presence of nitrogen oxides and UV-radiation, hydrocarbons are oxidized. In parallel to this oxidation ozone is formed (see Figure 3.2). The ketones and aldehydes formed during this reaction are themselves again the basic material for the formation of PAN (peroxyacetyl nitrate) (See Figure 3.3). These compounds, which are very polar, condense water and lead to the formation of smog. This phenomenon is the so called photosmog which is quite common during summer especially at noon when the UV-radiation is more important

than during the rest of the day (maximum between 12.00 and 2.00 pm).

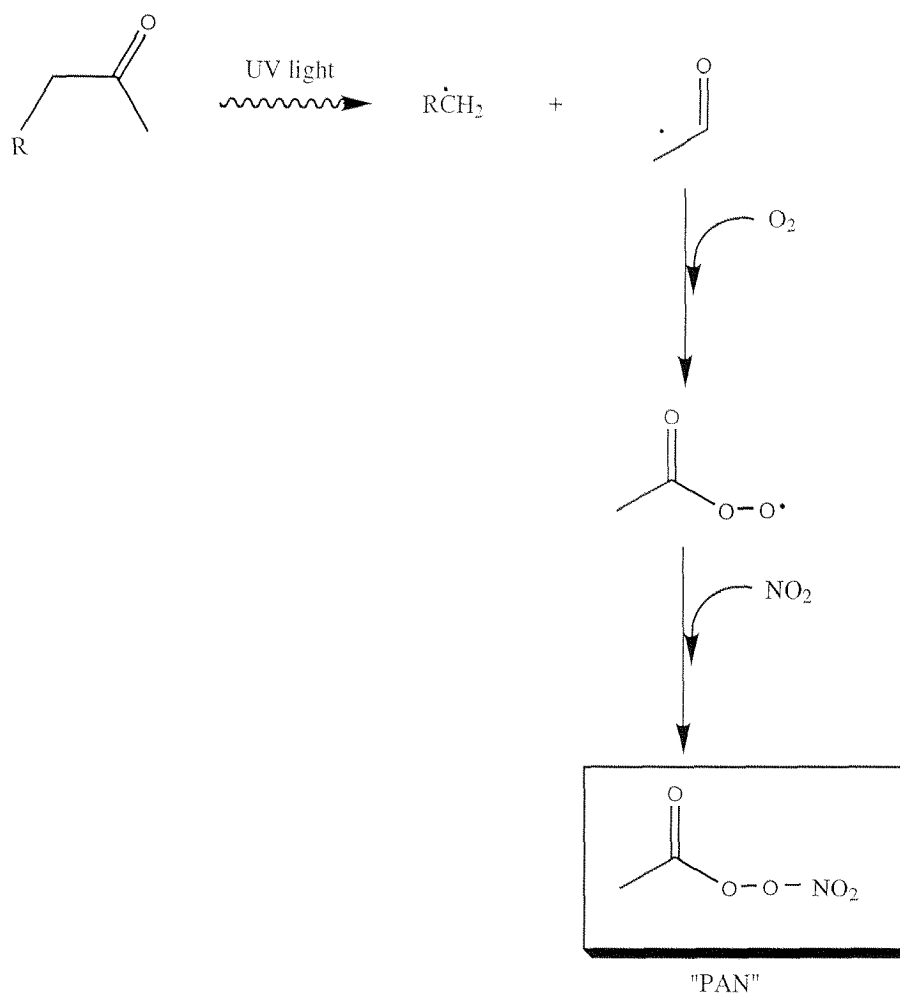


Figure 3.3: The "PAN" formation process (Hoigné, 1992)

3.8 UV - radiation

For certain photolytic reactions UV-radiation is necessary in order to create free radicals. These free radicals then initiate photolytic reactions which for example lead to the formation of sulfuric acid or nitric acid. Normally these photolytic reactions are very fast and could therefore play an important role in the formation of detached plume opacity. Some photolytic reactions that are likely to occur as well as their consecutive reactions are shown in Table 3.2. N_2O_5 is of a brownish colour and is mostly responsible for the smog situation in big agglomerations.

In the present work, plume opacity formation was studied in an experimental equipment in order to check some of the hypotheses mentioned above.

Table 3.2: List of main possible gas-phase reactions and constants: * F-P refers to Finlayson-Pitts and Pitts jr., (1986); S refers to Seinfeld (1986); D refers to Dahlin, Su and Peters (1981); WS refers to Wexler and Seinfeld, (1986)

Reaction	Rate constants	Units of rate constants	Ref.*
$NO_2 + h\nu \rightarrow NO + O(^3P)$	depends on light intensity	sec^{-1}	S
$O(^3P) + O_2 \rightarrow O_3$	$6.0 \times 10^{-34}(T/300)^{-2.3}$	$cm^6 molecule^{-2} sec^{-1}$	S
$SO_2 + O(^3P) \rightarrow SO_3$	3.3×10^{-14}	$cm^3 molecule^{-1} sec^{-1}$	F-P
$NO_2 + O_3 \rightarrow NO_3 + O_2$	$1.2 \times 10^{-13} \exp(-2450/T)$	$cm^3 molecule^{-1} sec^{-1}$	F-P
$NO + O_3 \rightarrow NO_2 + O_2$	$2.2 \times 10^{-12} \exp(-1430/T)$	$cm^3 molecule^{-1} sec^{-1}$	S
$O_3 + h\nu \rightarrow O_2 + O(^1D)$	$0.0 - 1.0 \times 10^{-5}$	sec^{-1}	S
$O(^1D) + H_2O \rightarrow 2 \cdot OH$	2.2×10^{-10}	$cm^3 molecule^{-1} sec^{-1}$	S
$\cdot OH + NO \xrightarrow{M} HNO_2$	6.6×10^{-12}	$cm^3 molecule^{-1} sec^{-1}$	S
$HNO_2 + h\nu \xrightarrow{M} NO + \cdot OH$	depends on light intensity	sec^{-1}	F-P
$\cdot OH + NO_2 \xrightarrow{M} HNO_3$	1.1×10^{-11}	$cm^3 molecule^{-1} sec^{-1}$	S
$SO_2 + \cdot OH \xrightarrow{M} HOSO_2 \cdot$	4.5×10^{-13}	$cm^3 molecule^{-1} sec^{-1}$	F-P
$HOSO_2 \cdot + O_2 \rightarrow SO_3 + HO_2 \cdot$	2.0×10^{-13}	$cm^3 molecule^{-1} sec^{-1}$	F-P
$HO_2 \cdot + NO \rightarrow \cdot OH + NO_2$	$3.7 \times 10^{-12} \exp(240/T)$	$cm^3 molecule^{-1} sec^{-1}$	S
$NO_2 + NO_3 \xrightarrow{M} N_2O_5$	$4.7 \times 10^{-13} \exp(259/T)$	$cm^3 molecule^{-1} sec^{-1}$	S
$N_2O_5 + H_2O \rightarrow 2HNO_3$	$\leq 2 \times 10^{-21}$	$cm^3 molecule^{-1} sec^{-1}$	S
$N_2O_5 \rightarrow NO_2 + NO_3$	$1.96 \times 10^{14} \exp(-10660/T)$	sec^{-1}	S
$SO_3 + H_2O \rightarrow H_2SO_4$	9.1×10^{-13}	$cm^3 molecule^{-1} sec^{-1}$	S
$NH_3 + HNO_3 \rightarrow NH_4NO_3$	11.6×10^6	$cm^3 mol^{-1} sec^{-1}$	WS
$NH_3 + HCl \rightarrow NH_4Cl$	11.4×10^6	$cm^3 mol^{-1} sec^{-1}$	D
$CO + \cdot OH \xrightarrow{O_2} CO_2 + HO_2 \cdot$	2.2×10^{-13}	$cm^3 molecules^{-1} sec^{-1}$	S
$2NO + O_2 \rightarrow 2NO_2$	$3.3 \times 10^{-39} \exp(530/T)$	$cm^6 molecules^{-2} sec^{-1}$	S

Chapter 4

Plume dispersion model

In the present work a plume dispersion model (Briggs, 1965; Damle, 1984; Damle, 1987; Fay et al., 1970; Hoult et al., 1969; Hoult et al., 1972; Ooms, 1972) was used in order to interpret the experimental results. It was checked if the assumptions of the theoretical model (constant wind velocity profile, turbulent exhaust gas stream) could be reproduced in our equipment. As it has been shown in the studies cited above, including those of Davidson (1989) and Netterville (1990), that this model describes accurately plume dispersion in the field as well as under laboratory conditions, it was used to interpret the experimental data collected in our wind tunnel (see Section 6.8).

As the exhaust gases leave the stack, they are diluted with ambient air (see figure 4.1). This dilution is due to the entrainment of ambient air into the plume with an entrainment rate V_e (m/s). The entrainment velocity depends on the plume buoyancy and the velocity difference between the plume (U (m/s)) and wind (V_a (m/s)). The entrainment rate V_e has been estimated by a semi-empirical method (Ooms, 1972; Hoult and Weil, 1972; Briggs, 1975) and can be written as:

$$V_e = \alpha_1(U - V_a \cos \Theta) + \alpha_2 V_a \sin \Theta + \alpha_3 g \left(\frac{T_a - T_p}{T_p} \frac{R}{U} \right) \quad (4.1)$$

α_1 , α_2 and α_3 are empirical constants; Θ is the plume inclination ($^\circ$) relative to the horizontal plane; g is the gravitational acceleration (m/s^2); T_a and T_p are the ambient and the plume temperatures, respectively

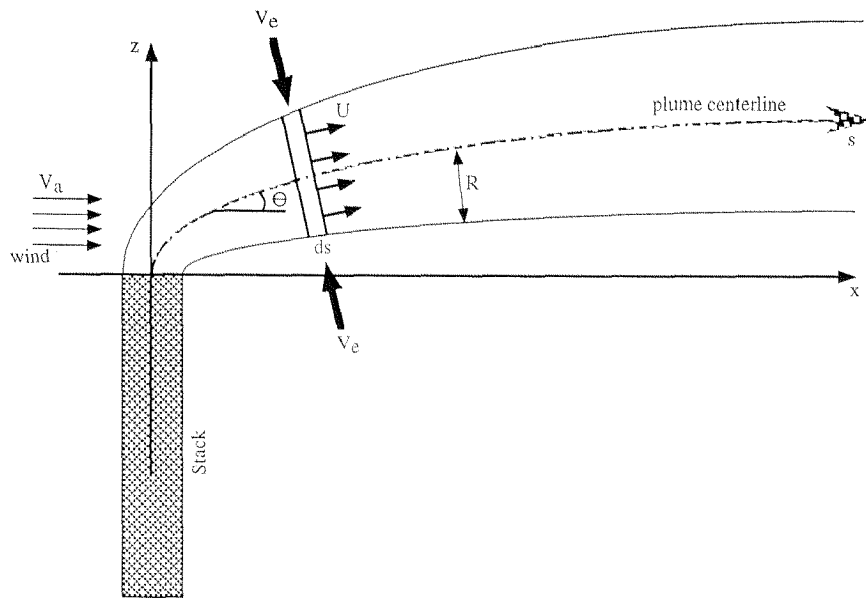


Figure 4.1: Scheme of the dispersion of plumes after the stack exit

(K); R is the effective plume radius (m).

In Equation 4.1 α_3 is often ignored (also in our case) as the corresponding term is usually very small compared to the two other terms. Term α_1 is assigned a mean value 0.11 and α_2 a mean value 0.6 (Hoult and Weil, 1972, Damle et al., 1984).

The entrainment of ambient air into the plume causes plume dilution. The rate of this dilution as well as the variation of plume temperature T_p , plume radius R , concentrations of the exhaust gas components C_p , plume inclination Θ as well as plume velocity U with time can be calculated by taking mass, momentum and energy conservation of a small portion ds of the plume into account. The variable x represents the horizontal distance downwind of the stack exit (m), z the vertical distance above the stack exit (m) and s the curvilinear coordinate (m) along the plume axis.

Conservation of mass: The increase of mass of the plume as it disperses downwind in a portion of length ds is equal to the mass of ambient air that is entrained

$$\frac{d}{ds}(\pi R^2 \rho_p U) = 2\pi R \rho_a V_e \quad (4.2)$$

where ρ_p and ρ_a (g/m³) are average densities of plume gases and ambient air, respectively.

Conservation of momentum in x-direction: The conservation of momentum in this direction takes into account the momentum of the entrained ambient air:

$$\frac{d}{ds}(\pi R^2 \rho_p U^2 \cos\Theta) = 2\pi R \rho_a V_e V_a \quad (4.3)$$

Conservation of momentum in z-direction: The conservation of momentum in z-direction takes into account the buoyancy effect which is due to the difference in density between the plume gases and ambient air. The difference in density is mainly related to the temperature difference of the exhaust gas and the ambient air, respectively.

$$\frac{d}{ds}(\pi R^2 \rho_p U^2 \sin\Theta) = \pi R^2 U g (\rho_a - \rho_p) \quad (4.4)$$

Conservation of thermal energy: This conservation describes the cooling of the plume.

$$\frac{d}{ds}(\pi R^2 \rho_p U T_p) = 2\pi R \rho_a V_e T_a \quad (4.5)$$

Conservation of species: With the help of this conservation formulation the evolution of the different species inside the plume can be described.

$$\frac{d}{ds}(\pi R^2 U C_p) = 2\pi R V_e C_a \quad (4.6)$$

with C_p and C_a being the compounds' concentrations in the plume gas and ambient air, respectively.

The average densities ρ_p and ρ_a can be expressed as a function of the respective molecular weights MW_p and MW_a (g/mol) and the temperatures T_p and T_a by using:

$$\rho_p = MW_p C_p \quad \text{and} \quad \rho_a = MW_a C_a \quad (4.7)$$

The relation:

$$dt = \frac{ds}{U} \quad (4.8)$$

can be used in Equations 4.2 to 4.6. After several simplifications, we obtain:

evolution of the plume radius with time

$$\frac{dR}{dt} = V_e \left[\frac{MW_a}{MW_p} + \frac{T_p}{T_a} \left(1 - \frac{MW_a V_a \cos \Theta}{MW_p U} \right) \right] - \frac{R g \sin \Theta}{2U} \left(\frac{MW_a T_p}{MW_p T_a} - 1 \right) \quad (4.9)$$

evolution of the plume velocity with time

$$\frac{dU}{dt} = \frac{2V_e MW_a T_p}{R MW_p T_a} (V_a \cos \Theta - U) + g \sin \Theta \left(\frac{T_p MW_a}{T_a MW_p} - 1 \right) \quad (4.10)$$

evolution of the plume inclination with time:

$$\frac{d\Theta}{dt} = \frac{g \cos \Theta}{U} \left(\frac{T_p MW_a}{T_a MW_p} - 1 \right) - \frac{2V_e T_p MW_a V_a \sin \Theta}{R T_a MW_p U} \quad (4.11)$$

evolution of the average molecular weight of the plume with time:

$$\frac{dMW_p}{dt} = \frac{2V_e T_p}{R T_a} (MW_a - MW_p) \quad (4.12)$$

evolution of the plume temperature with time:

$$\frac{dT_p}{dt} = \frac{2V_e MW_a T_p}{R MW_p T_a} (T_a - T_p) \quad (4.13)$$

evolution of the plume species concentration with time:

$$\frac{dC_p}{dt} = \frac{2V_e}{R} \left[C_a - C_p \left(\frac{MW_a}{MW_p} + \frac{T_p}{T_a} - \frac{MW_a T_p}{MW_p T_a} \right) \right] \quad (4.14)$$

as well as

$$\frac{ds}{dt} = U, \quad \frac{dz}{dt} = U \sin \Theta, \quad \frac{dx}{dt} = U \cos \Theta \quad (4.15)$$

As far as the simulations are concerned, only the initial conditions at stack height are needed to solve the equations above. At $t=0$, the plume radius equals the radius of the stack outlet. The initial plume velocity as well as its temperature, molecular weight and composition are given at the stack exit. The initial plume inclination is 90.0° ; x , z and s are equal to 0.0 (origin of the coordinate system).

In this model it is assumed that the temperature, plume velocity as well as the composition are uniform across the plume cross section (i. e. top hat profiles). This assumption is reasonable for a well mixed turbulent flow at the stack exit. In addition, the ambient region to be considered is large enough, compared to the extent of the plume, to neglect variations of temperature, composition and molecular weights. When a short time period (0.5 to 1 hour) during stable weather conditions is considered, it is reasonable to assume a constant wind velocity. So there are good reasons for using the present model to interpret the experimental results obtained in our laboratory equipment. In this equipment the wind velocity was controlled and therefore constant.

Chapter 5

Experimental equipment

5.1 Concept

As discussed in Section 1.2, the study of plume opacity phenomena in the field is quite problematic. This is why within the scope of this thesis an experimental equipment in lab scale was built in order to study plume opacity formation under controllable conditions. In this equipment visible plumes were produced in dependence of well defined variables as there are:

- atmospheric conditions:
 - ambient air temperature T_a
 - ambient air moisture content M_a
 - wind speed V_a
 - UV - light irradiation
- exhaust gas conditions:
 - exhaust gas temperature T_g
 - exhaust gas velocity u_i
 - chemical composition of the exhaust gas
 - * moisture content M_g
 - * oxygen concentration

- * ammonia concentration
- * hydrogen chloride concentration
- * sulfur dioxide concentration
- * nitrogen oxide concentration
- * dust concentration

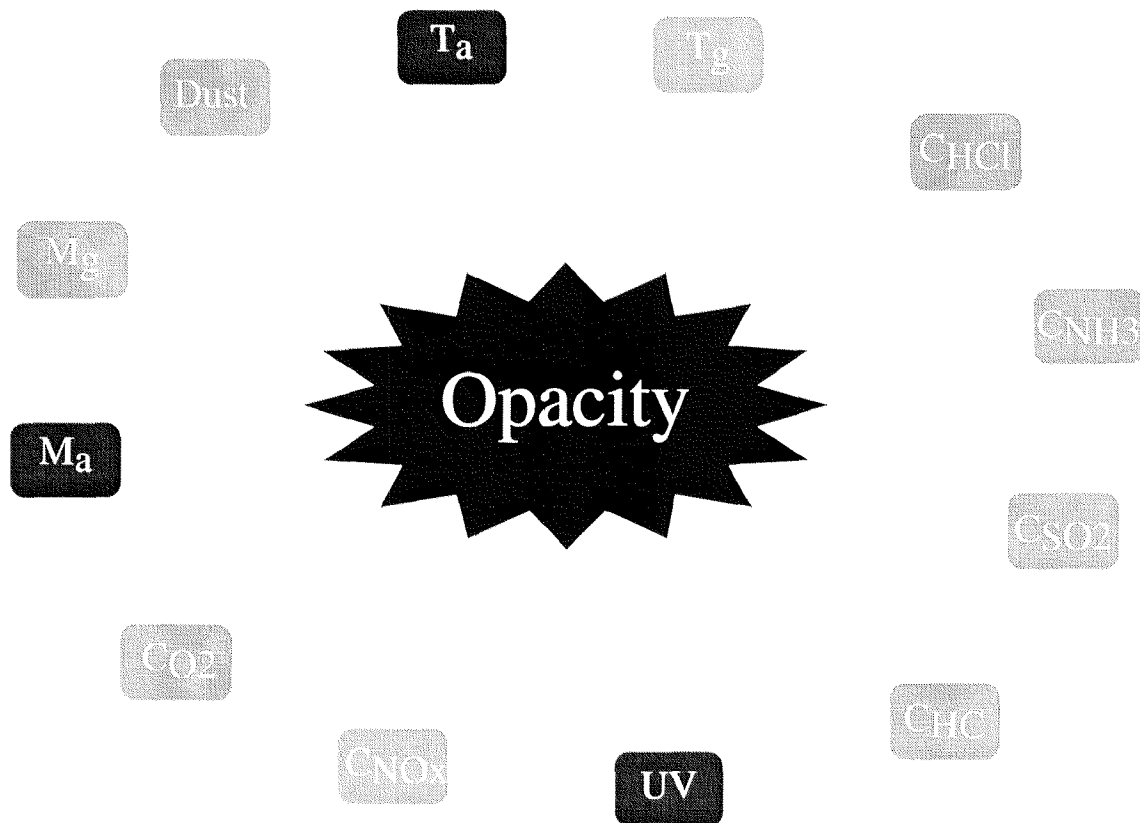


Figure 5.1: Main studied variables within this project

Figure 5.1 shows the main variables that have been considered in the present study. The dark grey variables are dependent on atmospheric conditions and hence can not be influenced in field experiments. The light grey variables are process variables and can be influenced within the range of design specifications of the equipment installed.

5.2 Equipment design

To reproduce the formation of a plume under controlled conditions, exhaust gases have to be led through a stack into a well defined atmo-

sphere. The conditions to be generated in the channel should reproduce the large scale shape and behaviour of the plume. Therefore several dimensions had to be chosen carefully, amongst them:

- the stack diameter b_i
- the exhaust gas velocity u_i
- the wind speed V_a
- the wind tunnel dimensions

The values of the first three quantities were determined by a scale-down using the relevant dimensionless parameters (Briggs, 1965; Fay et al., 1970; Hewett et al., 1971; Hoult et al, 1969). Hoult (1972) stated that it is most convenient to use the two dimensionless parameters \mathcal{R} and Fr for specifying the conditions of geometric similarity.

The first parameter \mathcal{R} is the dimensionless speed ratio \mathcal{R} which is useful in defining the conditions for which the plume will be unaffected by the aerodynamic wake of the stack.

$$\mathcal{R} = \frac{u_i}{V_a} \quad (5.1)$$

The second parameter is the densimetric Froude number Fr defined by

$$Fr = \frac{u_i}{\sqrt{g\Delta_i b_i}} \quad (5.2)$$

where $\Delta_i = \frac{T_i - T_1}{T_1}$ is the dimensionless temperature excess at the stack exit. The inverse of the square of the Froude number gives the ratio of buoyancy to inertia forces at the stack exit and can be expressed by the Richardson number Ri .

$$Ri = \frac{1}{Fr^2} \quad (5.3)$$

The value of the Richardson number Ri should be the same for the real stack and for the one in laboratory. This leads to

$$\frac{Ri_{field}}{Ri_{lab}} = \frac{(u_i)_{lab}^2 (g\Delta_i b_i)_{field}}{(u_i)_{field}^2 (g\Delta_i b_i)_{lab}} \approx 1 \quad (5.4)$$

A third dimensionless parameter that has to be used for the scale-down considerations is the Reynolds number Re which characterises the stack exit conditions.

$$Re = \frac{2u_i b_i}{\nu} \quad (5.5)$$

The Reynolds number Re for the laboratory equipment was chosen in such a way that the gas flow at the stack exit was fully turbulent. In (Hewett et al., 1971) a value of 300 is indicated as a lower limit for the Reynolds number for laboratory simulations of plumes. In our case a Reynolds number of 1500 was chosen.

The stack diameter b_i as well as the gas velocity u_i were determined by solving a system of two equations (5.4 and 5.5) with two unknowns (b_i and u_i). After the calculations of these values, Equation 5.1 was used to calculate the velocity of the air flow inside the wind tunnel.

Unfortunately a proper dimensioning of the wind tunnel according to the scale-down requirements was not possible due to the limited laboratory space at disposal. In addition a preliminary study (theoretical and experimental), required for specifying an inlet geometry, meeting standard aerodynamic design requirements, had to be dropped for lack of time and for financial reasons (Kunsch, 1996). Instead preliminary tests were made in order to determine the height of plume rise after the stack exit.

All the results related to the design as well as the assumptions of the field data needed are summarized in Table 5.1.

Due to technical reasons (large air flow rate that has to be air-conditioned) a wind speed of 0.45 (m/s) could not be guaranteed so that the value of the speed ratio \mathcal{R} in the laboratory (3.1) is slightly higher than in the field (2.4).

Table 5.1: Results of the equipment design by the way of scale-down considerations

parameter	Field data		Laboratory data	
stack diameter $2b_i$	4 (m)	13.12 (ft)	0.034 (m)	1.34 (in)
exhaust gas velocity u	12 (m/s)	26.84 (mi/hr)	1.09 (m/s)	2.44 (mi/hr)
wind speed V_a	5 (m/s)	11.18 (mph)	0.35 (m/s)	0.78 (mi/hr)
exhaust gas temperature T_g	150°C	302°F	150°C	302°F
ambient air temperature T_a	10°C	50°F	10°C	50°F
Reynolds number R_e	1.98·10 ⁶		1500	
speed ratio \mathcal{R}	2.4		3.1	
wind tunnel length			7 (m)	22.96 (ft)
wind tunnel width			1 (m)	3.28 (ft)
wind tunnel height			2 (m)	6.56 (ft)

5.3 Description of the experimental equipment

The experimental equipment consists mainly of two parts: the equipment for synthesizing the exhaust gas (see Figure 5.4) and the wind tunnel (see Figure 5.3). A schematic view of the experimental equipment is shown in Figure 5.2.

5.3.1 Preparation of simulated exhaust gases

The exhaust gases that will be used in the laboratory equipment have to be synthesized. Therefore the following gases will be used 1 :

- Nitrogen 4.5 tech. (≥ 99.995 %), pallet with 12 gas bottles 120 m³, 200 bar (PanGas, Luzern, CH)
- Oxygen techn. (PanGas, Luzern, CH)
- Carbon Dioxide 4.0 (≥ 99.99 %), (PanGas, Luzern, CH)
- Hydrogen Chloride 2.8 (≥ 99.8 %), (Linde, Höllriegelskreuth, D)
- Sulfur Dioxide 3.8 (≥ 99.98 %), (PanGas, Luzern, CH)
- 5 % Nitrogen Dioxide 1.8 (≥ 98 %) in 95% Nitrogen Oxide 2.5 (≥ 99.5 %), (Linde, Höllriegelskreuth, D)

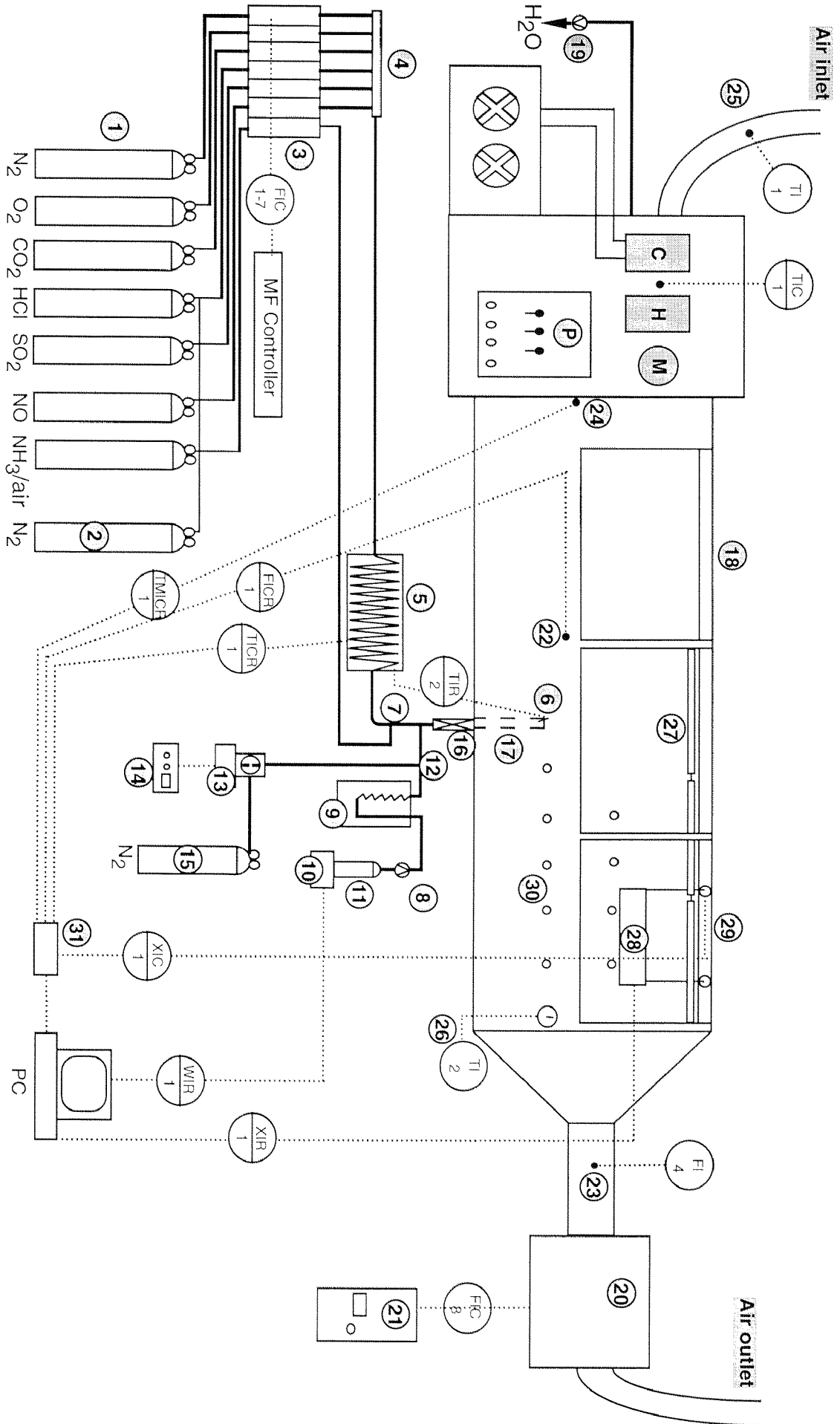


Figure 5.2: View of the equipment for synthesizing the exhaust gas: furnace, steam generator, aerosol generator

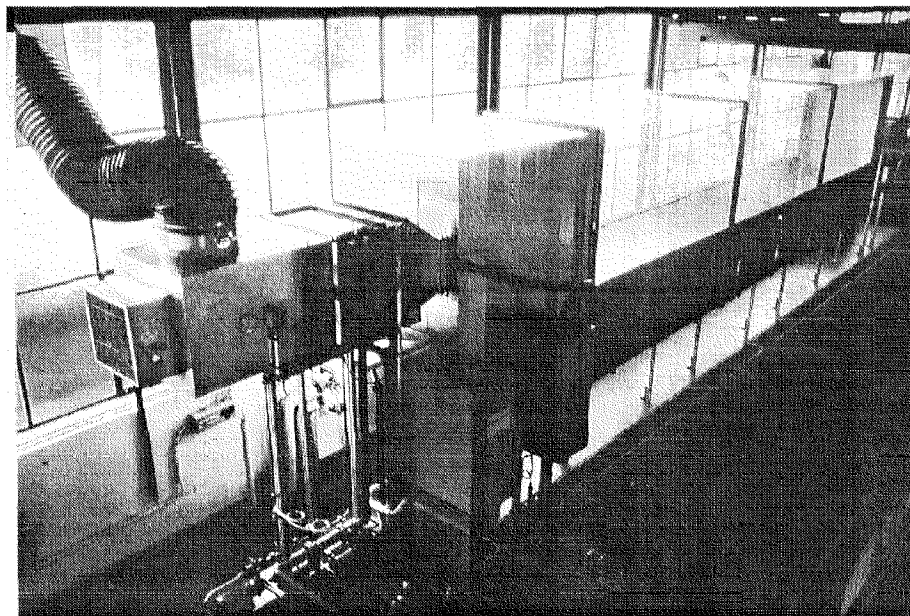


Figure 5.3: View of the air-conditioner and wind tunnel

- 1% Ammonia 3.8 ($\geq 99.8\%$) in Nitrogen 5.0 ($\geq 99.999\%$), (Pan-Gas, Luzern, CH)

An extra gas bottle with nitrogen [2] is used for flushing aggressive gases from the capillary tubes after an experiment has been finished. This should inhibit corrosion problems.

The flow of the different gases is controlled by 7 Mass Flow Controllers (Brooks 5850E) [3] which have already been calibrated for the different gases (see Figure 5.4). This calibration has been carried out by the manufacturer and has been checked in our laboratory. To simulate an exhaust gas, all the gases with the exception of ammonia are mixed [4] and are led through a stainless steel capillary ($\frac{1}{4}$ ") into a furnace [5] (Carbolite CTF 12/65/550). There the gas is heated up to a defined temperature. The furnace temperature is controlled on the basis of the temperature measured at the stack outlet [6]. Only after the gas mixture has been heated up, the ammonia/nitrogen mixture is added ($\frac{1}{8}$ " capillary tube) to the gas stream [7].

As all gases are dry, water has to be added to the exhaust gas stream in order to moisten the gas stream. After addition of ammonia, the gas

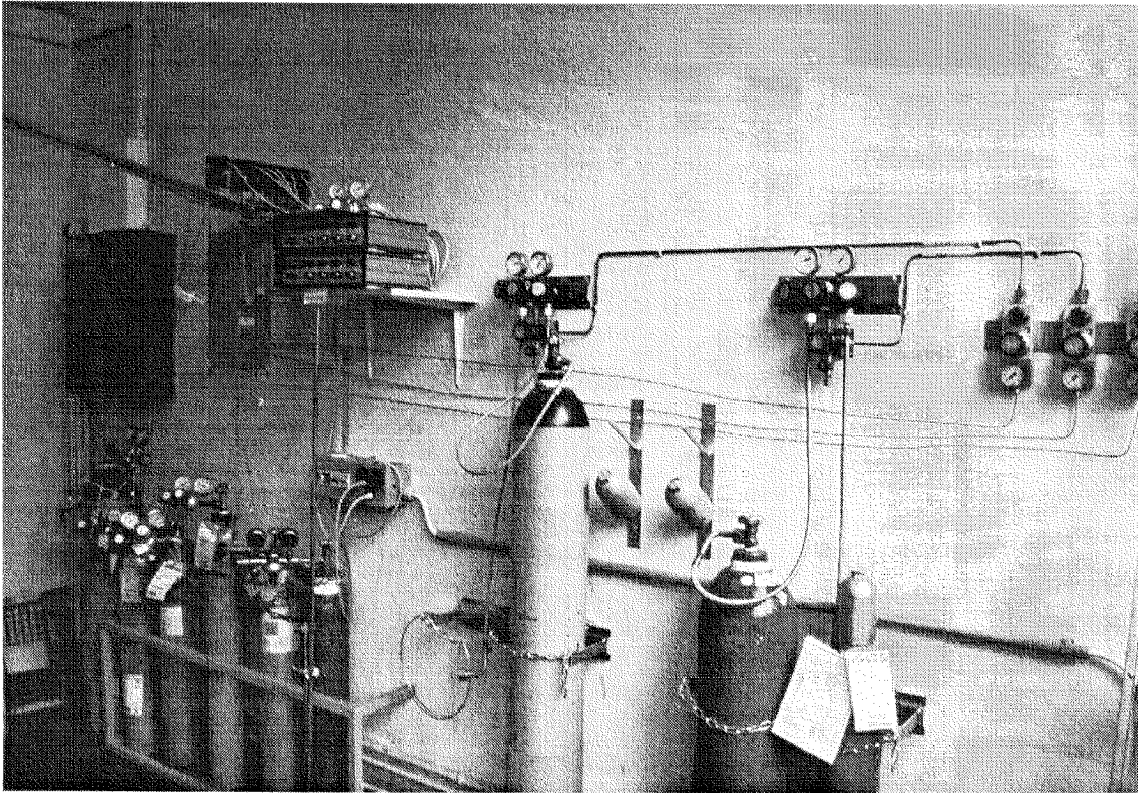


Figure 5.4: Gas bottles with mass flow controllers

moisture is adjusted by pumping bidistilled water [8] (Ismatec MS1-Reglo/8-160) through a stainless steel capillary ($\frac{1}{4}$ ") which is located in a second furnace [9] (Fractovap 2101). The water evaporates completely so that steam (150°C) can be added to the exhaust gas. The amount of water added is indicated by a balance [10] (Mettler PM 4600 Deltarange). The water is stored in a 5 l PE bottle [11]. At the same time dust can be added to the exhaust gas stream [12]. This dust consists of carbon aerosols which have been generated in a plasma cell [13] by applying a high voltage to two graphite electrodes. The voltage can be controlled by a high voltage transformer [14] (Fug HCN 14-12 500). The plasma cell has to be flushed with nitrogen [15] in order to eliminate oxygen on one hand and to serve as carrier gas for the carbon aerosols on the other hand. In fact in presence of oxygen the carbon aerosols would burn and would completely be oxidized to carbon dioxide.

Finally the gas passes a static mixer [16] (Sulzer Mixer DN 25, 3 mixing elements type SMV) before entering the wind tunnel through the stack

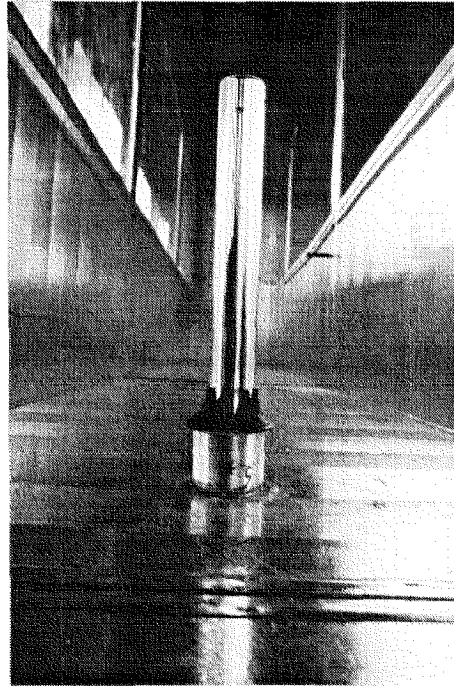


Figure 5.5: Double walled evacuated silvered glass stack

[17]. This stack is a double walled, evacuated, silvered glass tube (inner diameter 3.2 cm, outer diameter 5 cm, length 50 cm, see Figure 5.5). This well insulated stack prevents the exhaust gas from cooling down already inside the stack due to the wind cross-flow. All the capillaries are connected with Swagelok fittings.

5.3.2 Wind tunnel

The dispersion of the exhaust gas can be observed inside the wind tunnel (7 x 2 x 1 m) [18] that is purged with air-conditioned, ambient air simulating the atmosphere. This tunnel is made out of galvanized tin as well as Perspex. In order to avoid reflections during photometric measurements (see below), the tunnel walls have been coated with non-reflective, black paper (see Figure 5.6). Moreover the tunnel is coated with rock wool so that the heat transfer between the tunnel walls and the laboratory environment can be avoided.

The ambient air enters the equipment at the inlet [Air Inlet]. There the air is cooled down by the cooling unit [C]. With the help of this

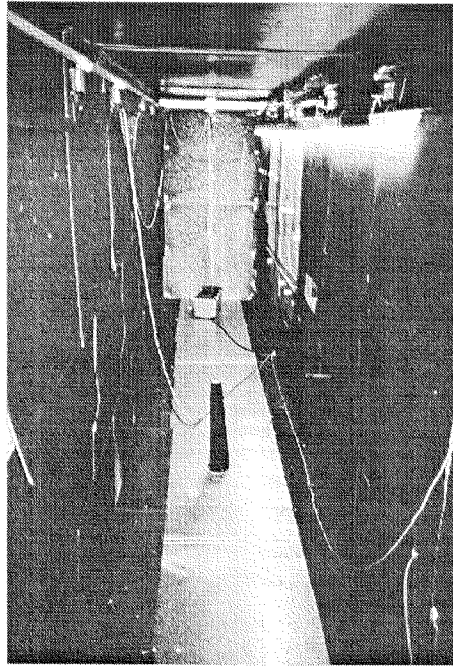


Figure 5.6: Inside view of the wind tunnel with the stack, dispersion photometer and UV - tubes

cooling down of the ambient air, a part of the ambient moisture can be condensed. This condensed water is eliminated with the help of a pump (WATSON MARLOW 601S stricture pump) [19]. Then the temperature of the air is adjusted by the heater (Axair ESCOhotair, 7.37 kW, Switzerland) [H] and passes the moistening unit (Axair Defensor Mk4, 30 kg steam/h [M] in order to adjust the relative humidity of the air. The available temperature range in the tunnel is 8 to 20°C ($\pm 0.5^\circ\text{C}$) and the moisture can be adjusted in a range of 55 to 95 % relative humidity ($\pm 2\%$).

The air-flow inside the tunnel is maintained by an industrial fan [20] (Stäfa, Switzerland, 2520 m³/h) which is located at the end of the tunnel. This fan is controlled by a frequency changer (Danfoss, VLT serie 3000) [21]. The velocity of the air-flow can be varied from 0.2 to 0.5 m/s and is measured by a velocity sensor [22] resp. [23]. The temperature as well as the moisture content inside the tunnel are indicated by a combined humidity/temperature sensor [24]. The temperature of the incoming as well as of the outgoing air are indicated by thermocouples [25] resp. [26]. The power switches for the equipment are located at

position [P].

In order to improve the mixing over the entire tunnel cross-section, four axial fans (Trial VC100A/A/220VAC, 380 m³/h each) were installed at the tunnel inlet right behind the air-conditioner according to Figure 5.7.

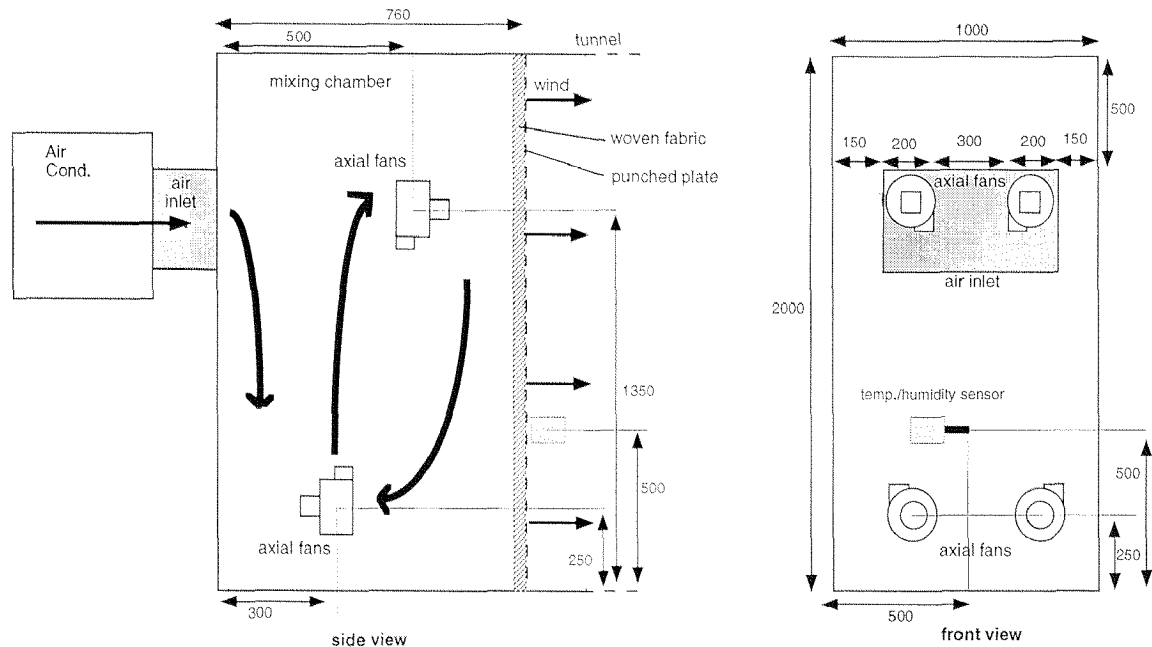


Figure 5.7: Wind tunnel entry in order to improve mixing (dimensions in mm)

These fans are circulating the incoming air from the air-conditioner in order to homogenize the temperature all over the tunnel cross-section. Moreover an additional pressure drop is created 0.76 m after the air inlet with the help of a punched plate that is coated with a woven fabric. By reducing the free cross section surface at this location, the air flow is strongly accelerated. Better homogeneity and uniformization of the flow is obtained by means of the punched plate. The recirculating flow generated is fully turbulent. This turbulence decays very rapidly with increasing distance from the punched plate. An identical punched plate is located at the tunnel end before the outlet cone. The air inside the tunnel is released to the ambient air at the equipment outlet [Air Outlet].

An equipment for irradiating the plume with UV-light was added as

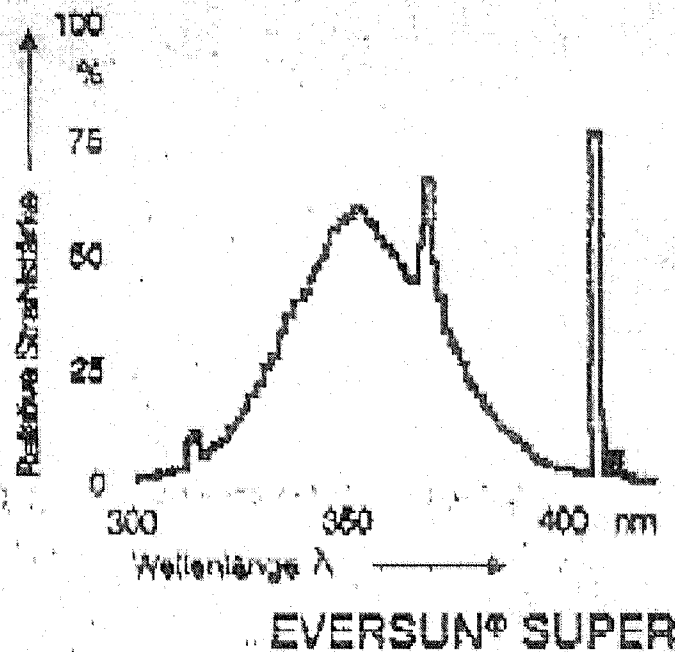


Figure 5.8: Spectrum of the Eversun sunbed tubes: Relative radiation intensity (%) plotted against the wavelength λ (nm)

UV - light can initiate several reactions by forming radicals. Three fluorescent tubes were installed along the tunnel parallel to the tunnel axis under the ceiling [27]. These tubes are sunbed tubes (OSRAM Eversun SUPER UVA L 100W/79). These tubes were chosen because they are easily available and meet important requirements for simulating atmospheric conditions. First the UV - light intensity should be similar to the one present at the earth surface (i.e. 20 W UVA and 0.3 to 1 W UVB). Moreover the light source emits some radiation in the visible range, so that light scattering can also be observed visually. Finally under no circumstances the tubes should emit IR radiation as the dispersion photometer is working with an IR beam. This would cause a malfunction of the photometer. Furthermore, infrared radiation causes a heating up of the environment which causes problems to the air flow profile. The OSRAM sunbed tubes were the most appropriate tubes (0.4 W UVB and 19 W UVA, some visible light radiation at 410 nm, no IR radiation; see Figure 5.8).

5.3.3 Dispersion photometer

The most important information that has to be collected during the experimental phase is the opacity of the plumes in our lab-scale equipment. However it turned out that the foreseen opacitymeter was not sensitive enough for our purpose. Commercially available opacitymeters could not measure opacity with a required accuracy of 0.01 % as they have not been designed or conceived for this purpose.

The idea of an in-house construction and development of a very sensitive opacitymeter was given up very soon for financial reasons and reasons of time. This is why the decision was taken to use a very sensitive dispersion photometer (SICK, RM210) [28] (Sick, 1995).

A scheme of this dispersion photometer can be seen in Figure 5.9. An emitter [1] radiates a modulated infrared beam in an angle $\Theta_1 = 90^\circ$. The infrared light that has been scattered by the particles is registered by a receiver [3] in an angle $\Theta_2 = 60^\circ$. The measured intensity of the scattered light indicates the amount of particles in the air flow. The emitted beam as well as the angle of the receiver define the region [4] where the particle concentration is measured. Reference measurements can be carried out periodically by shifting the emitter and the receiver in the corresponding position, so that the IR beam passes a reference filter [2] (see Figure 5.10).

The problem is that this instrument measures the light scattering on particles and not the opacity or light absorption by particles. The link between the dispersion photometer value and the opacity has been made by a calibration. During special series, two certified opacity readers (Mrs. S. Myers and Mr. J. Epperson, Holnam Inc., USA) read the opacity in the experimental equipment. At the same time photometer values were recorded. These readings made it possible to find a correlation between dispersion and opacity values for our equipment (see Figure 5.11).

In our case the correlation between opacity and dispersion can be expressed by:

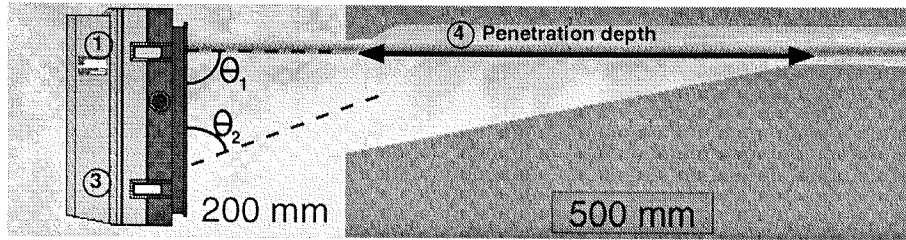


Figure 5.9: Scheme of the dispersion photometer RM210, Sick (1996)

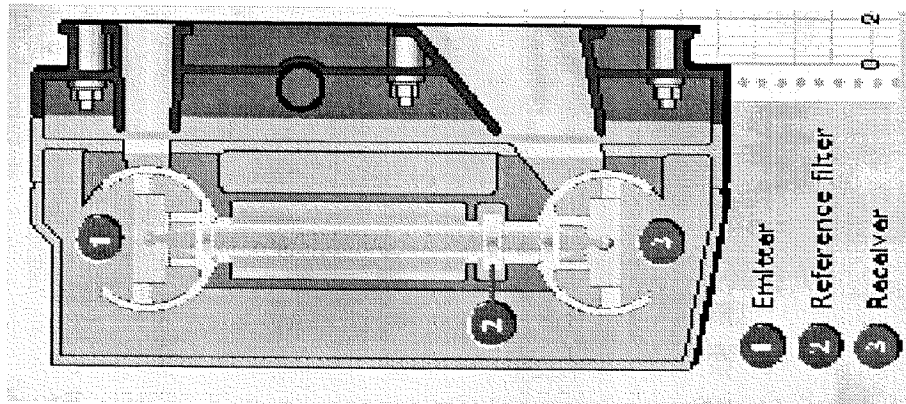


Figure 5.10: Reference measurement of the photometer, Sick (1996)

$$Opacity(\%) = 9.22 \ln(\text{dispersion value}) - 45.67 \quad (5.6)$$

Lou et al (1997) found correlations between plume opacity and sulfate particles from boilers whose curves show the same behaviour and have the same shape as the curves found during the test campaign. The correlation expressed by Equation 5.6 was used to convert light dispersion values into opacity values.

In order to move the photometer along and across the plume in three directions it was attached to a crane [29] (see Figures 5.12 and 5.13). This movement of the photometer is necessary in order to determine plume opacity along the plume and to read the maximum plume opacity (whose location depends on the conditions).

The crane is mounted on rails and is attached to an endless chain. An electric motor (motor 1) can move this chain and hence move the unit along the tunnel. The central unit can traverse the channel by means

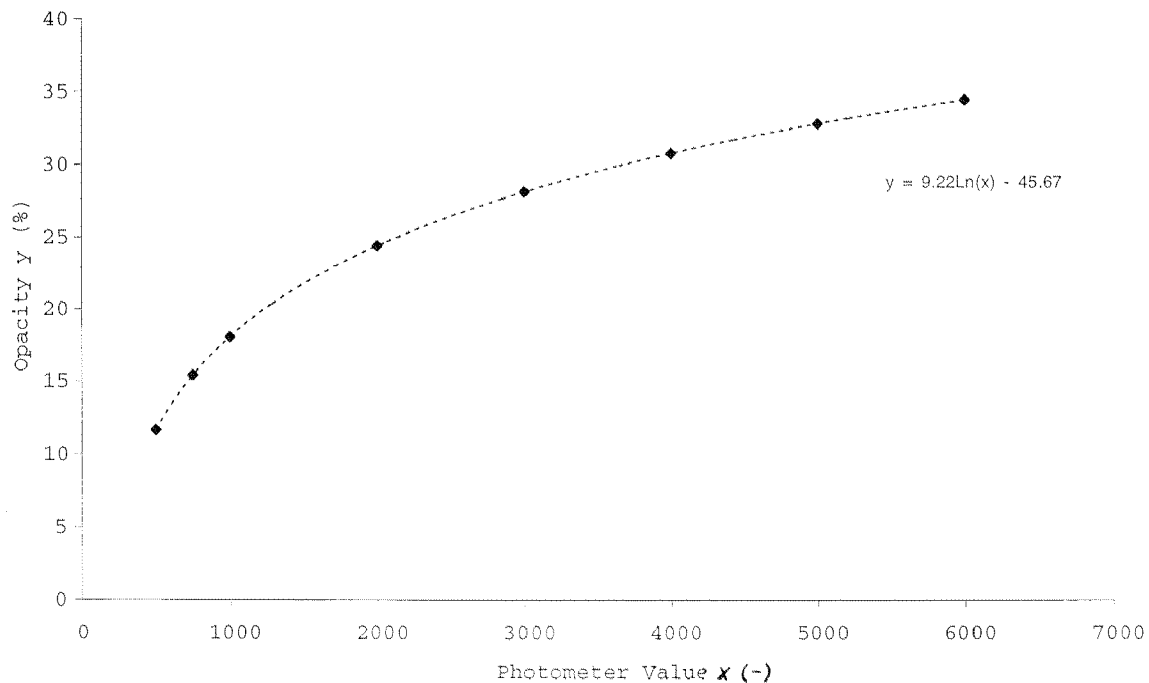


Figure 5.11: Opacities read during one experiment plotted versus the corresponding photometer values

of a second motor. To this central unit is fixed a shaft that can be moved by a third motor and which lifts or lowers two endless chains and hence the attached photometer.

5.3.4 Chemical analysis of aerosol particles

In order to determine the chemical composition of the aerosols formed, gas samples are taken. The sample train can be found in Figure 5.14. This special sample train has been used in order to collect only dry or wet particles (aerosols) with the filter. In fact it must be avoided that reactive gases such as ammonia and sulfuric acid react on the filter surface in order to form ammonium salts. In this case we would find aerosols in the sample which have not been present in the plume and hence overpredict the amount of aerosols formed inside the plume.

The sample is taken with the help of a nozzle which is made out of a Teflon tube (diameter 1 cm). The nozzle is inserted into the tunnel through an opening [30]. A gas sample is aspirated from the plume

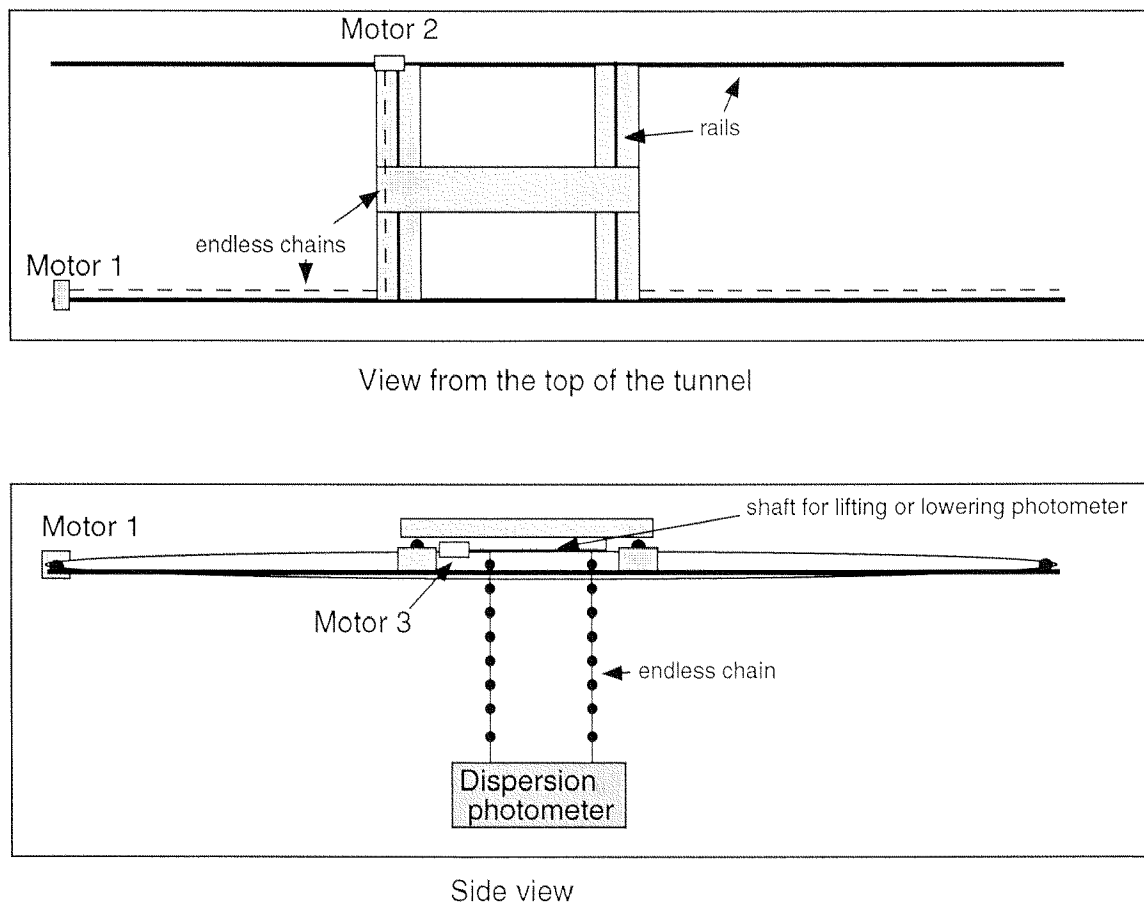


Figure 5.12: Top and side view of the crane for moving the photometer

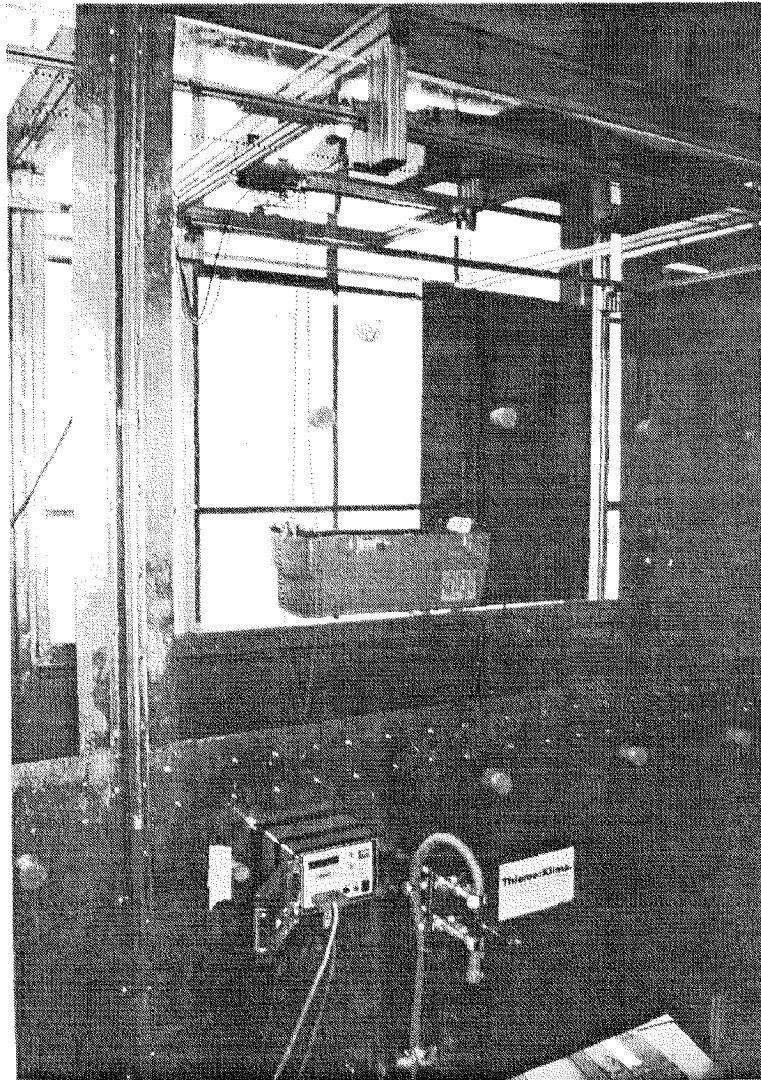


Figure 5.13: Picture of the crane moving the dispersion photometer in three directions

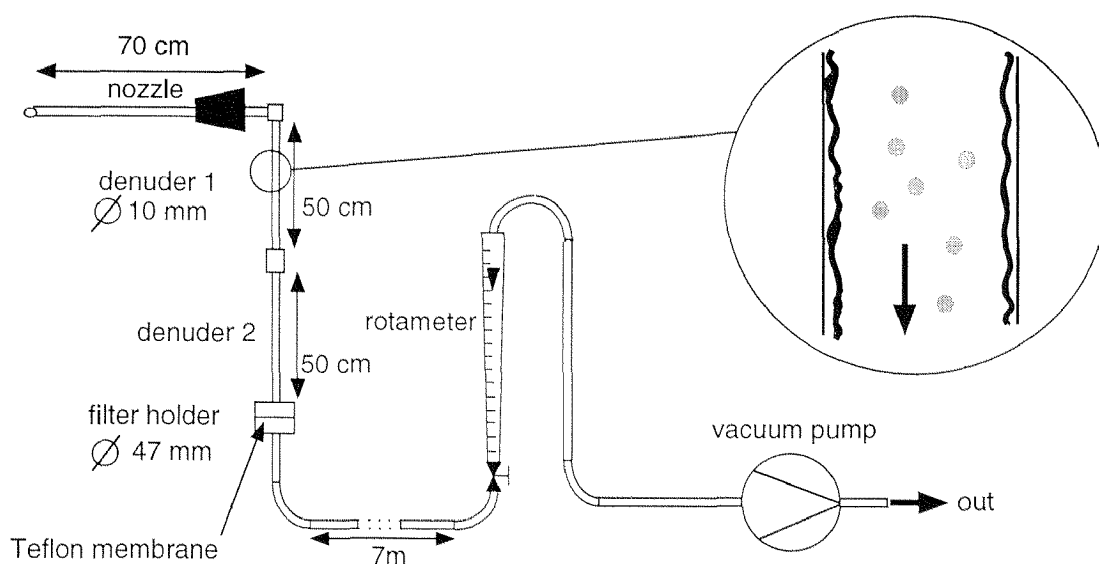


Figure 5.14: Sample train for chemical analysis of the aerosols formed, Oberholzer (1992)

with the help of a vacuum pump (Edwards, BS 2212, two stage) (see Figure 5.14). The gas flow can be determined with the help of a rotameter (MFG CO Ltd. Metric 10P, 0-25 $l_{n,dry}/min$). The exhaust gases as well as the formed aerosols pass two denuders. A denuder is a glass tube whose inner surface has been roughened by the way of a sandblast. The first denuder is coated with a 0.2 M H_3PO_4 solution in absolute Ethanol, the second one with a 0.5 M KOH solution in an ethanol/water (1/1) mixture (Oberholzer, 1992). Afterwards the denuders are dried and are ready for use. With the help of these denuders, active gases like ammonia or hydrogen chloride, which have not reacted so far, are absorbed. This measure is taken in order to avoid the formation of supplementary aerosols on the filter. The particles formed inside the wind tunnel as well as inert gases like nitrogen or carbon dioxide however can pass these denuders. The aerosols are filtered off with the help of a Teflon membrane that is placed in a filter holder.

This Teflon membrane is washed out with 10 ml bidistilled water. Then 100 μl of an internal standard (KI) (4 mM) are added to 900 μl of this solution. This solution is analyzed with ion chromatography (Dionex AS11 column, eluent: 2% NaOH 50mM 98% H_2O bidest.).

5.3.5 Controlling

Different instruments of the equipment are controlled by PC (using LabView) or separately. An example of a LabView program for controlling the movement of the photometer can be found in Appendix C.

Mass Flow Controllers

The flow of the different gaseous compounds is controlled by mass flow controllers. These mass flow controllers incorporate a highly accurate thermal mass flow sensor. A small amount of energy is continuously applied to the process gas. Temperature sensors located upstream and downstream detect the temperature difference which occurs when the gas flows. Based on the specific heat of the process gas the temperature difference is directly proportional to the mass flow rate. A voltage signal is generated as a result of temperature differences. This actual value is compared to the set point and the position of the control valve of the mass flow controller is adjusted accordingly.

Air - conditioning

The temperature of the incoming air, that has formerly been cooled down is measured with a temperature sensor. This actual value is compared to the set point and the control valve of the air conditioner (for dosing the refrigerant) is adjusted accordingly (Ero Electronic 4-digit temperature controller input: 1xPt-100, 1x0-10 VDC; output 0-20 mA). A second temperature sensor detects the temperature inside the wind tunnel. A second controller (Ero Electronic 4-digit temperature controller input: 1xPt-100, 1x0-10 VDC; output 0-20 mA) again compares actual temperature and set point and adjusts the power of the electric heater. The moisture content of the air inside the tunnel is measured and a third controller (Ero Electronic temperature controller SMART, input 0-10 VDC; output 0-20 mA) changes the position of the valve for adding water steam according to the set point.

The voltage signal generated by the temperature and moisture sensor as well as other analogue and digital signals (see below) are collected by a connector block (SCB-68 Shielded connector block for 68-pin MIO boards, National Instruments) [31].

These data are then recorded by a special data acquisition card DAQ card (National Instruments, AT-MIO-16XE-50; 16 SE/8 DI Analog inputs, 2 analog outputs, 8 Digital I/O, 16 bits resolution, 20kS/s sampling rate)

Exhaust gas furnace

The temperature of the exhaust gas furnace is adjusted by a cascade controller. The exhaust gas temperature at the stack exit is compared to the set point. The output signal of this first controller (Eurotherm 2408) then provides the set point of the second controller (Eurotherm 2416) for heating up the furnace (Carbolite, 1997). The output signal of this latter controller is collected by the connector block.

Photometer

The photometer can be operated with the help of a special software (MEPA 210, Sick) (Sick, 1995A). On the other hand photometer values can be recorded by the DAQ card by the way of a RS232 serial communication interface.

Balance

The mass values of the water added to the exhaust gas given by a balance are recorded by the way of a RS232 serial communication interface.

Fan

The fan that generates the air flow inside the tunnel is controlled by a frequency changer (Danfoss, VLT serie 3008) (Danfoss, 1993).

Crane for moving the photometer

The crane for moving the photometer is also controlled by PC. In fact this crane is moved by three electrical motors that can be operated by the way of digital signals (input as well as output signals). A rotation counter determines the position of the motors and hence the position of the dispersion photometer.

5.4 Experimental procedure

For each experiment the following procedure was used:

5.4.1 Starting - up of the equipment

The first step consists in stabilizing the air flow inside the wind tunnel. The fan as well as the air - conditioner are started up and the set point for the temperature of the ambient air are defined. After ca. 30 minutes the set point for the relative humidity of the ambient air is defined and the moistening unit is switched on. The air flow inside the tunnel becomes stable after about two to three hours.

In parallel the exhaust gas furnace is switched on. The set point of the exhaust gas temperature is defined. The capillary tubes are flushed with nitrogen (about 17 l/min). The hot nitrogen flow itself heats up the capillary tubes between the furnace and the stack as well as the mixing element. The actual value is measured at the stack exit. As soon as the actual value is about 110°C, water vapour is added to the exhaust gas. After about 1.5 hours the set points of the furnace and the actual values at the stack exit are identical.

5.4.2 Reference measurements

After the starting - up phase the reference measurements are made. The dispersion photometer is calibrated (once a day before the experiments)

by executing a standard reference cycle using the SICK RM 210 software. With the help of a reference filter, the intensity of the radiation emitted by the light emitting diode is adjusted. After this the dispersion value of the 'reference exhaust gas' (i.e. ambient air with a certain moisture content as well as the hot nitrogen exhaust gas (also with a certain moisture content)) is determined at the sampling point **J** (see Figure 5.15). Data are collected during 60 seconds (30 values) using the LabView program and the mean value is determined. The daily determination of this background 'opacity' is very important as it varies (photometer values ranging from 60 up to 900!) with the ambient air quality (for instance pollen, sulfates, dust concentration etc.).

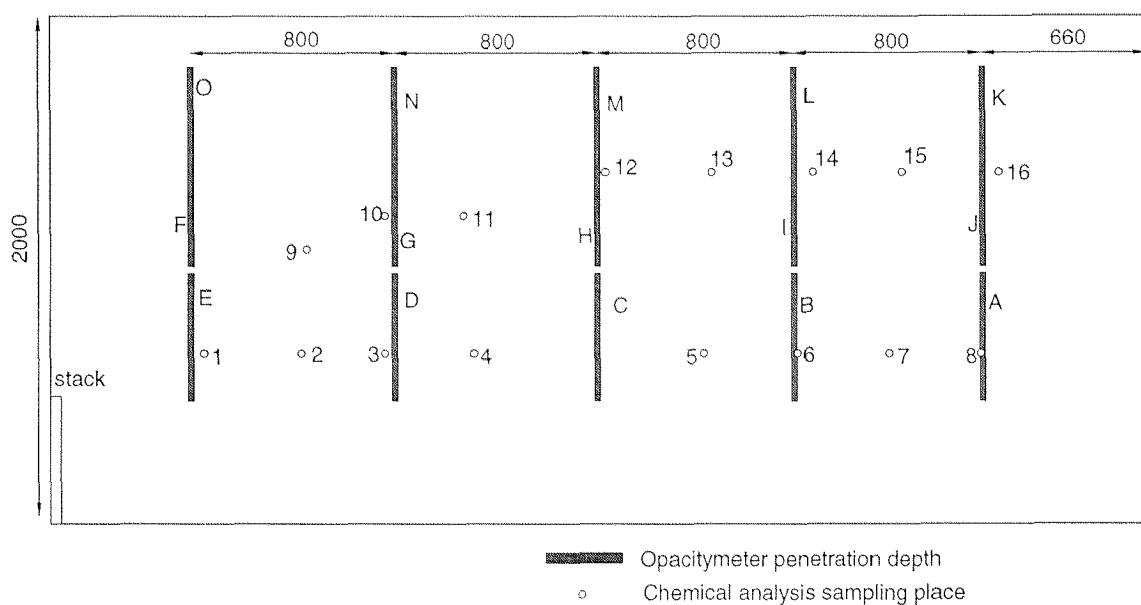


Figure 5.15: Scheme of the sampling locations (photometer as well as chemical analysis) inside the wind tunnel (dimensions in mm)

Afterwards a gas sample (100l/5 min) is taken with the help of a nozzle at location **3** (see Figure 5.15). The Teflon filter is transferred into a vial and 10 ml of bidistilled water are added. This water is used to extract the aerosols from the filter.

5.4.3 Measurements

Only then further gaseous components are added to the exhaust gas stream (according to the different experiments, see below). One has to wait for another 10 minutes until the temperature becomes stable again. After this the dispersion photometer values are collected. The photometer is moved to sampling point **A** and the data are recorded for 60 seconds. Then the photometer is moved to sampling point **B** and so on until sampling point **O** is reached.

The data can be imported into Microsoft Excel for evaluation.

The last step consists in the chemical analysis of the plume aerosols. Samples are taken at sample points **1** to **16**. The filters are washed out with 10 ml of bidistilled water. 100 μl of an internal standard (KI) are added to 900 μl of this solution. This mixture is analyzed with ion chromatography.

5.4.4 Shut - down of the equipment

After the experiment is finished, the furnace as well as the air - conditioner are shut down. All capillary tubes are flushed with nitrogen. The fan should not be shut down immediately as the heating elements of the air - conditioner, which are still very hot, would overheat in absence of fresh air. When the ambient air temperature is close to the setpoint temperature the fan is not shut down at all. This reduces the starting - up time of the equipment for the following experiment considerably.

Chapter 6

Experiments

As discussed in Section 2.2 many parameters can influence plume opacity formation. This is why a choice of variables had to be made in order to reduce the number of variables so that a systematic study of their influences could be made. In our experiments no hydrocarbons were added. The reason for this is that the influence of the inorganic matter on plume opacity has not been studied systematically either. This is why in a first step only these influences were studied as the number of reactions that could possibly occur in presence of inorganic matter is much smaller than in presence of organic matter. The study of the influence of organic matter itself from the point of view of complexity should definitely be studied in a separate project. As very little information was present in the beginning, the choice of not adding hydrocarbons to the exhaust gas is legitimate. However the equipment is designed in such a way that organic matter can be added with ease. With the help of well defined experiments the influence of different variables on plume opacity formation was investigated (see Figure 6.1). For all the experiments the general procedure (see Chapter 5) was used, whereas the details for the experimental series are described below.

At the beginning, the effects of these variables on plume opacity were not known at all (e. g. exhaust gas temperature T_g).

A distinction was made between experiments, where plume opacity formation at night (without UV - light) and during the day (in presence of UV - light) was studied because different reactions are assumed to

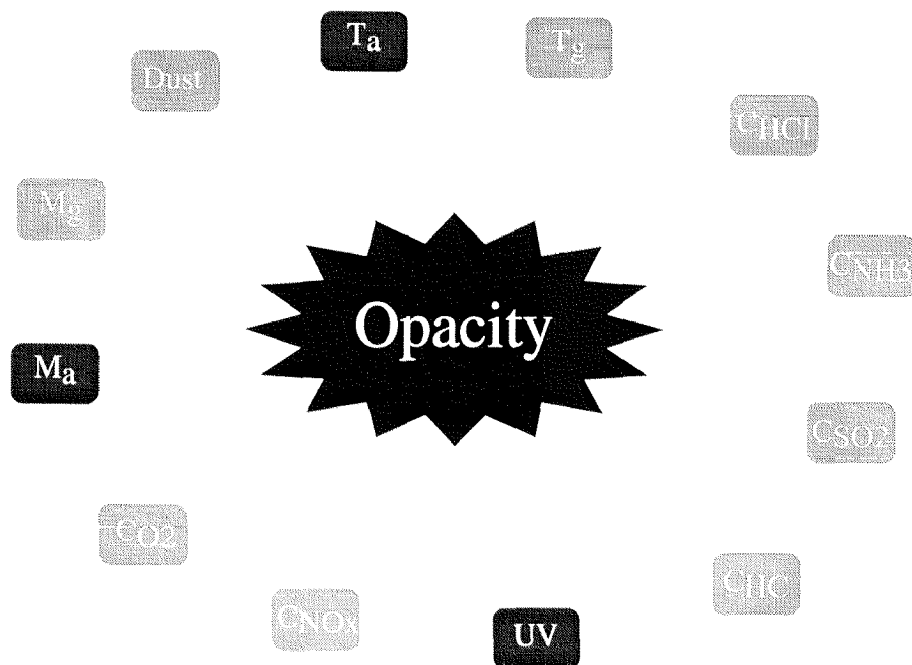


Figure 6.1: Main variables studied within this project

take place in the absence or the presence of sunlight (UV-light). For instance in absence of sunlight the formation of ammonium chloride is still possible whereas in presence of sunlight a photolytic reaction can take place so that ozone (O_3) as well as hydroxy radicals ($\cdot OH$) are produced (Finlayson - Pitts and Pitts jr., 1986). These hydroxy radicals can hydrolyze sulfur dioxide (SO_2) to $HSO_3\cdot$. This $HSO_3\cdot$ can then be oxidized to sulfur trioxide (SO_3) by oxygen (O_2).

As far as the experiments are concerned, two different approaches were possible. The first approach, using the "One-factor-at-a-time" - method, has to be rejected for reasons of effort, quality and time.

Figure 6.2 shows the response surface plot of an example showing the yield of a hypothetical reaction in function of time and temperature. First only the time t is varied while the temperature T is kept constant at $80^\circ C$. The time value is optimized. Afterwards the temperature is varied, the time being kept constant at the optimum. Despite the expense of time, this method normally never leads to the optimum.

In order to find this optimum, a factorial design is much more suitable as is shown in Figure 6.3. This is due to the fact that the plane of factors

(variables) is covered in a better way. Moreover interactions between different factors can be analyzed (in our case interactions between temperature and time). This method leads to a better understanding of the influence of variables on the target variable (in this case yield).

To put it in a nutshell the factorial design shows the following advantages (Grize, 1999; Scheffler, 1997):

- efficiency:
 - only experiments which are needed are carried out
 - all experiments that are needed are carried out
- reliability
 - the variables' plane is covered in an optimal way
 - the study of interactions between variables is possible
- rational procedure
 - systematical procedure
 - good documentation of the results

As far as factorial designs are concerned a further distinction has to be made. A factorial design can be full or fractional. However the number of variables that had to be studied in our case still caused a problem.

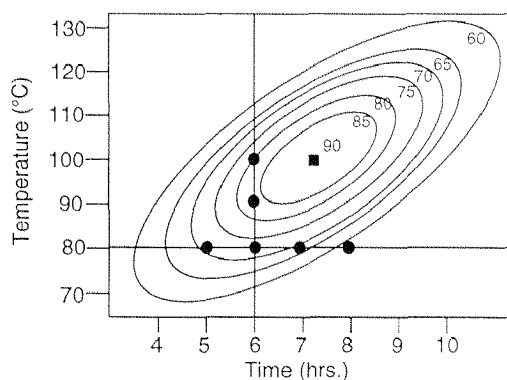


Figure 6.2: Surface plot of the one-factor-at-a-time method

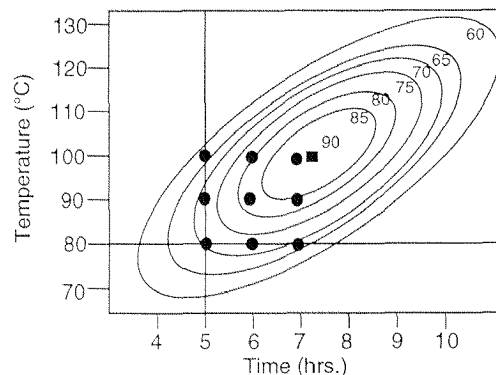


Figure 6.3: Surface plot of the factorial design method

In fact by studying the influence of 9 or 10 variables on plume opacity formation (night resp. day conditions) by using the full fractional design at two levels (every combination of variables is checked, every variable has a maximum and a minimum value), $2^9 = 512$ experiments (resp. $2^{10} = 1024$) should have been carried out. Following the experimental procedure described above only one experiment could be carried out per day. For this reason the full fractional design method approach could not be used within this project as it would have been much too time consuming.

This is why during this first experimental phase a different approach, the fractional factorial design (FFD), was chosen.

6.1 Fractional factorial design at two levels

The idea of the fractional factorial design at two levels is to change more than one variable at a time (Box and Hunter, 1987; Ripplin, 1992; Collombier, 1996; McLean and Anderson, 1984). Each variable are assigned two values: a minimum (-1) and a maximum value (+1). These variables which are used by this fractional factorial design method are actually normalized variables. The relation between the normalized variables and the quantitative variables of the experiments (for instance a temperature T) is given by:

$$x_1 = \frac{T - T_m}{\Delta T}, \quad \text{with } T = T_m \pm \Delta T \quad (6.1)$$

T being the high respectively the low value of a variable (in this example temperature), T_m being the mean value of the high and low value of the variable and ΔT being the difference between the high and low value of the variable.

Moreover this method uses a simple empirical model (it is assumed that this model is linear) which expresses the relation between the normalized variables x_i (in the example above temperature and time), their interactions and the target value y (in our case the yield of the

reaction). In the case of three normalized variables, the linear model has the following form:

$$y = \Theta_0 + \Theta_1 x_1 + \Theta_2 x_2 + \Theta_3 x_3 + \Theta_{12} x_1 x_2 + \Theta_{13} x_1 x_3 + \Theta_{23} x_2 x_3 + \Theta_{123} x_1 x_2 x_3 \quad (6.2)$$

y being the target function, x_i the normalized variables and Θ_i the parameters that have to be determined with the help of experiments.

In our case the fractional factorial design was used to find the variables which have an important influence on the target function (i. e. whose parameters Θ_i are large).

A fractional factorial design is a set of experiments for the same number of normalized variables, which however is only a part of the full factorial design. A 2^{k-p} fractional factorial design consists of 2^{k-p} experiments, which are the $2^{p^{th}}$ part of a full 2^k factorial design. In a 2^{k-p} fractional factorial design the influence of k normalized variables is studied while $k-p$ is the number of main normalized variables and p is the number of the rest of the variables which are interactions between main variables. One condition however that has to be respected in all these designs is that the number of variables studied is always smaller than the number of experiments carried out, i. e. $k < 2^{k-p}$.

A typical 2^{3-1} fractional factorial design (the influence of 3 variables is studied in 4 experiments, using 2 main variables and one variable defined by the way of an interaction) can be written in the following form (see Table 6.1):

Table 6.1: 2^{3-1} Fractional Factorial Design

exp.#	design matrix			regression matrix								results
	x_1	x_2	$x_3=x_1x_2$	x_0	x_1	x_2	x_3	x_1x_2	x_1x_3	x_2x_3	$x_1x_2x_3$	y
1	-	-	+	+	-	-	+	+	-	-	+	y_1
2	+	-	-	+	+	-	-	-	-	+	+	y_2
3	-	+	-	+	-	+	-	-	+	-	+	y_3
4	+	+	+	+	+	+	+	+	+	+	+	y_4

Once these matrices have been created, the design matrix will be used for the realization of the experiments. The design matrix in Table 6.1 shows for instance that in the second experiment the first normalized variable x_1 should be allocated the maximum value whereas variables x_2 and x_3 should be allocated their minimum values.

These experiments are carried out and the response values y_i of the target function will be noted in the last column of the matrices (see Table 6.1).

The regression matrix as well as the result column will then be used for the data evaluation (i.e. the determination of the values for the different parameters Θ_i) (see Equation 6.2).

The values of the different empirical parameters Θ_i can be determined by multiplying the column of the corresponding variable x_i of the design or the regression matrix with the results column and by dividing the result by the number of experiments. In case of parameter Θ_1 we will have:

$$\Theta_1 = \frac{1}{4}(-y_1 + y_2 - y_3 + y_4) \quad (6.3)$$

The parameter Θ_0 represents the mean value for an empirical value. However as can be seen from the regression matrix of Table 6.1, some columns are identical as there are:

$$x_1 = x_2x_3 \quad (6.4)$$

$$x_2 = x_1x_3 \quad (6.5)$$

$$x_3 = x_1x_2 \quad (6.6)$$

$$x_0 = x_1x_2x_3 \quad (6.7)$$

This means that the influence of the different columns of the normalized variables can not be determined separately which is a disadvantage of this method. These interactions are actually taken into account in the values of the different Θ_i (1 interaction had to be considered in addition to the two main variables!). For instance the influence of x_1

on the target function was not studied separately but the influence of x_1 and x_2 x_3 was investigated at the same time.

According to what has been said, Equation 6.3 for example should be written in a more correct way:

$$\Theta_1 + \Theta_{23} = \frac{1}{4}(-y_1 + y_2 - y_3 + y_4) \quad (6.8)$$

The same is true for the three other equations.

After determination of the different Θ_i 's the important variables (or the important combination of different variables) can be found. In fact all those variables x_i (or combinations) have an important influence on the response function y whose corresponding parameters Θ_i have a large value. This is expressed by a large absolute value of these Θ_i 's.

A large positive value of Θ_i means that its corresponding variable x_i has a large proportional effect on y whereas a negative value of Θ_i corresponds to a inversely proportional effect of x_i on y .

6.2 Night experiments

6.2.1 Experimental conditions

To start with, the night conditions (no UV-light) were chosen since the number of possible reactions that could take place inside the plume is much smaller than for simulations taking place in presence of UV-light. As the number of variables that had to be studied was still quite large (9 variables) a fractional design (cf. above) was made.

The variables that were studied with the help of this 2^{9-5} fractional factorial design are: temperature of the air T_a , moisture of the air M_a , temperature of the exhaust gas T_g , moisture content of the exhaust gas M_g , concentration of ammonia C_{NH_3} , concentration of sulfur dioxide C_{SO_2} , concentration of hydrogen chloride C_{HCl} , concentration of nitrogen oxides C_{NO_x} and concentration of oxygen C_{O_2} . This design was chosen as the influence of 9 variables can be studied in 16

experiments which is reasonable within this project.

Their maximum as well as their minimum values can be found in Table 6.2. The symbol '-' stands for the minimum value of the normalized variable, '+' for the maximum one.

Table 6.2: Main normalized variables for the night plume experiment

x_i	variable	'-' value	'+' value
x_1	T_a [$^{\circ}\text{C}$]	9	18
x_2	M_a [%]	60	85
x_3	T_g [$^{\circ}\text{C}$]	150	200
x_4	M_g [g/m^3]	100	180
x_5	C_{NH_3} [mg/m^3]	0	75
x_6	C_{SO_2} [mg/m^3]	0	2500
x_7	C_{HCl} [mg/m^3]	0	60
x_8	C_{NO_x} [mg/m^3]	0	50
x_9	C_{O_2} [%]	0	10

The model according to the method described above (see Equation 6.2 can be simplified in our case (only interactions of the second order are considered):

$$y = b_0 + b_1x_1 + b_2x_2 + \dots + b_9x_9 \quad (6.9)$$

with

$$b_0 = \Theta_0 \quad (6.10)$$

$$b_1 = \Theta_1 + \Theta_{25} + \Theta_{36} + \Theta_{47} \quad (6.11)$$

$$b_2 = \Theta_2 + \Theta_{15} + \Theta_{38} + \Theta_{49} \quad (6.12)$$

$$b_3 = \Theta_3 + \Theta_{16} + \Theta_{28} \quad (6.13)$$

$$b_4 = \Theta_4 + \Theta_{17} + \Theta_{29} \quad (6.14)$$

$$b_5 = \Theta_5 + \Theta_{12} + \Theta_{68} + \Theta_{79} \quad (6.15)$$

$$b_6 = \Theta_6 + \Theta_{13} + \Theta_{58} \quad (6.16)$$

$$b_7 = \Theta_7 + \Theta_{14} + \Theta_{59} \quad (6.17)$$

$$b_8 = \Theta_8 + \Theta_{23} + \Theta_{56} \quad (6.18)$$

$$b_9 = \Theta_9 + \Theta_{24} + \Theta_{57} \quad (6.19)$$

The regression matrix of this 2^{9-5} design can be found in Table 6.3. The values of the different variables during the experiments were set according to this matrix. In experiment 8 for instance the value "+" for x_3 stands for an exhaust gas temperature of 200°C, the value "-" for x_9 for an oxygen concentration of 0 %. The y_i represent the response of the different experiments (in our case the photometer value, i. e. the amount of light that has been scattered by aerosols inside the wind tunnel).

In order to avoid trends during the same type of experiments (for instance in experiments 1 to 8, x_4 has the same value), the experiments were carried out in a random order: 15, 6, 10, 12, 4, 14, 3, 7, 2, 8, 11, 10, 5, 9, 1, 9, 13. Experiment 9 was made twice in order to check the reproducibility of the experiments.

Table 6.3: 2^{9-5} Fractional Factorial Design of the night experiments

exp.#	x_0	x_1	x_2	x_3	x_4	x_5	x_6	x_7	x_8	x_9	y
						$=x_1x_2$	$=x_1x_3$	$=x_1x_4$	$=x_2x_3$	$=x_2x_4$	
1	+	-	-	-	-	+	+	+	+	+	y_1
2	+	+	-	-	-	-	-	-	+	+	y_2
3	+	-	+	-	-	-	+	+	-	-	y_3
4	+	+	+	-	-	+	-	-	-	-	y_4
5	+	-	-	+	-	+	-	+	-	+	y_5
6	+	+	-	+	-	-	+	-	-	+	y_6
7	+	-	+	+	-	-	-	+	+	-	y_7
8	+	+	+	+	-	+	+	-	+	-	y_8
9	+	-	-	-	+	+	+	-	+	-	y_9
10	+	+	-	-	+	-	-	+	+	-	y_{10}
11	+	-	+	-	+	-	+	-	-	+	y_{11}
12	+	+	+	-	+	+	-	+	-	+	y_{12}
13	+	-	-	+	+	+	-	-	-	-	y_{13}
14	+	+	-	+	+	-	+	+	-	-	y_{14}
15	+	-	+	+	+	-	-	-	+	+	y_{15}
16	+	+	+	+	+	+	+	+	+	+	y_{16}

6.2.2 Results of the night experiments

The d experiments were carried out according to the procedure described above. The results (the photometer values) are listed in Table 6.4.

The values in brackets have not been considered for the following calculations. In fact these values are much too high (probably due to some reflection inside the wind tunnel). In Table 6.4 the first column represents the number of the experiment. The second column indicates the photometer values of the reference measurements (measurement of the dispersed light in presence of only wet nitrogen exhaust gas). Columns 3 to 17 represent the corrected values collected at the different sample locations [A] to [O] (see Figure 5.15). These corrected values are not the actual photometer values at this sampling point but only the additional light scattering value due to additional aerosol formation. In other terms:

$$\text{corrected value}_{[i]} = \text{actual photometer value}_{[i]} - \text{reference value}_{[i]}$$

[i] stands for the sampling point ([A] to [O]), the reference value is the photometer value of a plume that only consists of water steam and nitrogen).

Finally the last column represents the mean value of the sample points [A] to [O] for each experiment (i. e. a mean dispersion value over the entire plume).

The next step consisted in the calculation of the different b_i 's in order to determine the influence of each variable (respectively their combinations (see Table 6.5)). The different b_i 's can be calculated by multiplying the corresponding column of the regression matrix by the results column (see above). However in our case, the photometer values were collected at different locations. This involves that we do not only have one column with results but 16 columns (see Table 6.4). This is why different values for b_i could be calculated (see Table 6.5):

- *max*: the parameters b_i have been calculated for the maximum

6.2. NIGHT EXPERIMENTS

Table 6.4: Night plume experiments results

exp.#	ref.	A	B	C	D	E	F	G	H	I	J	K	L	M	N	O	\bar{y}
1	163	28	106	114	150	210	602	559	557	574	516	(1223)	485	483	485	475	381
2	651	3	13	29	2	2	20	4	30	77	79	9	71	79	68	63	36
3	151	5	11	26	42	18	87	165	33	294	390	6	141	50	26	86	92
4	67	10	17	22	46	12	39	57	4	188	181	0	102	111	112	102	67
5	133	47	64	87	224	341	601	505	581	561	464	(983)	414	395	342	402	359
6	693	46	210	388	184	75	95	95	91	95	95	23	20	29	131	78	110
7	79	3	2	9	7	6	80	132	17	114	214	0	27	30	37	15	46
8	601	76	6	10	30	0	100	89	2	103	176	13	79	72	84	78	61
9a	268	25	113	77	137	0	558	558	528	512	386	(1320)	420	415	411	427	326
9b	146	47	69	73	290	(6112)	521	(3104)	479	513	389	(1106)	385	386	390	386	320
10	592	17	37	38	136	105	48	79	6	186	201	115	211	142	162	109	106
11	599	11	46	205	620	471	25	20	102	36	0	14	150	150	119	47	134
12	169	0	34	98	36	0	350	369	323	397	542	303	404	398	386	387	287
13	130	65	121	85	211	355	44	37	18	38	92	(1386)	122	133	132	126	112
14	615	2	12	18	30	1	163	86	1	264	373	1	96	187	205	97	102
15	63	445	463	467	447	406	157	432	495	247	270	0	0	0	0	0	255
16	960	0	0	0	781	806	906	1222	160	0	610	3	154	716	204	244	387

Table 6.5: Fractional factorial design coefficients for the night plume simulation according to three different methods: mean values of y_i , maximum values of y_i and the values of y_i of each sampling location

coeff.	Max(y_i)	Mean(y_i)	A	B	C	D	E	F
b_0	442.50	178.81	48.93	78.43	104.56	192.68	175.50	242.18
b_1	-84.62	-34.31	-29.68	-37.31	-29.18	-37.06	-50.37	-27.06
b_2	-1.12	-12.68	19.81	-6.06	0.06	58.43	39.37	-24.18
b_3	43.75	0.18	36.36	31.31	28.43	46.56	73.25	26.06
b_4	65.00	34.81	21.68	24.81	18.93	107.06	92.50	39.18
b_5	96.25	68.68	-17.56	-20.81	-42.00	9.18	40.00	157.81
b_6	59.12	20.31	-24.81	-15.43	0.18	54.06	22.12	74.81
b_7	85.12	41.18	-36.18	-45.18	-55.81	-16.93	10.37	112.43
b_8	-37.37	20.93	25.68	14.06	-11.56	18.56	16.37	66.68
b_9	134.37	64.81	23.56	38.56	68.93	112.81	113.37	102.31
G	H	I	J	K	L	M	N	O
275.56	184.25	230.37	286.81	337.43	181.00	211.87	181.50	171.00
-25.43	-107.12	-66.62	-4.68	-279.06	-38.87	4.87	-12.50	-26.25
35.18	-42.25	-58.00	11.06	-295.06	-48.87	-21.00	-60.50	-51.12
49.18	-13.63	-52.62	-0.06	-36.31	-67.00	-16.62	-39.62	-41.00
74.81	19.87	-20.37	22.43	55.31	13.62	55.75	20.87	8.62
148.93	87.37	66.25	84.06	316.43	91.50	128.50	88.00	109.12
73.68	0	4.37	31.43	-12.66	12.12	50.87	26.62	20.50
114.06	25.50	68.37	126.93	-8.18	60.50	88.25	49.37	55.87
108.81	40.12	-3.75	19.68	-2.06	-0.12	30.25	-0.12	5.37
125.18	108.12	18.00	35.18	-17.68	31.25	69.37	35.37	41.00

$$\begin{aligned}
 b_0 &= \Theta_0 \\
 b_1 &= \Theta_1 + \Theta_{25} + \Theta_{36} + \Theta_{47} \\
 b_2 &= \Theta_2 + \Theta_{15} + \Theta_{38} + \Theta_{49} \\
 b_3 &= \Theta_3 + \Theta_{16} + \Theta_{28} \\
 b_4 &= \Theta_4 + \Theta_{17} + \Theta_{29} \\
 b_5 &= \Theta_5 + \Theta_{12} + \Theta_{68} + \Theta_{79} \\
 b_6 &= \Theta_6 + \Theta_{13} + \Theta_{58} \\
 b_7 &= \Theta_7 + \Theta_{14} + \Theta_{59} \\
 b_8 &= \Theta_8 + \Theta_{23} + \Theta_{56} \\
 b_9 &= \Theta_9 + \Theta_{24} + \Theta_{57}
 \end{aligned}$$

x_i	variable	-1	+1
x_1	T_a [°C]	9	18
x_2	M_a [%]	60	85
x_3	T_g [°C]	150	200
x_4	M_g [g/m ³]	100	180
x_5	C_{NH_3} [mg/m ³]	0	75
x_6	C_{SO_2} [mg/m ³]	0	2500
x_7	C_{HCl} [mg/m ³]	0	60
x_8	C_{NO_x} [mg/m ³]	0	50
x_9	C_{O_2} [%]	0	10

photometer values of each experiment (only one maximum photometer value per experiment). This has been done by forming a new column with the maximum values of each line of the columns [A] to [O] (of Table 6.4). This column was multiplied with the corresponding column x_i of the regression matrix (see Table 6.3) in order to obtain the value of the corresponding b_i . This procedure could be compared to the one of EPA Method 9, where only the maximum opacity in a plume has to be read.

- *mean*: In this case the result column is composed of the mean photometer values \bar{y} (see Table 6.4) of one experiment (corresponds to the mean opacity of a plume).
- *different sample locations*: Each column of each sampling location is multiplied by the corresponding regression matrix column. This corresponds to an evaluation of the photometer values for each sampling location.

A small Matlab program was written to make these simple calculations described above. The results of these calculations can be found in Table 6.5.

As far as the importance of the different variables is concerned, Table 6.5 shows that the evaluation of the maximum photometer values leads to the same results (same trends) as the one for the mean values. For the different sample point data, some small deviations can occur, however the trend is the same as for the mean or maximum value. The small deviations can be explained by the fact, that according to the location of the plume, some variables are more or less important. For instance in the neighbourhood of the stack ([E]), the influences of b_3 as well as of b_4 (the gas exhaust variables and interactions) are very important, whereas at the tunnel exit ([J]) b_7 and b_5 (ammonia and hydrogen chloride as well as the different interactions) become important. This is why the evaluation of the data for a defined sample point can lead to erroneous general conclusions and should therefore not be done. Instead the mean respectively the maximum values, which moreover are most in compliance with EPA Method 9, should be used.

The higher the absolute value of $|b_i|$ the more important the influence of the corresponding variable. A positive value of b_i indicates that the answer y_i of an experiment is proportional to the corresponding variable x_i whereas a negative value of b_i indicates a negative correlation between y_i and x_i . However it has to be noted that a high absolute value of for example $|b_7|$ does not mean that the variable x_7 alone (in our case the HCl concentration) has a big influence on the photometer value but the sum of the variable x_7 and the interactions between variables x_1 and x_4 as well as x_5 and x_9 (see equations 2 to 12). In order to check which relation is most important, more experiments have to be made.

A first look at Table 6.5 shows that b_1 , b_5 , b_7 as well as b_9 seem to influence the photometer value mostly. This is why these values should be discussed in detail:

- The parameter b_0 simply indicates a mean value of the dispersion photometer value of all the experiments. In fact it is obtained by multiplication of the column containing only '+1' values with the result column. This involves that the mean maximum increase of the photometer (for the maximum values) signal due to aerosol formation for the sixteen experiments was 442.50. The average increase of the mean values (mean value of the average values over the plume for all the experiments) of the photometer signal was 178.8.
- The coefficient b_1 has a negative value. This means that the higher the value of the variable, the lower the photometer value (and vice versa). In addition to the ambient temperature (x_1) also the interactions between the ambient air humidity / ammonia concentration (x_2x_5), exhaust gas temperature / sulfur dioxide concentration (x_3x_6) as well as the exhaust gas humidity / hydrogen chloride concentration (x_4x_7) are taken into account. The influence of the ambient temperature (negative value!) seems to be even more important when considering that the negative value of b_1 is the sum of the ammonia and hydrogen chloride influence (positive value)

and the negative value of the temperature.

- The high value for b_5 indicates a large influence of the ammonia concentration (x_5) as well as the ambient air temperature / humidity (x_1x_2), sulfur dioxide conc. / NO_x conc. (x_6x_8) as well as hydrogen chloride conc. / oxygen conc. (x_7x_9).
- b_7 : the hydrogen chloride concentration (x_7) as well as the ambient air temperature / exhaust gas moisture (x_1x_4) and the ammonia conc. / oxygen conc. (x_5x_9) interactions.
- b_9 : the oxygen concentration (x_9) as well as the ambient air humidity / exhaust gas humidity (x_2x_4) and the ammonia conc. / hydrogen chloride conc. (x_5x_7).

Analyzing the results above, it seems that mainly the ambient temperature, the ammonia concentration, the hydrogen chloride concentration and all their interactions seem to influence the formation of aerosols during the night. The nitrogen oxide concentration seems to play only a minor role in this set of experiments. The influence of sulfur dioxide can not be proven by this fractional factorial design as the formation of sulfates inside the tunnel is masked by the presence of sulfates in the ambient air (as shown below). The values of b_6 and b_8 can be explained by the fact that mostly the ambient temperature (x_1x_3) as well as the ammonia concentration (x_5x_8) respectively (x_5x_6) contribute mostly to the values of b_6 and b_8 .

This involves that mainly ammonium chloride is formed during the night. However more experiments are needed to prove this.

6.2.3 Chemical analysis

The hypotheses about the chemical reactions taking place (see previous section) and hence the hypotheses about the chemical composition of the aerosols have been checked with the help of a qualitative chemical analysis. The analysis was only semi-quantitative, i. e. only the different anions were identified as well as their relative concentrations (ion

chromatography peak area of a component in relation to the peak area of a fixed amount of inner standard (KI) added to a sample). With this procedure it was possible to check whether chlorides or sulfates were formed during an experiment or not. Moreover it was possible to see if more or less chlorides were formed in different experiments. In fact at this stage, a quantitative analysis was not intended because these first series only consisted of screening experiments. A quantitative chemical analysis was carried out in the different series where the influences of different variables on plume opacity were studied individually (see Section 6.5 ff.).

The qualitative chemical analysis for the night plume experiments confirmed the formation of ammonium chloride. No sulfates were formed inside the wind tunnel. The sulfates found by ion chromatography were already present in the ambient air. Moreover the amount of sulfates was very small and varied very much during one experiment.

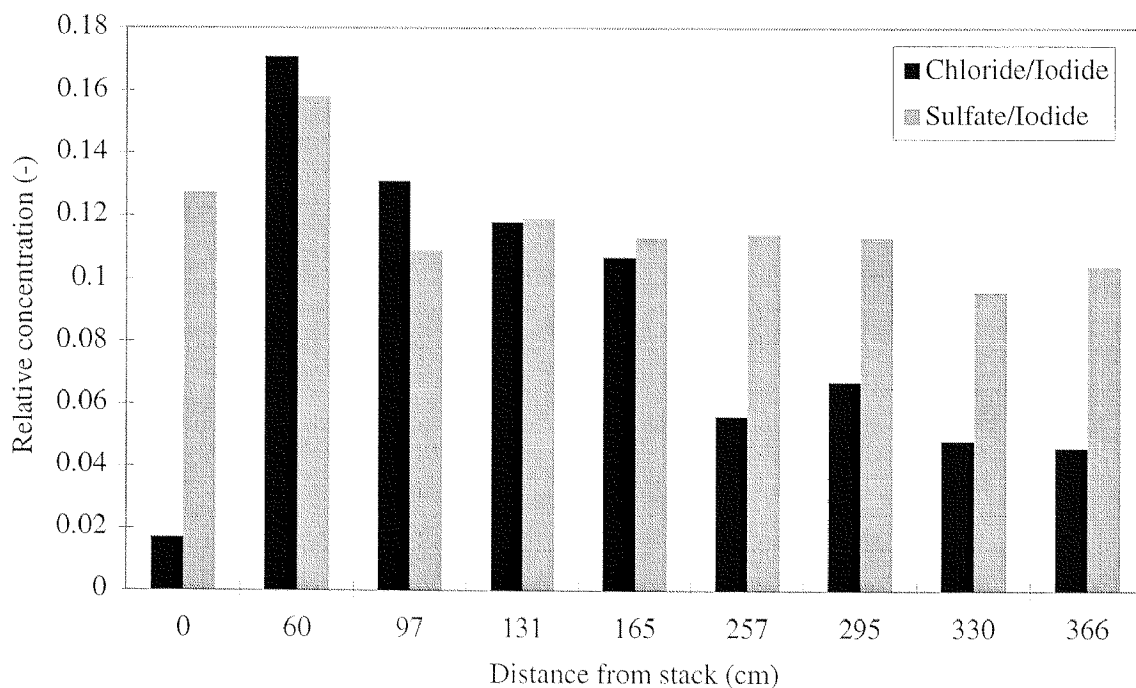


Figure 6.4: Relative chloride and sulfate concentrations along the wind tunnel at stack height

In Figure 6.4 it can be seen that at stack height the ammonium chloride concentration decreases in the downwind direction. The concentration

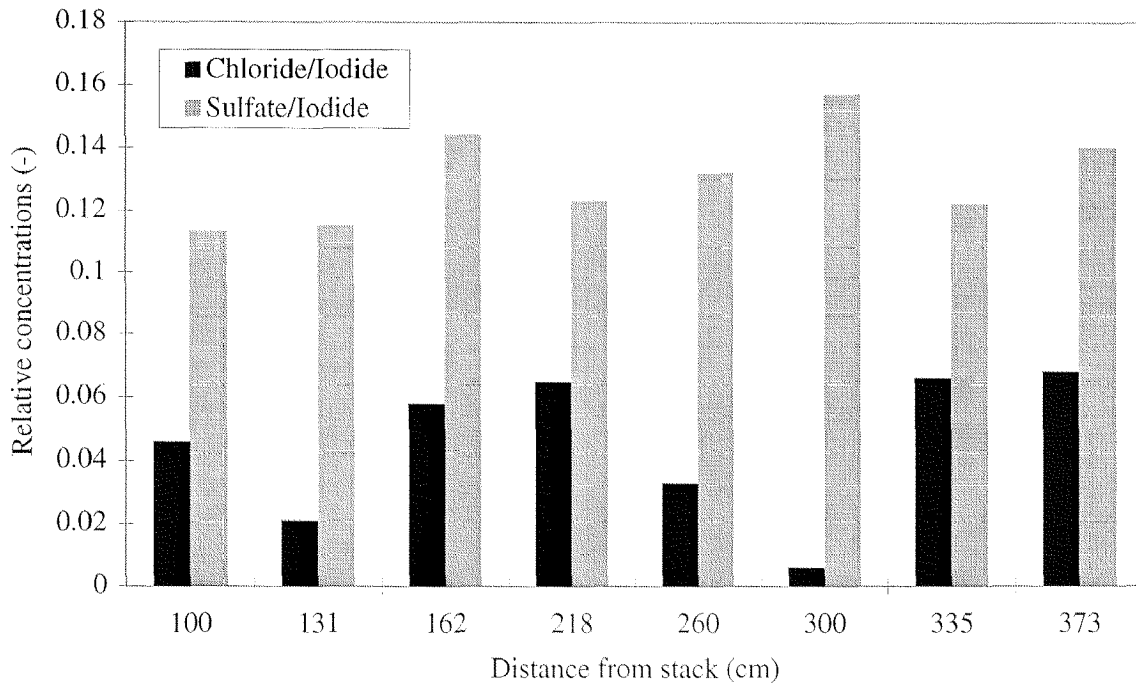


Figure 6.5: Relative chloride and sulfate concentrations along the wind tunnel at 50 to 70 cm above stack height

of the first sample at the stack exit is very small. This value is due to the fact that the plume's diameter is very small (3.2 cm) and that the nozzle was not completely within the plume during the sampling. However at the stack exit the chloride concentration is at its maximum. Due to the entrainment of the ambient air, the chloride concentration decreases until the equilibrium concentration (in our case the chloride concentration of the ambient air) is reached. In fact in Figure 6.4 are represented the relative sulfate and chloride concentrations at stack height. It can be seen that due to ambient air entrainment the chloride concentration decreases whereas the sulfate relative concentration is constant and oscillates around a value 0.12. This can be explained by the fact that the chloride concentration of the ambient air was lower than the concentration inside the plume. This is not the case for the sulfates concentration. The fact that ambient air is entrained into the plume and that the sulfate concentration is constant leads to the conclusion that the sulfate concentration measured is the one of ambient air.

This conclusion can be verified by another chemical analysis 70 cm above stack height (see Figure 6.5). At this height the plume was not present due to the experimental conditions. Moreover this fact could be checked by having a look at the plume. The chloride concentration is relatively low which proves that chlorides were present inside the plume. The sulfate concentration still oscillates around the value of 0.12 which must be the ambient air's concentration as the plume is not present there.

The conclusion that can be drawn from these observations is that chlorides but no sulfates were formed during this experiment.

6.3 Day experiments

6.3.1 Experimental conditions

In order to study the influence of UV-light (day situation), an additional variable (UV-light) was introduced. The experiments were planned with the help of a 2^{10-6} Fractional Factorial Design. This means that 10 variables are studied in 16 experiments (4 independent variables and 6 interactions). The list of the variables can be found in Table 6.6.

Table 6.6: Main normalized variables for the day plume experiment

x_i	variable	'-' value	'+' value
x_1	T_a [$^{\circ}\text{C}$]	9	18
x_2	M_a [%]	60	85
x_3	T_g [$^{\circ}\text{C}$]	150	200
x_4	M_g [g/m^3]	100	180
x_5	C_{NH_3} [mg/m^3]	0	75
x_6	C_{SO_2} [mg/m^3]	0	2500
x_7	C_{HCl} [mg/m^3]	0	60
x_8	C_{NO_x} [mg/m^3]	0	50
x_9	C_{O_2} [%]	0	10
x_{10}	UV-light	no light	light

Also for this design one obtains a model similar to that for the 2^{9-5} design, which after simplifications has the following form (again only interactions of order 2 or smaller are considered):

$$y = b_0 + b_1x_1 + b_2x_2 + \cdots + b_{10}x_{10} \quad (6.20)$$

with

$$b_0 = \Theta_0 \quad (6.21)$$

$$b_1 = \Theta_1 + \Theta_{25} + \Theta_{36} + \Theta_{47} \quad (6.22)$$

$$b_2 = \Theta_2 + \Theta_{15} + \Theta_{38} + \Theta_{49} \quad (6.23)$$

$$b_3 = \Theta_3 + \Theta_{16} + \Theta_{28} + \Theta_{410} \quad (6.24)$$

$$b_4 = \Theta_4 + \Theta_{17} + \Theta_{29} + \Theta_{310} \quad (6.25)$$

$$b_5 = \Theta_5 + \Theta_{12} + \Theta_{68} + \Theta_{79} \quad (6.26)$$

$$b_6 = \Theta_6 + \Theta_{13} + \Theta_{58} + \Theta_{710} \quad (6.27)$$

$$b_7 = \Theta_7 + \Theta_{14} + \Theta_{59} + \Theta_{610} \quad (6.28)$$

$$b_8 = \Theta_8 + \Theta_{23} + \Theta_{56} \quad (6.29)$$

$$b_9 = \Theta_9 + \Theta_{24} + \Theta_{57} \quad (6.30)$$

$$b_{10} = \Theta_{10} + \Theta_{24} + \Theta_{57} + \Theta_{34} + \Theta_{67} \quad (6.31)$$

The regression matrix according to which the experiments were planned and carried out can be found in Table 6.7.

It can be noted that the results of experiments 5 to 12 of Table 6.7 are exactly the same than those of experiments 5 to 12 of Table 6.3. In fact in order to save time for the second set of experiments, only experiments 1 to 4 and 13 to 16, which differ from those of the first 2^{9-5} design, were carried out. For the experiments 5 to 12 the results of the first set of experiments (no UV-light) were used.

6.3.2 Results of the day experiments

The results of these 'day' experiments are summarized in Table 6.8. Also in this case the values in brackets were not considered for the

Table 6.7: 2^{10-6} Fractional Factorial Design

exp.#	x ₀	x ₁	x ₂	x ₃	x ₄	x ₅ =x ₁ x ₂	x ₆ =x ₁ x ₃	x ₇ =x ₁ x ₄	x ₈ =x ₂ x ₃	x ₉ =x ₂ x ₄	x ₁₀ =x ₃ x ₄	Y
1	+	-	-	-	-	+	+	+	+	+	+	Y ₁
2	+	+	-	-	-	-	-	-	+	+	+	Y ₂
3	+	-	+	-	-	-	+	+	-	-	+	Y ₃
4	+	+	+	-	-	+	-	-	-	-	+	Y ₄
5	+	-	-	+	-	+	-	+	-	+	-	Y ₅
6	+	+	-	+	-	-	+	-	-	+	-	Y ₆
7	+	-	+	+	-	-	-	+	+	-	-	Y ₇
8	+	+	+	+	-	+	+	-	+	-	-	Y ₈
9	+	-	-	-	+	+	+	-	+	-	-	Y ₉
10	+	+	-	-	+	-	-	+	+	-	-	Y ₁₀
11	+	-	+	-	+	-	+	-	-	+	-	Y ₁₁
12	+	+	+	-	+	+	-	+	-	+	-	Y ₁₂
13	+	-	-	+	+	+	-	-	-	-	+	Y ₁₃
14	+	+	-	+	+	-	+	+	-	-	+	Y ₁₄
15	+	-	+	+	+	-	-	-	+	+	+	Y ₁₅
16	+	+	+	+	+	+	+	+	+	+	+	Y ₁₆

calculations as they are outliers.

Again in Table 6.8 the second column represents the reference measurements whereas columns 3 to 17 represent the corrected values of sample locations $\boxed{\text{A}}$ to $\boxed{\text{O}}$.

Also in this case, the evaluation of the collected photometer data (and hence the determination of the different parameters b_i of the linear model) is identical to the one described above (i.e. using maximum values, mean ones or the values collected at each sampling location). The results of this evaluation can be found in Table 6.9.

Also in this case, only the mean, respectively the maximum values of the different experiments are used in order to avoid errors (see above). Using the maximum values of the experiments, several important coefficients of the model can be found (the coefficients b_i are again combinations of different parameters Θ_i see Table 6.9). For the day experiments

6.3. DAY EXPERIMENTS

Table 6.8: Day plume simulation results

exp.#	ref.	A	B	C	D	E	F	G	H	I	J	K	L	M	N	O	\bar{y}
1	118	43	88	94	168	132	276	196	190	234	204	(679)	160	163	157	147	161
2	149	5	0	4	0	0	178	142	146	180	69	(1196)	252	250	233	235	121
3	146	4	35	18	0	0	95	0	0	58	0	(1598)	70	85	110	83	40
4	152	1	0	0	0	0	154	122	111	153	70	(878)	190	202	203	191	100
5	133	47	64	87	224	341	601	505	581	561	464	(983)	414	395	342	402	359
6	693	46	210	388	184	75	95	95	91	95	95	23	20	29	131	78	110
7	79	3	2	9	7	6	80	132	17	114	214	0	27	30	37	15	46
8	601	76	6	10	30	0	100	89	2	103	176	13	79	72	84	78	61
9	268	25	113	77	137	0	558	558	528	512	386	(1320)	420	415	411	427	326
10	592	17	37	38	136	105	48	79	6	186	201	115	211	142	162	109	106
11	599	11	46	205	620	471	25	20	102	36	0	14	150	150	119	47	134
12	169	0	34	98	36	0	350	369	323	397	542	303	404	398	386	387	287
13	150	0	47	32	9	0	273	163	236	223	137	(1762)	322	314	316	321	171
14	152	0	0	2	0	0	224	100	97	167	14	(1177)	118	123	132	113	77
15	143	6	10	16	(1614)	593	329	199	261	298	157	(1881)	272	245	240	268	223
16	182	20	124	405	231	/	180	185	328	245	277	(1231)	291	253	231	218	230

Table 6.9: Fractional factorial design coefficients for the day plume simulation according to three different methods: mean values of y_i , maximum values of y_i and for y_i of each sampling location **A to **O****

coeff.	Max(y_i)	Mean(y_i)	A	B	C	D	E	F
b_0	379.81	161.50	19.00	51.00	92.68	121.43	120.18	222.87
b_1	-79.68	-22.50	1.62	0.37	25.43	-44.31	-72.68	-56.75
b_2	-21.93	-20.12	-3.87	-18.87	2.43	14.18	38.56	-58.75
b_3	33.31	-0.25	5.75	6.87	25.93	-15.68	31.68	12.37
b_4	54.56	34.37	-9.12	0.37	16.43	44.81	50.93	25.50
b_5	53.31	52.37	7.50	8.50	7.68	-17.06	-36.06	88.62
b_6	-35.18	-18.25	9.12	26.70	57.18	49.81	-10.43	-28.75
b_7	-9.18	2.62	-2.25	-3.00	1.18	-21.18	-22.18	8.87
b_8	-44.18	-1.12	5.37	-3.50	-11.06	-12.68	9.31	-4.25
b_9	127.56	42.75	3.25	21.00	69.43	81.56	106.31	31.37
b_{10}	-81.68	-17.12	-9.12	-13.00	-21.31	-50.31	-4.56	-9.25
G	H	I	J	K	L	M	N	O
184.62	188.68	222.62	187.87	274.75	212.50	204.12	205.87	194.93
-37.00	-50.68	-31.87	-7.37	-115.50	-16.87	-20.50	-10.62	-18.81
-45.12	-45.68	-47.12	-8.37	-136.00	-27.12	-24.75	-29.62	-34.06
-1.12	12.93	3.12	3.87	-30.50	-19.62	-21.50	-16.75	-8.31
24.50	46.43	35.37	26.37	61.12	61.00	50.87	43.75	41.31
88.75	98.68	80.87	94.12	168.25	72.50	72.37	60.37	76.43
-29.25	-21.43	-41.37	-43.87	-27.25	-49.00	-42.87	-34.00	-46.06
11.12	4.06	22.62	51.62	-23.37	-0.62	-5.50	-11.25	-10.68
12.87	-3.93	11.37	22.62	20.00	1.50	-7.87	-11.50	-10.68
29.25	64.06	33.12	38.12	4.37	32.87	31.25	24.00	27.81
-46.25	-17.56	-27.87	-71.87	-71.62	-3.12	0.25	-3.12	2.06

$$b_0 = \Theta_0$$

$$b_1 = \Theta_1 + \Theta_{25} + \Theta_{36} + \Theta_{47}$$

$$b_2 = \Theta_2 + \Theta_{15} + \Theta_{38} + \Theta_{49}$$

$$b_3 = \Theta_3 + \Theta_{16} + \Theta_{28} + \Theta_{410}$$

$$b_4 = \Theta_4 + \Theta_{17} + \Theta_{29} + \Theta_{310}$$

$$b_5 = \Theta_5 + \Theta_{12} + \Theta_{68} + \Theta_{79}$$

$$b_6 = \Theta_6 + \Theta_{13} + \Theta_{58} + \Theta_{710}$$

$$b_7 = \Theta_7 + \Theta_{14} + \Theta_{59} + \Theta_{610}$$

$$b_8 = \Theta_8 + \Theta_{23} + \Theta_{56}$$

$$b_9 = \Theta_9 + \Theta_{24} + \Theta_{57}$$

$$b_{10} = \Theta_{10} + \Theta_{24} + \Theta_{57} + \Theta_{34} + \Theta_{67}$$

x_i	variable	-1	+1
x_1	T_a [$^{\circ}\text{C}$]	9	18
x_2	M_a [%]	60	85
x_3	T_g [$^{\circ}\text{C}$]	150	200
x_4	M_g [g/m^3]	100	180
x_5	C_{NH_3} [mg/m^3]	0	75
x_6	C_{SO_2} [mg/m^3]	0	2500
x_7	C_{HCl} [mg/m^3]	0	60
x_8	C_{NO_x} [mg/m^3]	0	50
x_9	C_{O_2} [%]	0	10
x_{10}	UV - light	no light	light

b_1 , b_4 , b_5 , b_9 and b_{10} seem to influence the dispersion photometer value mostly.

- The coefficient b_1 has a big negative influence on the photometer value. This is mainly due to the inversely proportional effect of the temperature (see night plume experiments). This effect is more important as ammonia (Θ_{25} in the x_2x_5 interaction) and hydrogen chloride (Θ_{47} in the x_4x_7 interaction) have a positive influence on the light dispersion value.
- The relatively high value of b_4 is due to the positive effect of hydrogen chloride (Θ_{17} in the x_1x_7 interaction) on the light dispersion. This effect is masked by the negative influence of the ambient temperature (Θ_{17} in the x_1x_7 interaction) and should even be more important. After this FFD (fractional factorial design) it is not clear whether the moisture content of the exhaust gas x_4 has an influence on opacity or not.
- The relatively high value of b_5 is due to the positive effect of hydrogen chloride (Θ_{79} in the x_7x_9 interaction) and ammonia (Θ_5) on the light dispersion. This effect is masked by the negative influence of the ambient temperature (Θ_{12} in the x_1x_2 interaction) and should even be more important.
- The very high value of b_9 is due to the big influence of the ammonia-hydrogen chloride interaction. This factor underlines the importance of the formation of ammonium chloride during plume opacity phenomena.
- b_{10} has a relatively important negative value. This is due to the fact that for the experiments without light (first set of experiments) the increase of the photometer value was more important than for the experiments with light. In fact in Table 6.8 the values of the difference between the plume 'opacity' and the reference (columns \boxed{A} to \boxed{O}) were higher for the experiments without UV-light (exp. 5 to 12) than for those with UV-light (exp. 1 to 4 and 13 to 16). It was noticed that for the first set of experiments

the aerosol concentration of the ambient air was higher than in the second set of experiments. These higher values of the photometer readings in the first set can be explained when the initial particles are considered as condensation nuclei. In fact during the first set of experiments, the ambient air contained high quantities of pollen whereas during wintertime the air in Zurich was cleaner as far as dust or pollen are concerned. The air contained higher amounts of sulfur dioxide which however has no influence on the dispersion photometer value.

6.4 Summary of the fractional factorial design series

The preliminary results of the fractional factorial design campaign are summarized in Figure 6.6. The variables will be discussed in the clockwise direction, starting with the ambient temperature T_a .

The ambient temperature T_a shows a strong inversely proportional influence on plume opacity.

The fractional factorial design did not show any important influence of exhaust gas temperature T_g . However this temperature should have the same influence as the ambient temperature T_a as the important factor is the temperature difference $T_g - T_a$. In fact the formation of ammonium chloride is faster the lower the temperature inside the plume (see Section 3.1). The cooling rate of the plume is dependent on the temperature difference between environment and plume. This is why the exhaust gas temperature should have the same inversely proportional effect as the ambient temperature.

The ammonia concentration C_{NH_3} , the hydrogen chloride concentration C_{HCl} and all their interactions influence the formation of aerosols during the day.

No sulfates were formed in these first experiments and no significant influence of neither sulfur dioxide nor the sulfur dioxide/ammonia in-

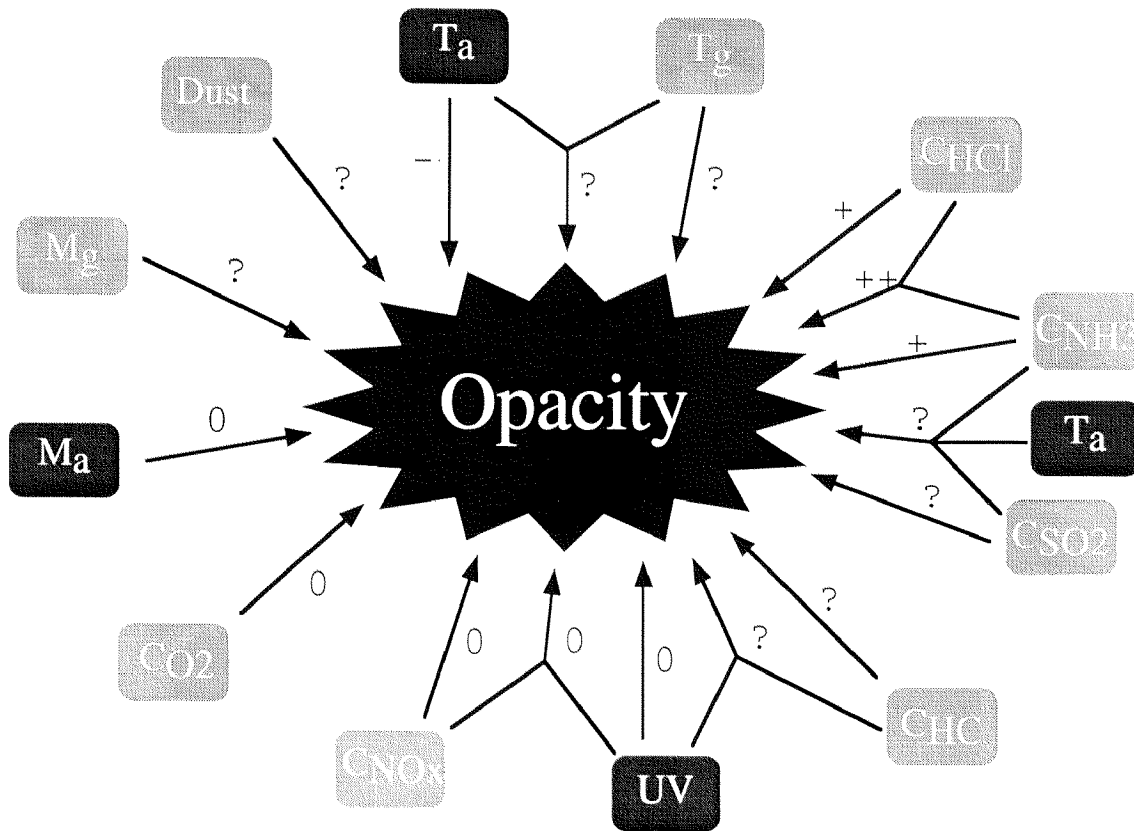


Figure 6.6: Influences of different variables during the 'night' and 'day' experiments on opacity: 0 no influence; + proportional influence; ++ very strong proportional influence; - inversely proportional influence; -- very strong inversely proportional influence; ? influence not known yet

teraction on plume opacity could be found.

During this FFD phase (as well as during the rest of this project) no organic matter was added to the exhaust gas stream (see Section 6.1). This is why the influence of organic matter on opacity is not known at the moment.

In our experiments a significant influence of UV-light with the inorganic components could not be shown. In fact it is supposed that UV-light is only important in the presence of organic matter in combination with nitrogen oxides in the exhaust gas (photooxidation).

The nitrogen oxide concentration seems to play no significant role in this set of experiments and was not considered during further experiments as organic matter was not added to the exhaust gas either.

In fact the formation of ozone and hence possible oxidations are only possible in presence of NO_x , UV-light as well as organic matter (see Figure 3.2). In absence of one of these three components the ozone formation process is interrupted.

Oxygen had no significant influence on the aerosol formation in these series. The exhaust gas moisture content as well as the ambient air moisture content M_a could possibly be important for sulfate formation however in this series the effect could not be shown. The influence of dust was not studied so far.

According to the results presented in this section, it can be concluded that only ammonium chloride was formed as new aerosols in our experiments. This result was confirmed by the chemical analysis of the gas samples.

6.4.1 Consequences for further experiments

At the end of this FFD series different questions concerning plume opacity remained unanswered, as there are:

- influence of the exhaust gas temperature T_g
- influence of the sulfur dioxide concentration C_{SO_2}
- influence of the exhaust gas moisture content M_g
- influence of dust

This is why these influences were studied in a second phase of the experiments (see Section 6.5 and following). Moreover in these series opacity formation was studied in a more quantitative way than during the screening phase (fractional factorial design). This is why in these series the dispersion photometer results were converted to opacity values (using the correlation of Section 5.3.3) in order to study different effects concerning plume opacity. In the following only the maximum opacity value of a plume was considered as this maximum value is most in accordance with EPA Method 9 (see Section 2.1.2).

A list of factors that could possibly influence plume opacity and that have been studied in these different series can be found in Table 6.10

Table 6.10: List of influences that have been studied in different series as well as sections where the results can be found

series	x ₁	x ₂	x ₃	x ₄	x ₅	x ₆	x ₇	x ₈	x ₉	x ₁₀	x ₁₁	section
HCl					X		X					6.5
SO ₂						X						6.6.1
SO ₂	X	X				X						6.6.2
SO ₂				X								6.6.4
SO ₂						X					X	6.6.5
SO ₂	X											6.6.6
T _g			X									6.7

x _i	variable	variable
x ₁	T _a [°C]	ambient air temperature
x ₂	M _a [%]	ambient air moisture content
x ₃	T _g [°C]	exhaust gas temperature
x ₄	M _g [g/m ³]	exhaust gas moisture content
x ₅	C _{NH₃} [mg/m ³]	ammonia concentration
x ₆	C _{SO₂} [mg/m ³]	sulfur dioxide concentration
x ₇	C _{HCl} [mg/m ³]	hydrogen chloride concentration
x ₈	C _{NO_x} [mg/m ³]	nitrogen oxide concentration
x ₉	C _{O₂} [%]	oxygen concentration
x ₁₀	UV - light	UV - light
x ₁₁	dust	dust

Moreover in Section 6.8 the results of the comparison of the experimental data with the data predicted by the theoretical model are presented.

6.5 Hydrogen chloride series

In order to know the quantitative influence of hydrogen chloride on opacity, a hydrogen chloride series was carried out. The experimental conditions can be found in Table 6.11.

During the first series the ammonia concentration was kept constant

Table 6.11: Experimental conditions for the hydrogen chlorides series

variable	units	value
T_a	[°C]	9
M_a	[% r.h.]	60
T_g	[°C]	200
M_g	[g/m ³ _{n,dry}]	180
C_{NH_3}	[mg/m ³ _{n,dry}]	75 resp. 240.4
C_{SO_2}	[mg/m ³ _{n,dry}]	0
C_{HCl}	[mg/m ³ _{n,dry}]	0 to 204
C_{NO_x}	[mg/m ³ _{n,dry}]	0
C_{O_2}	[vol%]	10
C_{CO_2}	[vol%]	10
UV - light	[W/m ²]	yes

at 75 mg/m³_{n,dry} compared to 240.4 mg/m³_{n,dry} during the second series. This extremely high ammonia concentration was used in order to check if the ammonium chloride formation rate could be enhanced by additional ammonia.

The opacity results are shown in Figure 6.7, the results of the chemical analysis can be found in Figure 6.8. Figure 6.8 clearly shows that an increase in hydrogen chloride concentration leads to an increase of the ammonium chloride concentration. Comparing the two series (one with 75 mg NH₃/m³_{n,dry} and one with 240.4 mg NH₃/m³_{n,dry}) it can be noted that a significant increase of ammonia alone does not increase the ammonium chloride concentration. In fact the ammonium chloride concentration is the same at a given hydrogen chloride concentration. This means that a ammonia concentration of 75 mg/m³_{n,dry} is already sufficient to produce ammonium chloride. Only the hydrogen chloride concentration influences the concentration of the ammonium chloride formed. This can be explained by the fact that for a given hydrogen chloride concentration the HCl/NH₃ molar ratio is smaller than 1. Hydrogen chloride is the rate determining component.

Comparing Figure 6.8 to Figure 6.7 one can see that opacity increases with increasing chloride concentration. In this case the formation of

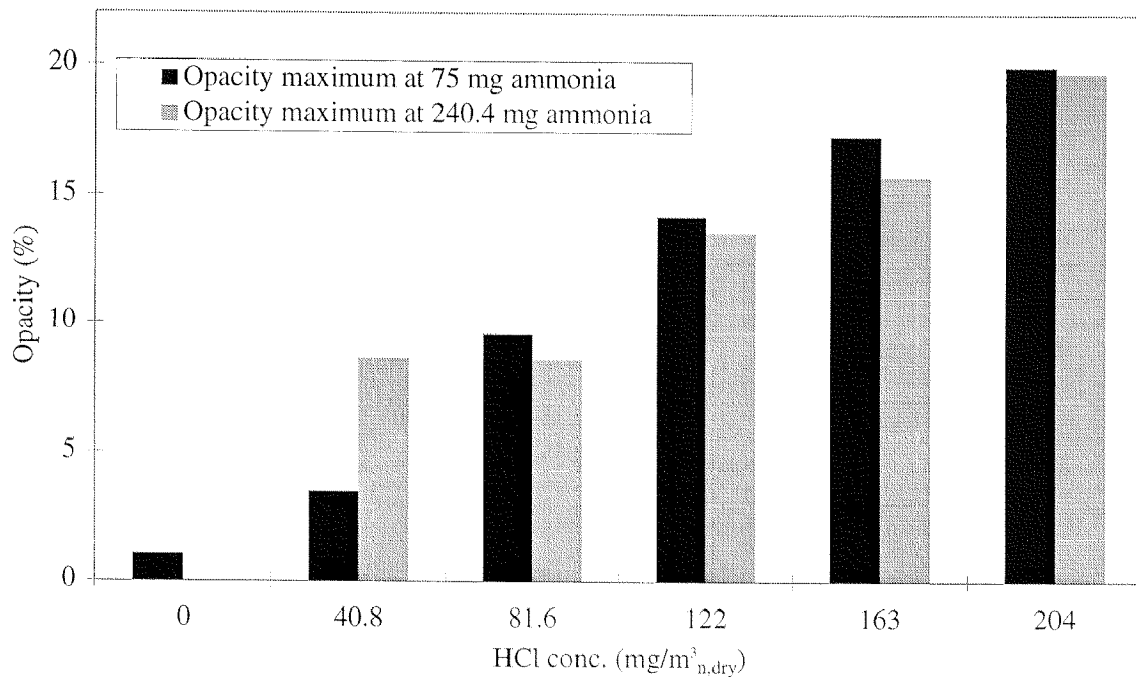


Figure 6.7: Opacity readings (maximum values) of the hydrogen chloride series at two different ammonia concentration levels 75 resp. 240 mg/m³_{n,dry}; $T_a=9^{\circ}\text{C}$, $T_g=150^{\circ}\text{C}$

ammonium chloride clearly leads to an increased opacity which in our experimental equipment can be as high as 20 %.

An increase of the hydrogen chloride concentration in presence of ammonia leads to an increase in ammonium chloride concentration and hence to increased opacity.

6.6 Sulfur dioxide series

6.6.1 Influence of the sulfur dioxide concentration on opacity

At the end of the screening phase it was not sure whether sulfur dioxide has an influence on plume opacity formation or not. This is why several additional series, in which sulfur dioxide was added to the exhaust gas in different concentrations and under different conditions, were carried out. The experimental conditions for the sulfur dioxide series can be found in Table 6.12.

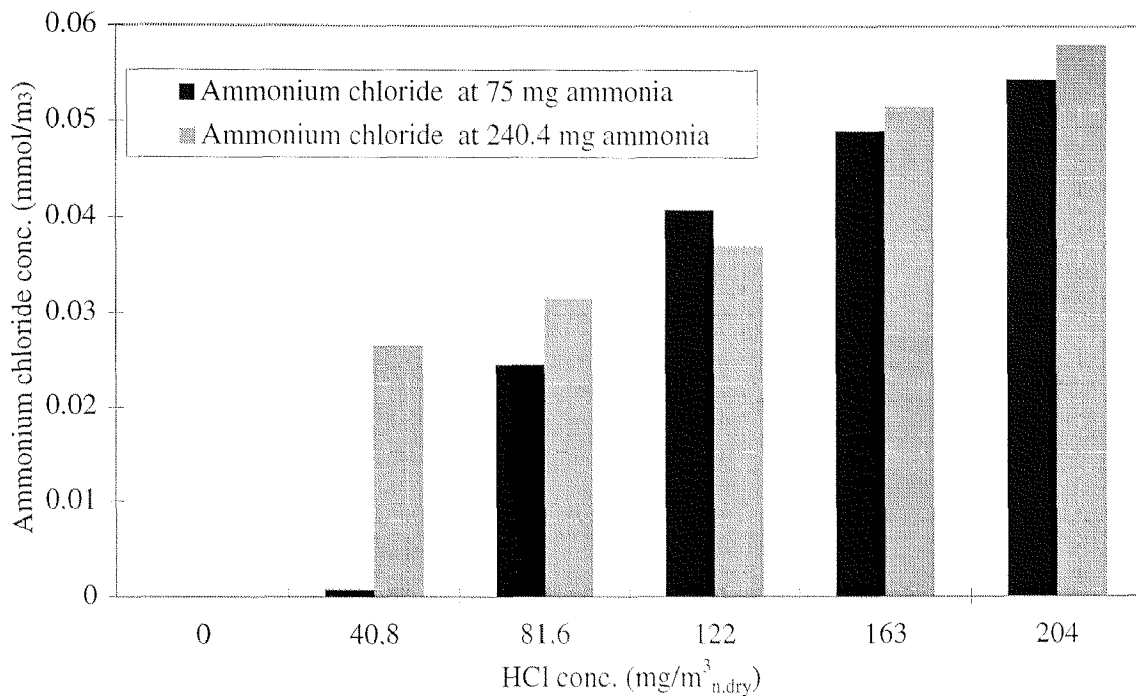


Figure 6.8: Ammonium chloride concentration results of the hydrogen chloride series at two different ammonia concentration levels 75 resp. 240 $\text{mg}/\text{m}^3_{n,dry}$; $T_a=9^\circ\text{C}$, $T_g=150^\circ\text{C}$

The experiment during which the sulfur dioxide concentration was increased continuously was repeated three times. The opacity results of these series are summarized in Figure 6.9, the results of the chemical analysis can be found in Figure 6.10.

In Figure 6.9 it can be seen that for these experiments no correlation between opacity and the sulfur dioxide concentration was found. This confirmed the results of the screening experiments. However the same trend for the three experiments can be seen. With increasing sulfur dioxide concentration opacity increases then decreases and increases again. However this variation of the opacity can not be due to sulfate aerosols formed. This can be seen from Figure 6.10. The amount of sulfates inside the wind tunnel is extremely low (approximately 1 ppb). An explanation for the observed trends as far as opacity is concerned is that these changes in opacity are due to changes of the ambient air quality. In fact the air for simulating the atmosphere inside the wind tunnel is ambient air from the Zurich city area. Moreover each

Table 6.12: Experimental conditions for the sulfur dioxide series

variable	units	series 1	series 2	series 3
T_a	[°C]	9	9	9
M_a	[% r.h.]	60	60	60
T_g	[°C]	200	200	200
M_g	[g/m ³ _{n,dry}]	180	180	180
C_{NH_3}	[mg/m ³ _{n,dry}]	75	75	75
C_{SO_2}	[mg/m ³ _{n,dry}]	0 to 3571	0 to 3571	0 to 3571
C_{HCl}	[mg/m ³ _{n,dry}]	0	0	0
C_{NO_x}	[mg/m ³ _{n,dry}]	0	0	0
C_{O_2}	[vol%]	10	10	10
C_{CO_2}	[vol%]	10	10	10
UV - light	[W/m ²]	yes	yes	yes
dust	[mg/m ³ _{n,dry}]	no	no	no

experiment was done at the same period of the day. An experiment started at noon and ended at 7.00 pm. This involves that the first opacity increase could be observed between 1.30 pm and 2.00 pm, the second one between 6.00 pm and 7.00 pm. This corresponds to the period of day where traffic is most heavy. This is why it seems that opacity increases at 714.3 (1428.6) and 3571 mg/m³_{n,dry} sulfur dioxide. But in these experiments under the conditions listed in Table 6.12 no sulfates were formed and sulfur dioxide did not influence opacity at all. Only ambient air influenced the opacity measured in the wind tunnel. This fact was taken in account in the future and the periods in question (1.00-2.00 pm as well as 6.00-7.00 pm) were avoided when carrying out experiments.

One conclusion that was drawn from the series was that the ambient humidity possibly was not high enough. In fact the sulfur dioxide oxidation needs an aqueous phase. This hypothesis was tested during further experiments.

An increase of the sulfur dioxide concentration in presence of ammonia alone is not sufficient for the sulfur dioxide oxidation reaction to occur.

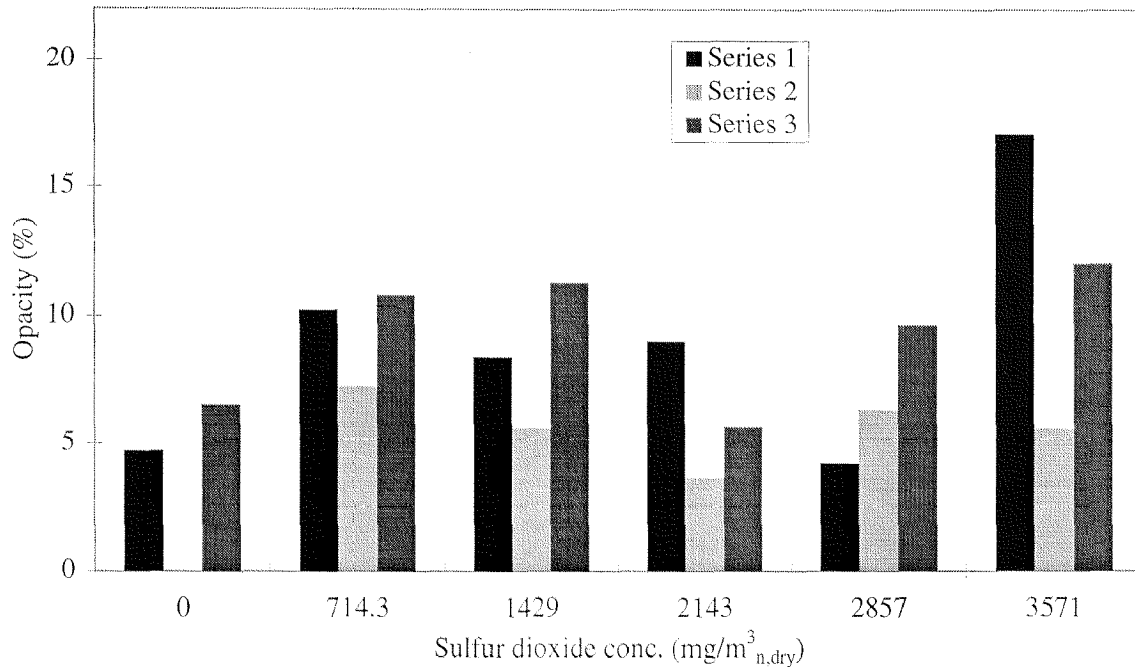


Figure 6.9: Opacity readings (maximum values) of the sulfur dioxide series; $T_a=9^\circ\text{C}$, $T_g=200^\circ\text{C}$, $C_{NH_3}=75 \text{ mg}/\text{m}^3_{n.dry}$ for all three series

6.6.2 Influence of the sulfur dioxide concentration in combination with the ambient relative humidity on opacity

The oxidation of sulfur dioxide to sulfate requires the presence of ammonia as well as an aqueous phase (see Section 3.3). This is why the influence of sulfur dioxide in combination with the ambient air moisture content was studied. The experimental conditions for the two experiments can be found in Table 6.13.

It has to be noted that the ambient temperature in the first experiment was higher than in the second experiment. This is due to the fact that unfortunately meteorological conditions (extremely low relative ambient humidity) in April were so that in order to reach an ambient relative humidity of 82 % the ambient air had to be cooled down to 3.2°C . An artificial moistening of the ambient air up to 80 % was not possible at that moment. In fact the tunnel walls were so cold at that moment that the steam added immediately condensed on the wall surface. This is why the ambient humidity was adjusted by choosing the corresponding ambient air temperature. The first experiment is the

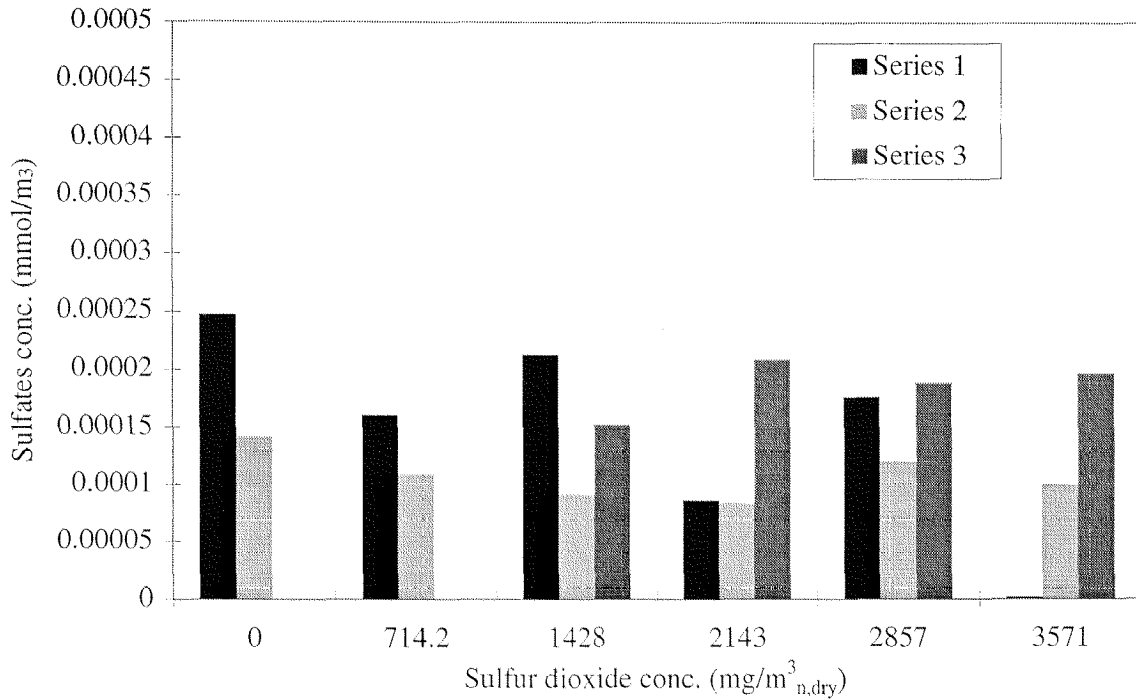


Figure 6.10: Results of the chemical analysis of the sulfur dioxide series; $T_a=9^\circ\text{C}$, $T_g=200^\circ\text{C}$, $C_{NH_3}=75 \text{ mg}/\text{m}^3_{n,dry}$ for all three series

same than experiment series 3 of Chapter 6.6.1.

The results of the two experiments can be found in Figure 6.11 (opacity results) and in Figure 6.12 (results of chemical analysis).

From Figure 6.11 it becomes obvious that at high values of relative ambient humidity, the opacity increases in a continuous way. Moreover Figure 6.12 clearly shows that at high values of relative ambient humidity formation of sulfates inside the wind tunnel took place (up to 6 times more sulfates were present in the exhaust gas samples compared to the experiment where no sulfates were formed inside the wind tunnel). Another indication for the formation of sulfates inside the tunnel is the following. The sulfates concentration was determined about 1 m after the stack exit as well as at the wind tunnel exit. At the first location the sulfate concentration increased with increasing sulfur dioxide concentration. At the tunnel exit the concentration was close to 0 and constant. This concentration (which is much lower than the sulfate's concentration in the neighbourhood of the stack) is the concentration

Table 6.13: Experimental conditions for the sulfur dioxide and moisture content of the ambient air series

variable	units	exp. at low r.h.	exp. at high r.h.
T_a	[°C]	9	3.5
M_a	[% r.h.]	60	82
T_g	[°C]	200	200
M_g	[g/m ³ _{n,dry}]	180	180
C_{NH_3}	[mg/m ³ _{n,dry}]	75	75
C_{SO_2}	[mg/m ³ _{n,dry}]	0 to 3571	0 to 3571
C_{HCl}	[mg/m ³ _{n,dry}]	0	0
C_{NO_x}	[mg/m ³ _{n,dry}]	0	0
C_{O_2}	[vol%]	10	10
C_{CO_2}	[vol%]	10	10
UV - light	[W/m ²]	yes	yes
dust	[mg/m ³ _{n,dry}]	no	no

of the sulfates present in the ambient air. In fact the higher sulfate concentration (due to formation of additional sulfates inside the wind tunnel) is decreasing due to the entrainment of ambient air until the very low sulfate concentration of ambient air is reached.

After this experiment it was evident that the formation of sulfates inside the wind tunnel is possible and that these sulfates formed increase opacity. However it still was not clear whether this formation of sulfates was due to increased ambient relative humidity or to the reduced ambient temperature or due to an interaction of both of them. This is why the influence of humidity (see Section 6.6.4) and ambient temperature (see Section 6.7) on the sulfur dioxide oxidation process were studied separately.

An increase of both the sulfur dioxide concentration and the ambient air relative humidity and at the same time a decrease of the ambient air temperature in presence of ammonia leads to the formation of sulfates and increased opacity.

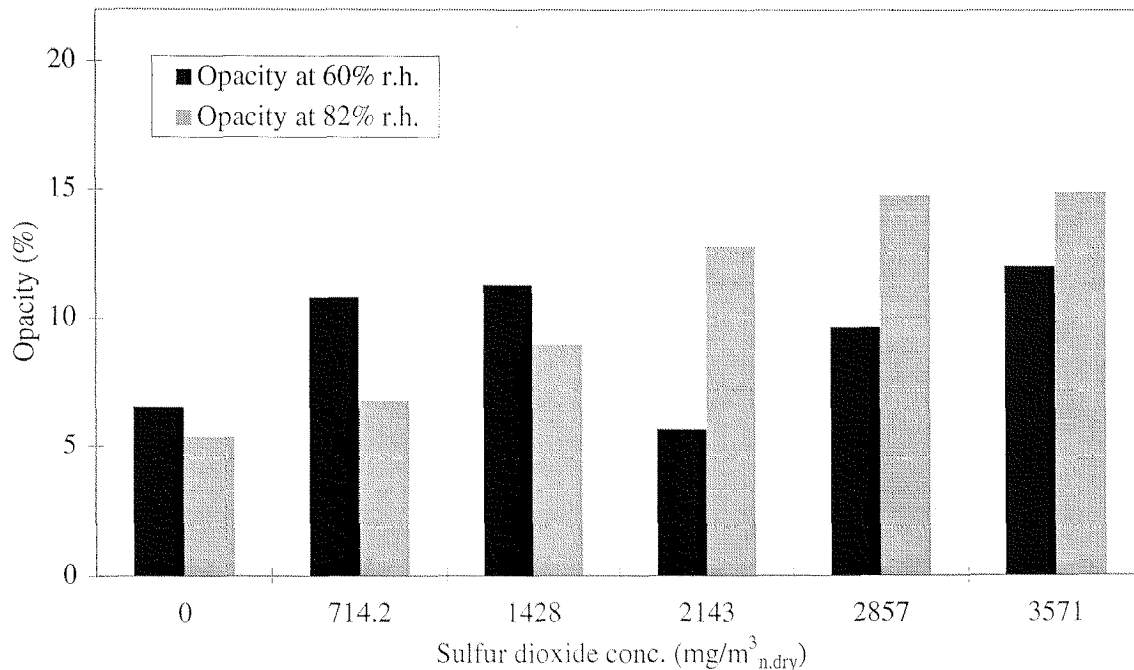


Figure 6.11: Opacity readings (maximum values) of the sulfur dioxide and ambient humidity series at $T_a=9^\circ\text{C}$ and $M_a=60\%$ resp. at $T_a=3.5^\circ\text{C}$ and $M_a=82\%$; $T_g=200^\circ\text{C}$, $C_{NH_3}=75 \text{ mg}/\text{m}^3_{n.dry}$

6.6.3 Comparison between the influence of the sulfur dioxide concentration and hydrogen chloride concentration on opacity

In Figure 6.13 a comparison between the influence of the sulfur dioxide and hydrogen chloride concentrations on opacity is shown.

This figure clearly shows that the formation of ammonium chloride has a much more important influence on plume opacity than the formation of sulfates. An increase of the hydrogen chloride concentration from 0 to 204 $\text{mg}/\text{m}^3_{n.dry}$ involves an opacity increase from almost 0 to 20 % whereas the same increase in the sulfur concentration only increases opacity by 1 to 2 % (-x- line in Figure 6.13). Only in the case of the series represented by -x- sulfates were formed. For this curve an increase in opacity can be seen whereas for the other sulfate series, opacity varies in function of the quality of the ambient air. This is why only the $-\Delta-$ curve is representative for the influence of sulfates on opacity. However the influence on opacity of sulfates is much smaller

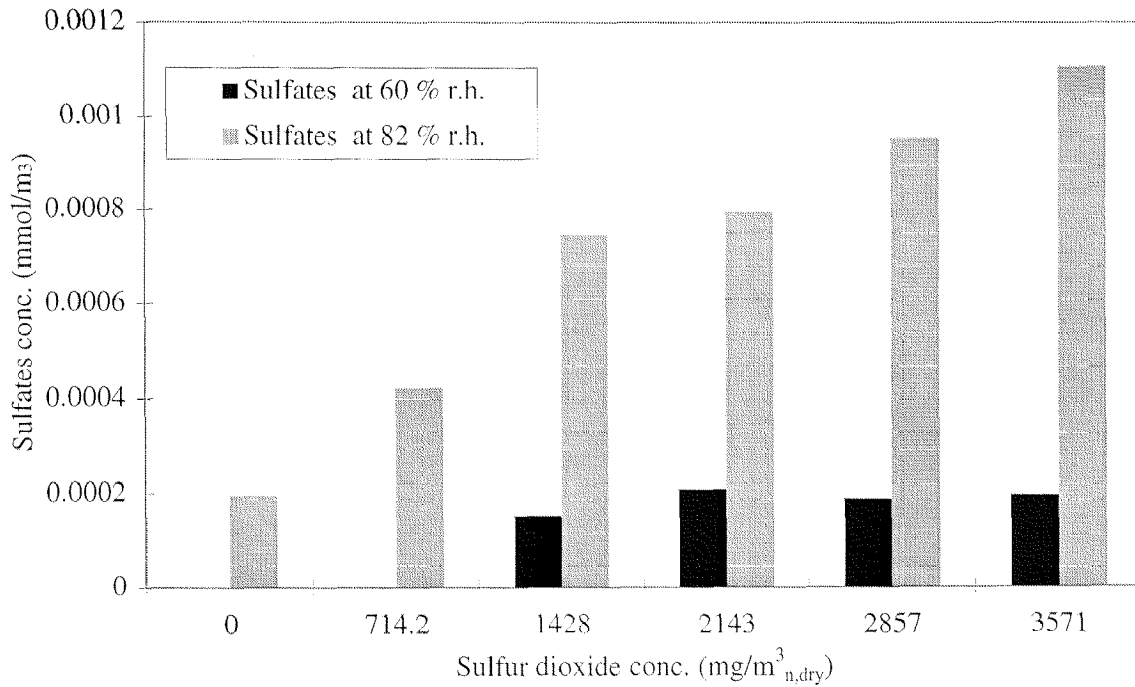


Figure 6.12: Results of the chemical analysis of the sulfur dioxide and ambient humidity series at $T_a=9^\circ\text{C}$ and $M_a=60\%$ resp. at $T_a=3.5^\circ\text{C}$ and $M_a=82\%$; $T_g=200^\circ\text{C}$, $C_{NH_3}=75 \text{ mg}/\text{m}^3_{n,\text{dry}}$

than that of chlorides.

An increase of the hydrogen chloride concentration has a much bigger influence on plume opacity than the same increase of the sulfur dioxide concentration.

6.6.4 Moisture content of the exhaust gas series

For studying the influence of humidity on the sulfur dioxide oxidation process the exhaust gas moisture content was varied. The reason for this is that the absolute water content in the exhaust gas is higher than in the ambient atmosphere. For instance at 15°C and 60 % relative humidity the air contains approximately 6.5 g water per $\text{m}^3_{n,\text{dry}}$ of air whereas the exhaust gas contains for instance 180 g water per $\text{m}^3_{n,\text{dry}}$. This is why by changing the exhaust gas moisture content instead of the ambient relative humidity the variation of the amount of water introduced into the plume is much more important.

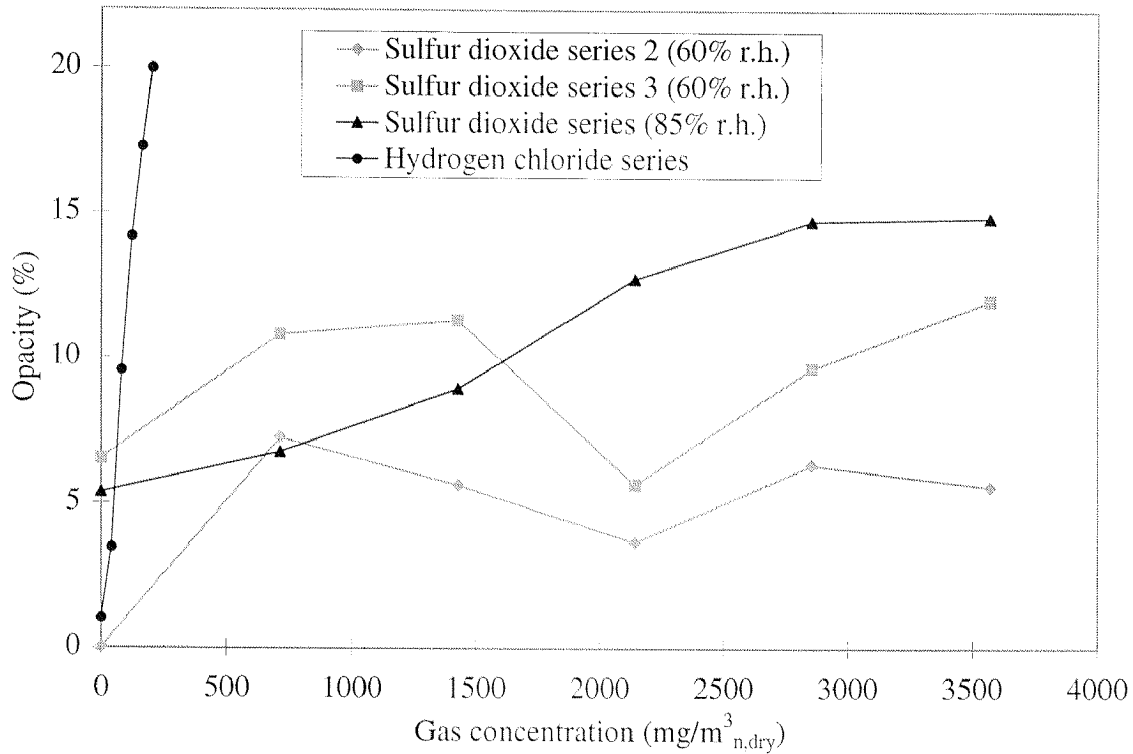


Figure 6.13: Comparison between the influence of the sulfur dioxide concentration and hydrogen chloride concentration on opacity at $T_a=9^\circ\text{C}$ and $M_a=60\%$ resp. at $T_a=3.5^\circ\text{C}$ and $M_a=82\%$; $T_g=200^\circ\text{C}$, $C_{NH_3}=75\text{ mg}/\text{m}^3_{n,dry}$

The experimental conditions for this experiment can be found in Table 6.14.

Figure 6.15 clearly shows that independently from the exhaust gas moisture content, no sulfates were formed inside the wind tunnel. This means that the formation of sulfates shown in Section 6.6.2 was due to the ambient temperature drop and not to an increased ambient relative humidity. This is why the influence of the ambient temperature drop on the oxidation of sulfur dioxide was studied separately (see Section 6.7). Moreover the opacity was constant until an exhaust gas moisture content of $250\text{ g}/\text{m}^3_{n,dry}$ was reached (see Figure 6.14). The slightly increased opacity in this case was due to the fact that at these extremely high exhaust gas moisture contents the steam plume did not dissipate completely before the wind tunnel exit. Once a steam plume has been formed opacity is always increased at this point (at the maximum opacity of a steam plume is 100 %). However this opacity is not

Table 6.14: Experimental conditions for the exhaust gas moisture content series

variable	units	value
T_a	[°C]	8.5
M_a	[% r.h.]	80
T_g	[°C]	200
M_g	[g/m ³ _{n,dry}]	0 to 320
C_{NH_3}	[mg/m ³ _{n,dry}]	75
C_{SO_2}	[mg/m ³ _{n,dry}]	2500
C_{HCl}	[mg/m ³ _{n,dry}]	60
C_{NO_x}	[mg/m ³ _{n,dry}]	0
C_{O_2}	[vol%]	10
C_{CO_2}	[vol%]	10
UV - light	[W/m ²]	yes
dust	[mg/m ³ _{n,dry}]	no

interesting in our case as opacity has to be read after the steam plume has evaporated. Moreover the ammonium chloride concentration was relatively constant. However these salts are very hygroscopic. This is an explanation why at very high exhaust gas moisture contents opacity is higher than at lower moisture contents. In fact at high exhaust gas moisture contents these salts absorb water. These wet particles than scatter light to a much higher extend than do dry particles of the same salt.

An increase of the exhaust gas moisture content did not lead to a significant increase of opacity.

6.6.5 Dust series

A further aspect of plume opacity formation that was not clear so far was the influence of dust on aerosol formation. Dust could possibly act as condensation nuclei and initiate the formation of sulfates. This is why the sulfur dioxide concentration was varied from 0 to 3571 mg/m³_{n,dry} once in absence of dust and once in presence of dust.

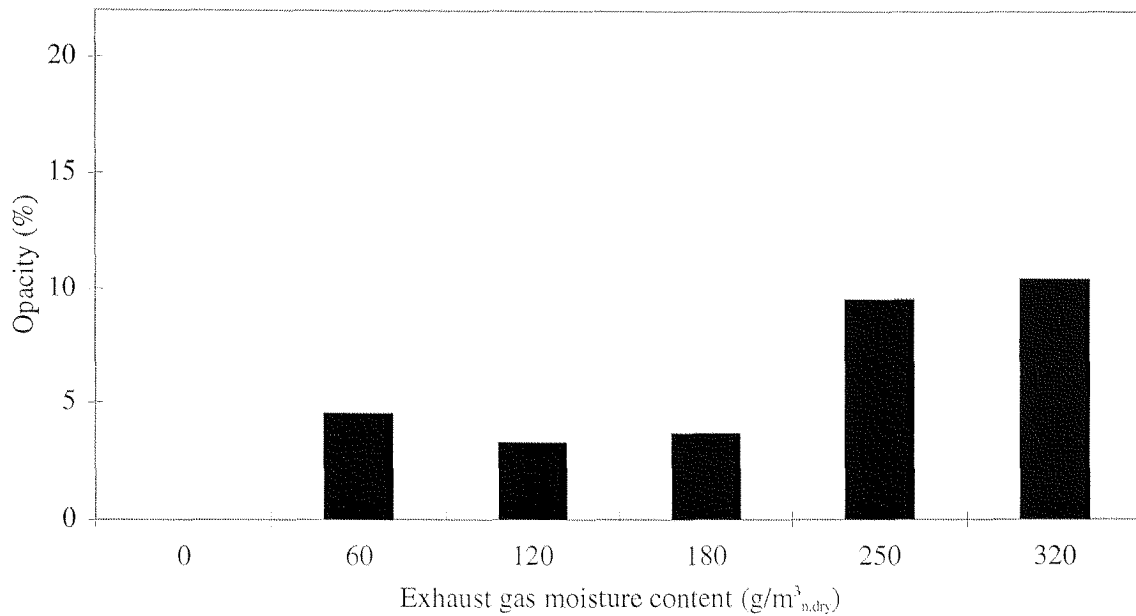


Figure 6.14: Opacity values of the exhaust gas moisture content series at $T_a=8.5^\circ\text{C}$ and $M_a=80\%$ (r. h. relative humidity); $T_g=200^\circ\text{C}$, $C_{NH_3}=75\text{ mg}/\text{m}^3_{n,dry}$, $C_{HCl}=60\text{ mg}/\text{m}^3_{n,dry}$

The dust consist of carbon aerosols that were generated on-line in the plasma reactor (see Section 5.3.1).

The experimental conditions of the dust series can be found in Table 6.15.

Looking at Figure 6.16 it can clearly be seen that the addition of dust to the exhaust gas has no significant influence on plume opacity. This can be due to the fact that the amount of dust added has been too small for the amount of gas emitted. However it was not possible to add dust in a different form to the exhaust gas. In fact according to experts (Ilmac, 1996) it is impossible to dose about 1 mg of dust per minute. This is why no conclusion concerning the influence of dust on plume opacity formation can be drawn. Moreover Figure 6.17 shows that no additional sulfates were produced in the wind tunnel, neither in absence nor in presence of dust. The sulfates found in the samples have already been present in the ambient air.

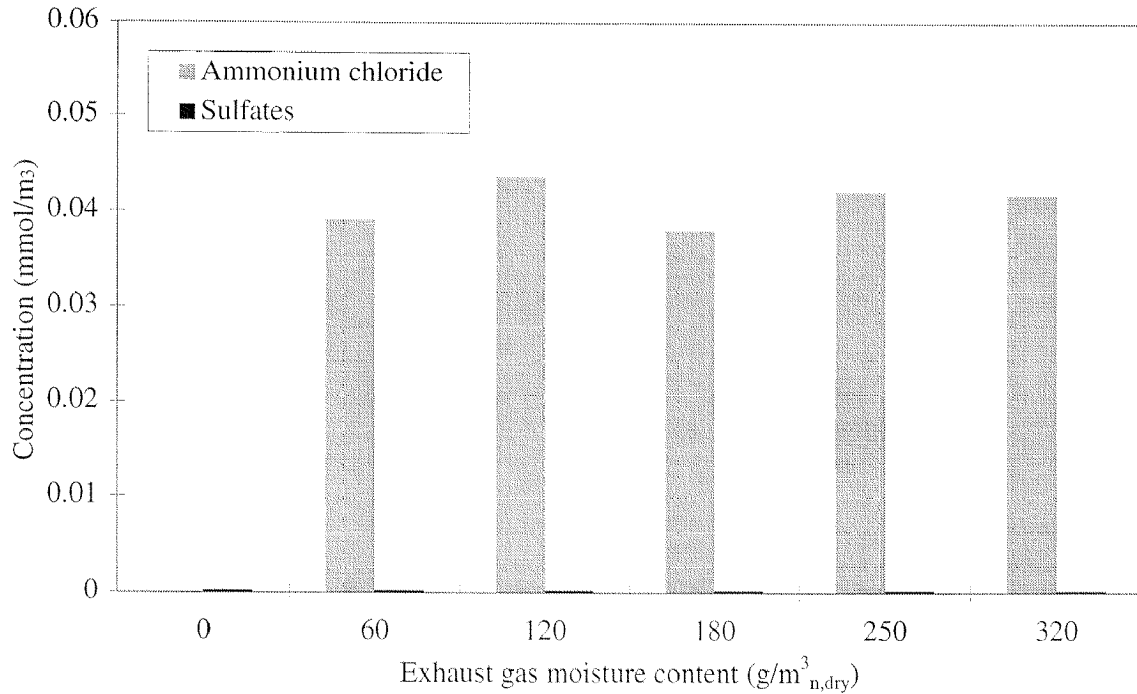


Figure 6.15: Results of the chemical analysis of the exhaust gas moisture content series at $T_a=8.5^\circ\text{C}$ and $M_a=80\%$ (r. h. relative humidity); $T_g=200^\circ\text{C}$, $C_{\text{NH}_3}=75 \text{ mg}/\text{m}^3_{\text{n.dry}}$, $C_{\text{HCl}}=60\text{mg}/\text{m}^3_{\text{n.dry}}$

In this series no significant influence of dust on plume opacity was found.

6.6.6 Influence of the ambient air temperature

In Section 6.6.2 it was shown that the formation of sulfates resulting from an oxidation of sulfur dioxide inside the wind tunnel was possible. However the ambient temperature was very low (3.5°C) and the ambient humidity was increased (82 % r.h.). In Section 6.6.4 it was shown that the increased moisture content was not responsible for this oxidation. As a consequence of this only the low ambient temperature could be at the origin for this sulfate formation. This is why an experimental series, where the ambient temperature was varied, was made.

The experimental conditions of this exhaust gas temperature series can be found in Table 6.16.

The results of this ambient air temperature series can be found in Figure

Table 6.15: Experimental conditions for the dust series

variable	units	witout dust	with dust
T_a	[°C]	9	9
M_a	[% r.h.]	60	60
T_g	[°C]	200	200
M_g	[g/m ³ _{n,dry}]	180	180
C_{NH_3}	[mg/m ³ _{n,dry}]	75	75
C_{SO_2}	[mg/m ³ _{n,dry}]	0 to 3571	0 to 3571
C_{HCl}	[mg/m ³ _{n,dry}]	0	0
C_{NO_x}	[mg/m ³ _{n,dry}]	0	0
C_{O_2}	[vol%]	10	10
C_{CO_2}	[vol%]	10	10
UV - light	[W/m ²]	yes	yes
dust	[mg/m ³ _{n,dry}]	no	yes

6.18.

Due to adverse meteorological conditions the lower limit for the ambient air temperature was 5.1°C. However the result is relatively clear. At low ambient air temperatures the formation of sulfates is possible. With increasing temperature the sulfate's concentration decreases considerably. Opacity decreases in the same manner than does the sulfate concentration. The opacity and sulfate concentration values at higher ambient temperatures are probably upper limits. This is due to the fact that the first experiment was done at 5.1°C. Afterwards the ambient temperature was increased to 7.5°C. However this step is rather time consuming as the temperature profile has to stabilize inside the wind tunnel. Unfortunately it was not possible to wait for 3 hours in order to reach this stabilization. In fact the experiment had to be finished within 4 hours as the meteorological conditions were acceptable only within this short period of time (5.00 am to 9.00 am). Therefore the effect that can be seen in Figure 6.18 would be even more pronounced (opacity would be lower if the temperature drop had taken place in a more homogeneous way over the entire wind tunnel cross section). In this case the values of opacity would be lower and the effect would even be more important. However also under these conditions it is obvious

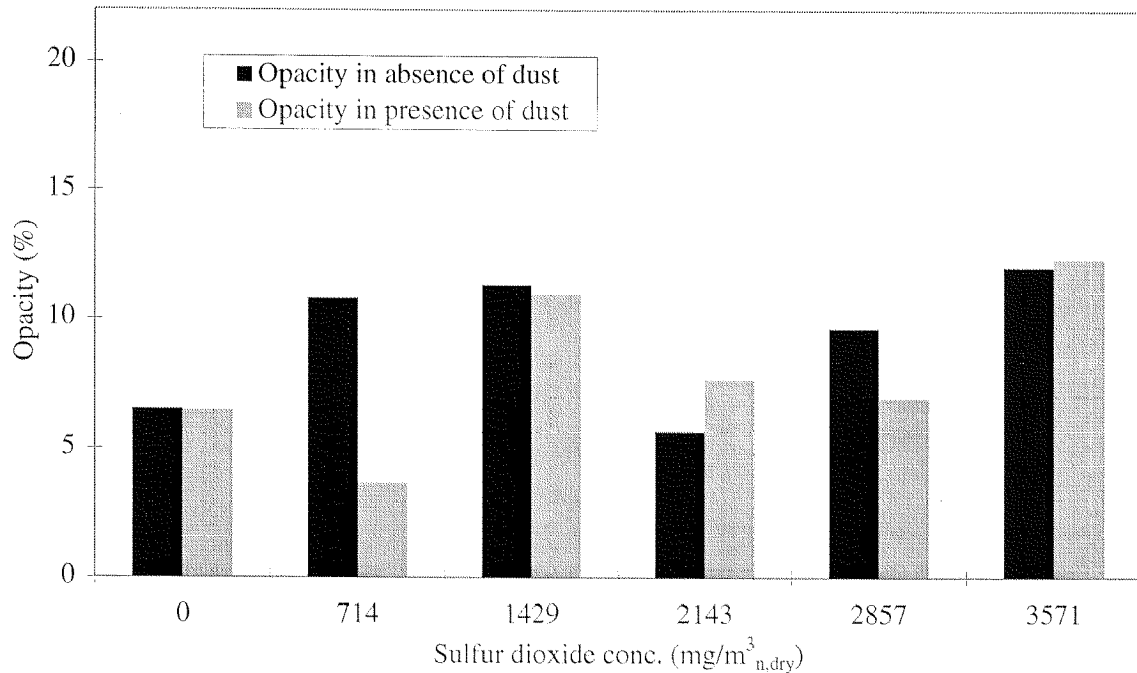


Figure 6.16: Opacity readings of the dust series at $T_a=9^\circ\text{C}$ and $M_a=60\%$; $T_g=200^\circ\text{C}$, $C_{NH_3}=75\text{ mg}/m^3_{n,dry}$

that the sulfates' concentration and hence opacity decreases with increasing ambient air temperature. It seems that 6°C to 7°C is a critical limit above which the formation of sulfates is negligible.

A decrease of the ambient air temperature in presence of sulfur dioxide and ammonia resulted in the formation of sulfates and increased opacity.

6.7 Exhaust gas temperature series

As shown in Section 6.4 the ambient air temperature has a strong inversely proportional influence on plume opacity. For the reasons exposed in Section 6.4 the exhaust gas temperature should have the same effect on plume opacity. This has been studied in a separate exhaust gas temperature series.

The experimental conditions of this exhaust gas temperature series can be found in Table 6.17. It has to be noted that the limits for the exhaust

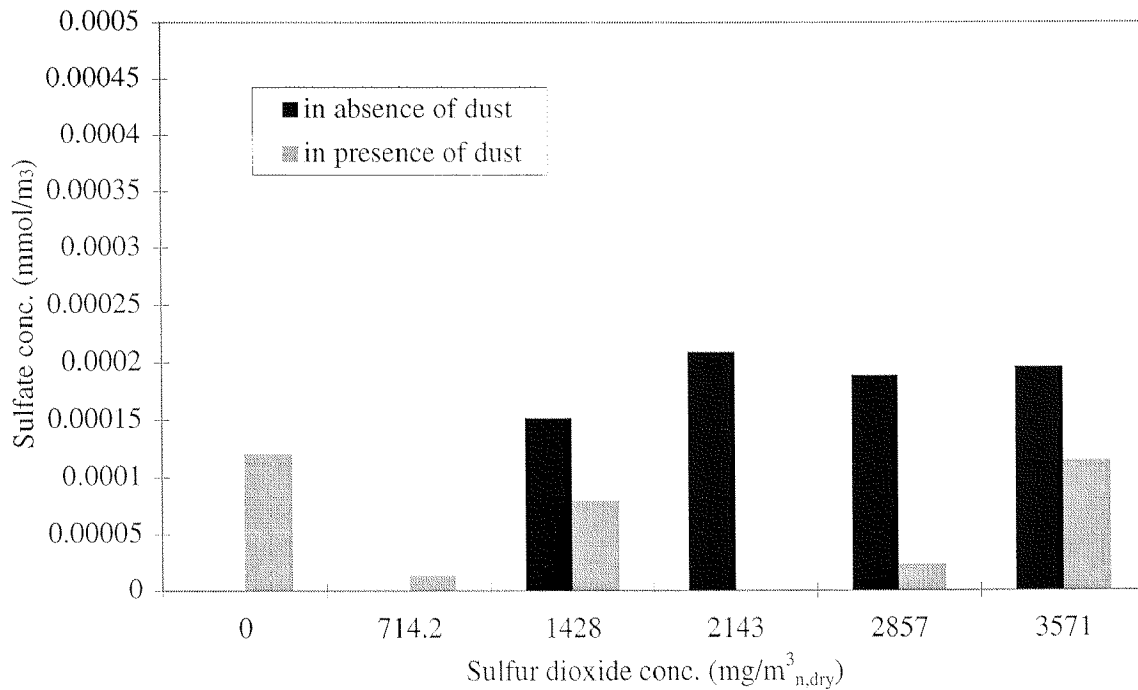


Figure 6.17: Results of the chemical analysis of the dust series at $T_a=9^\circ\text{C}$ and $M_a=60\%$; $T_g=200^\circ\text{C}$, $C_{NH_3}=75\text{ mg}/m^3_{n,dry}$

gas temperature are due to technical reasons. In fact 150°C is the lower limit because otherwise ammonium chloride would solidify inside the capillary tubes, while 230°C is the upper limit because of the melting point of the Teflon connection between the capillary tube and the glass stack (227°C) (Küpfer, 1999).

Figure 6.19 clearly shows that the expected inversely proportional effect of the exhaust gas temperature could be observed. Opacity decreases drastically when the exhaust gas temperature increases from 150°C to 190°C . When the exhaust gas temperature rises from 190°C to 230°C , opacity still decreases. However this decrease is not as high as the one resulting from a temperature increase from 150°C to 190°C . Figure 6.20 shows that the sulfate concentration is negligible compared to the ammonium chloride concentration.

The exhaust gas temperature has an inversely proportional influence on plume opacity.

Table 6.16: Experimental conditions for the ambient air temperature series

variable	units	value
T_a	[°C]	5.1 to 10.0
M_a	[% r.h.]	60
T_g	[°C]	150
M_g	[g/m ³ _{n,dry}]	180
C_{NH_3}	[mg/m ³ _{n,dry}]	75
C_{SO_2}	[mg/m ³ _{n,dry}]	2500
C_{HCl}	[mg/m ³ _{n,dry}]	0
C_{NO_x}	[mg/m ³ _{n,dry}]	0
C_{O_2}	[vol%]	10
C_{CO_2}	[vol%]	10
UV - light	[W/m ²]	yes
dust	[mg/m ³ _{n,dry}]	no

6.8 Validation of the wind tunnel's fluid dynamics

Another part of the studies consisted of the testing of the flow field inside the wind tunnel. It was checked if the assumptions of the theoretical model (uniform wind profile, turbulent exhaust gas stream) could be reproduced in our equipment. Therefore the chloride concentrations of the different samples collected were compared to the concentrations predicted by the model described in Chapter 4. The theoretical concentrations for the experiments in lab-scale (stack diameter 3.2cm, wind velocity 0.35 m/s) were calculated using Equation 4.1 as well as the Equations 4.9 to 4.14. The theoretical as well as experimental chloride concentration profiles for two different ambient conditions are represented in Figure 6.21 ($T_g = 150^\circ C$, $T_a = 18^\circ C$, $M_a = 85\%$) and in Figure 6.22 ($T_g = 150^\circ C$, $T_a = 9^\circ C$, $M_a = 60\%$).

The comparison of the experimental with the theoretical chloride concentrations inside the tunnel permits to evaluate the down-scaling of the equipment (stack, tunnel, etc.). The formation of chloride is a practically instantaneous and at ambient temperatures irreversible reaction so that the ammonium chloride formed can be considered as a tracer. In fact the concentration profile is mainly influenced by the

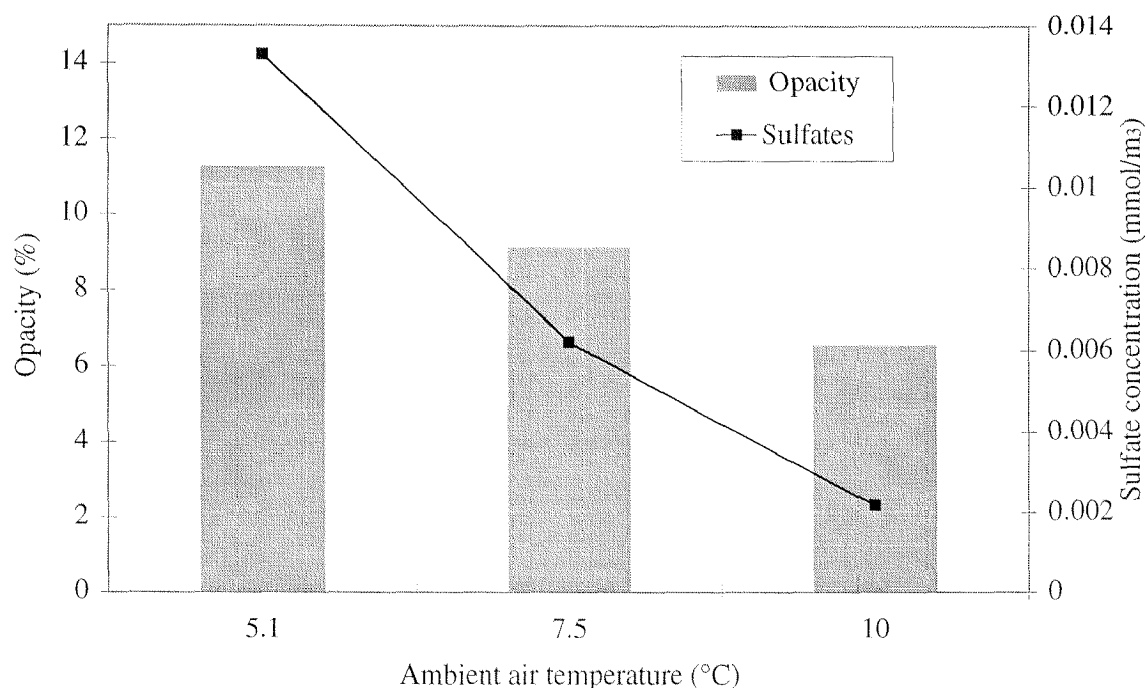


Figure 6.18: Opacity values and sulfate concentrations of the ambient air temperature series at $M_a=60\%$, $T_g=150^\circ\text{C}$, $C_{NH_3}=75\text{ mg}/m_{n,dry}^3$, $C_{SO_2}=2500\text{ mg}/m_{n,dry}^3$

entrainment rate of ambient air. This entrainment rate itself is influenced by the geometry of the plume (plume inclination angle) as well as the different velocities, i. e. wind speed and exhaust gas velocity (see Equation 4.1). It has been shown that the model presented in Chapter 4.1 describes the dispersion of plumes both in the field as well as under laboratory conditions in small wind tunnels well (Hoult et al., 1969; Fay et al, 1970; Hewett et al., 1971; Hoult and Weil, 1972; Damle et al., 1984).

In our case there is a very good agreement between the theoretical and experimental chloride concentration values. In fact the largest deviation between the measured and predicted values is 50 % (see Figure 6.21) and 60 % (see Figure 6.22). These values are rather low considering that the dimensions of the wind tunnel are large with respect to the air-conditioning of the wind tunnel, compared to other comparable wind tunnels. In fact the thermal influences on the air flow profile can be enormous. This was the case during the start-up phase of the

Table 6.17: Experimental conditions for the exhaust gas temperature series

variable	units	value
T_a	[°C]	9
M_a	[% r.h.]	60
T_g	[°C]	150 to 230
M_g	[g/m ³ _{n,dry}]	180
C_{NH_3}	[mg/m ³ _{n,dry}]	75
C_{SO_2}	[mg/m ³ _{n,dry}]	2500
C_{HCl}	[mg/m ³ _{n,dry}]	60
C_{NO_x}	[mg/m ³ _{n,dry}]	0
C_{O_2}	[vol%]	10
C_{CO_2}	[vol%]	10
UV - light	[W/m ²]	yes
dust	[mg/m ³ _{n,dry}]	no

experimental equipment. However a lot of efforts were made so that in the end the flow inside the wind tunnel behaved quite satisfactorily (see Appendix B). Moreover the concentrations of the salts that have been compared are extremely small (ppb) so that very small deviations are quite obvious.

The fact that for low ambient temperatures, the deviation between experimental and theoretical concentrations values is a little bit higher shows that the thermal effects on the air flow are enormous. In fact at low ambient temperatures the problem of stratification is more important than at higher ambient temperatures. This is why differences of 60% in case of low ambient temperatures can be considered as rather low. The fact that the experimental values are higher than the theoretical ones indicates that the air flow predicted by the model is more turbulent than the actual flow inside our wind tunnel. The reason for this is that the entrainment rate predicted by the model is more important than the one observed in the wind tunnel. Therefore the ammonium chloride concentration is slightly lower in the predictions than in the experiments.

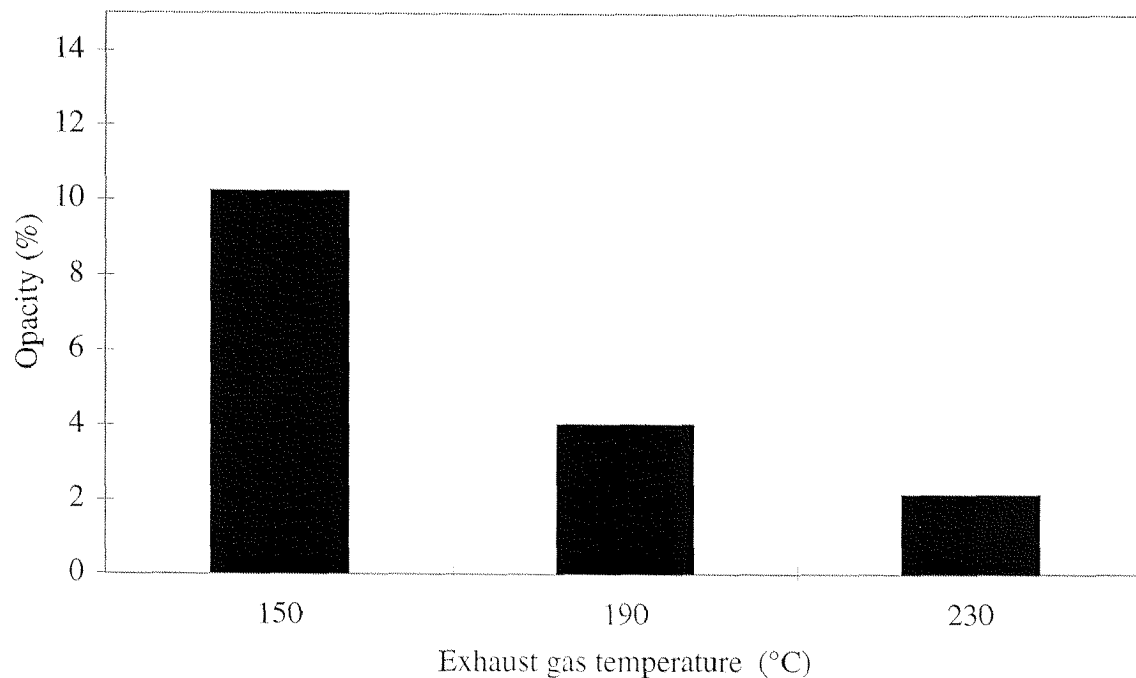


Figure 6.19: Opacity readings of the exhaust gas temperature series at $T_a=9^\circ\text{C}$ and $M_a=60\%$; $C_{NH_3}=75\text{ mg}/m_{n,dry}^3$, $C_{HCl}=60\text{ mg}/m_{n,dry}^3$

The experiments in our equipment can reproduce the assumptions of the theoretical plume dispersion model (roughly constant wind profile, turbulent exhaust gas stream).

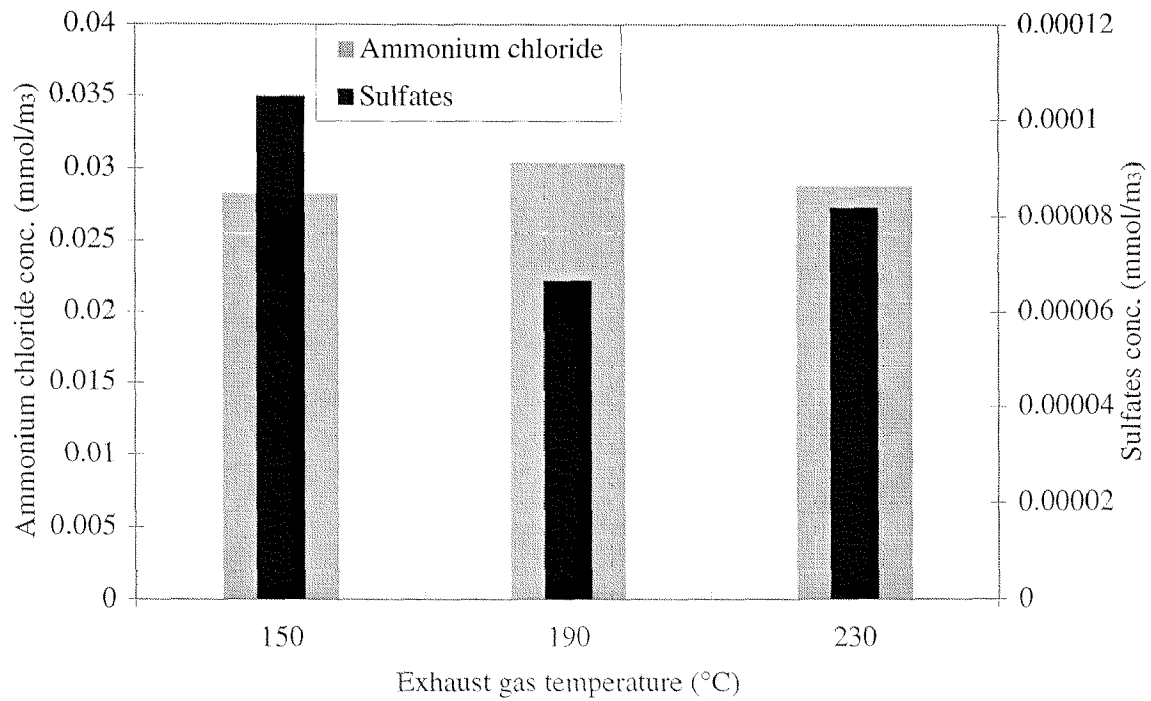


Figure 6.20: Results of the chemical analysis of the exhaust gas temperature series at $T_a=9^\circ\text{C}$ and $M_a=60\%$; $C_{\text{NH}_3}=75 \text{ mg}/\text{m}^3_{n,\text{dry}}$, $C_{\text{HCl}}=60 \text{ mg}/\text{m}^3_{n,\text{dry}}$

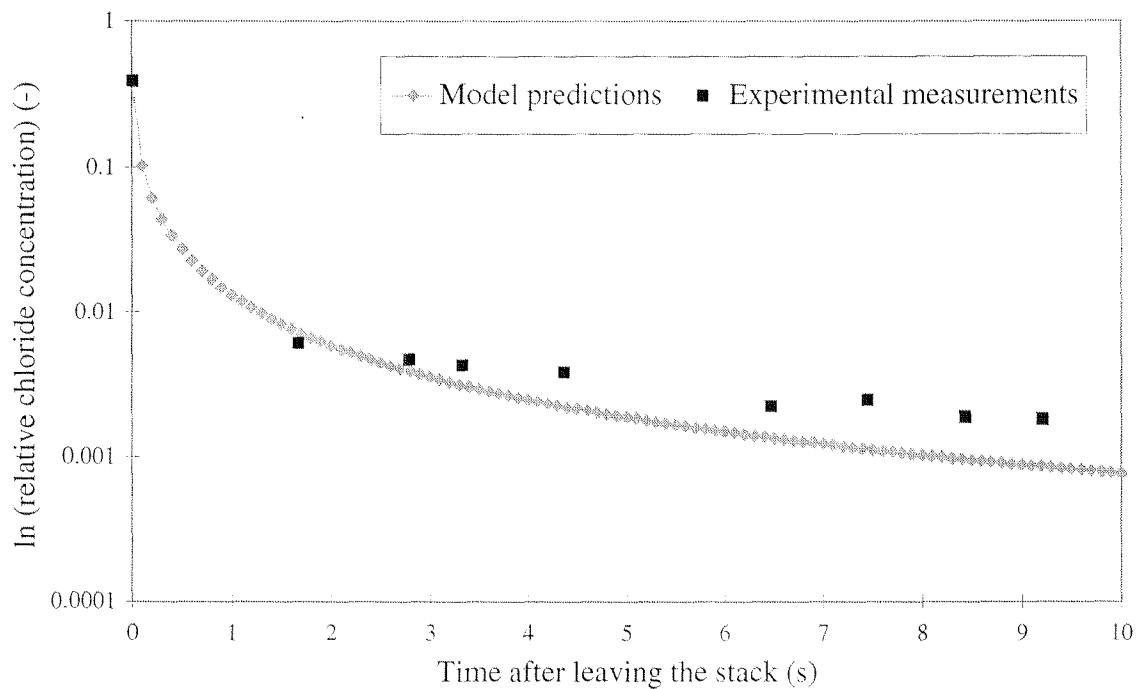


Figure 6.21: Experimental and predicted (model) ammonium chloride concentrations along the wind tunnel at stack height vs. time after leaving the stack; $T_g = 150^\circ\text{C}$, $T_a = 18^\circ\text{C}$, $M_a = 85\%$, $v_a = 0.35 \text{ m/s}$

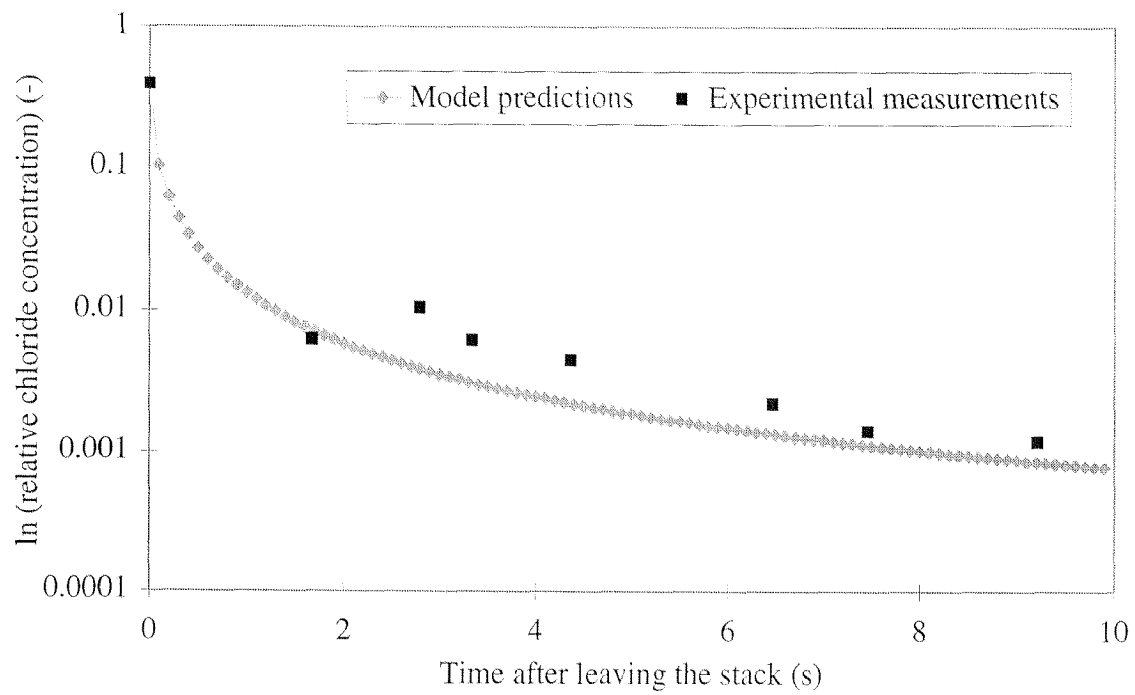


Figure 6.22: Experimental and predicted (model) ammonium chloride concentrations along the wind tunnel at stack height vs. time after leaving the stack; $T_g = 150^\circ C$, $T_a = 9^\circ C$, $M_a = 60\%$, $v_a = 0.35$ m/s

7.1 Influence of temperature

As far as the temperature of the exhaust gas T_g as well as of the ambient air T_a are concerned, the expected inversely proportional influence on plume opacity was shown. There are several reasonable explanations for this influence.

First of all an increase of the exhaust gas temperature leads to a dilution effect. Given a constant molar emission of different components an increase of the temperature leads to an increase of the molar volume. This is why the concentrations of the different components at higher temperatures are lower as the same number of moles of the components are dispersed over a larger volume. The lower the concentrations of the reacting components the lower the reaction rate and hence the formation of aerosols.

However as this effect could be foreseen, this dilution effect was controlled in our experiments. While increasing the exhaust gas temperature the gas flow rates of the different exhaust gas components were adjusted in such a way that the concentrations of the different components were identical no matter the exhaust gas temperature. It has been shown in Chapter 3 that the lower the temperature the more the formation of ammonium chloride salts is favoured.

In order to have a lower plume temperature two possibilities exist. First of all if the exhaust gas temperature is already low at the stack exit, more ammonium chloride aerosols will be formed than if the exhaust gas temperatures were higher. On the other hand, given an exhaust gas temperature the cooler the ambient air the faster the plume temperature is decreased as the temperature gradient (and hence the driving force of the cooling process) is higher. In fact at the stack exit two competing phenomena are occurring. Ambient air is entrained into the plume. This decreases the concentrations of the different components in the plume and hence the reaction rate between these components.

On the other hand not only the concentrations are decreased due to this entrainment but also the temperature of the plume. Equation 4.13

shows that the change in temperature is directly proportional to the temperature gradient. This is not the case for the change in concentrations (see equation 4.14). This means that in our case the cooling of the plume is the dominant effect during the ambient air entrainment. In case of the ammonium chloride formation reaction the decrease of the temperature leads to an increase in the amount of ammonium chloride formed and hence to an increase of opacity.

In addition a higher exhaust gas temperature leads to a higher buoyancy as the difference between the ambient air's density and the plume's density is more important. The temperature influences directly the ratio of inertia to buoyancy forces at the stack exit by the way of the temperature excess Δ_i (see equation 5.4).

Moreover the lower the ambient air temperature the more important the steam plume formation and the slower the dissipation of this steam plume. This is very important during the sulfur dioxide oxidation (see Section 7.3).

7.2 Formation of ammonium chloride

Given the presence of both ammonia and hydrogen chloride in the exhaust gas it could be shown that ammonium chloride is formed. The formation of these aerosols occurs by the following steps:

1. First of all there is an extremely fast (nearly instantaneous) reaction between HCl and NH_3 (reaction rate $11.4 \times 10^6 [\text{cm}^3 \text{mol}^{-1} \text{sec}^{-1}]$ at 25°C (Dahlin, 1981; Countess and Heiklen, 1973)). This gas phase reaction proceeds sufficiently far for the supersaturation ratio to exceed unity.
2. Afterwards, in absence of dust (in our equipment no significant amounts of dust were added to the exhaust gas), a homogeneous nucleation takes place. This homogeneous nucleation can either be homomolecular or heteromolecular (for example in presence of water droplets). The homogeneous-homomolecular nucleation does

not occur unless the vapour phase is supersaturated. Under atmospheric conditions, heteromolecular nucleation with water droplets can occur at a rate many orders of magnitude above that of homomolecular nucleation because the heteromolecular nucleation can take place even when a mixture of vapours is undersaturated with respect to the pure vapours as long as it is supersaturated with respect to the critical solution. In addition to this the heterogeneous condensation of reactive vapour species on an aerosol particle takes place.

3. The nucleation process is quenched due to the loss of the nucleating species from the gas phase by diffusion to the freshly formed aerosol on one side and by decreasing the vapour concentrations (and hence the saturation ratio) of the reactive components due to ambient air entrainment on the other hand. Only heterogeneous condensation can take place at this point.
4. The last step consists in the accumulation mode where particles can coagulate. However during the very short time interval considered in our experiments this event may be neglected.

The conditions for the formation of ammonium chloride are fulfilled in theory and the formation of ammonium chloride could be proven with the help of experiments in our wind tunnel. In our case the formation of ammonium chloride is due to the nucleation of dry NH_4Cl . This can be shown by the fact that the absence or presence of water in the exhaust gas has no influence on the ammonium chloride formation in our experiments. This is why the binary nucleation $\text{NH}_4\text{Cl}-\text{H}_2\text{O}$ can be neglected. Moreover there was no significant influence of ambient humidity neither on the formation of ammonium salts nor on plume opacity.

The fact that ammonia as well as hydrogen chloride show a small proportional influence on plume opacity can be explained by the characteristic properties of the fractional factorial design. Ammonia as well as hydrochloric acid taken separately have an influence on plume opacity

but the effect becomes even more important when the two components are present at the same time in the exhaust gas. An increase of the hydrogen chloride concentration at a constant ammonia concentration leads to a higher ammonium chloride formation and hence to a higher opacity. However in absence of ammonia, the influence of HCl on opacity was small. What has been said for HCl is also true for ammonia. Ammonia taken alone does not absorb visible light and hence does not contribute to opacity directly. However ammonia is essential for the ammonium chloride formation as well as for the sulfate formation by the way of sulfur dioxide oxidation (see Section 7.3).

7.3 Sulfate formation and its influence on opacity

No influence of sulfur dioxide taken alone on plume opacity could be observed. Moreover the tests in which sulfur dioxide, ammonia and an aqueous phase were combined, were not successful as far as the formation of sulfates is concerned. The hypotheses that under these conditions sulfur dioxide can be oxidized within 15 seconds to sulfates (Dellinger, 1980) was only verified by introducing another very important variable, the ambient temperature T_a . The hypotheses and mechanisms described in Section 3.3 were verified for ambient temperatures below 6°C. For the formation of sulfates by oxidation of sulfur dioxide, not only the fact that moisture is present in the exhaust gas is important but also the dimensions of the steam plume. The dimensions of this steam plume are influenced by ambient temperature. The lower the ambient air temperature the longer the steam (primary) plume.

As described in Dellinger (1980) sulfur dioxide can be oxidized in the presence of water and ammonia to sulfates. However in our experiments it was shown that the ambient temperature (and hence the dimensions of the steam plume) are very important. At temperatures below 6°C the steam plume was present long enough (5 to 6 seconds) so that there was enough time for the sulfur dioxide oxidation to occur. The higher the ambient temperature, the sooner the steam plume dissipates.

However it is evident that the aqueous phase in the plume is present in form of fine droplets. The variation of the moisture content of the exhaust gas at constant ambient temperature did not influence the formation of sulfates.

However it has to be noted that the amount of sulfates formed was not as important as the amount of ammonium chloride formed even when the sulfur dioxide concentration was much higher ($2500 \text{ mg/m}_{n,dry}^3$) than the hydrogen chloride concentration ($60 \text{ mg/m}_{n,dry}^3$). The reason for this is that hydrogen chloride reacts readily with ammonia whereas sulfur dioxide has to be oxidized to sulfuric acid first before reacting with ammonia.

The fact that a large quantity of ammonium chloride was formed compared to ammonium sulfates indicates that the impact of ammonium chloride on opacity was more important too.

7.4 Hydrocarbons/UV - light/ NO_x

For the reasons mentioned in Chapter 6 the experiments were focused on inorganic exhaust gas components. This is why no influence of hydrocarbons could be studied in this work. In absence of these hydrocarbons neither UV - light nor nitrogen oxides did show any effect on plume opacity. Nitrogen monoxide does not absorb visible light. Nitrogen dioxide vapours are of brown colour, however their concentrations were so small ($2.5 \text{ mg NO}_2/\text{m}_{n,dry}^3$ / ($47.5 \text{ mg NO}/\text{m}_{n,dry}^3$)) that these vapours were not visible in our equipment. This is also the case for exhaust gases in the field as the plume is detached at the stack exit because the exhaust gases are invisible at that point.

In our experiments UV - light did not show any influence on chemistry or opacity either. However in presence of NO_x , UV - light as well as hydrocarbons, the formation of ozone will take place (see Figure 3.2). This ozone then will react readily to form other species.

7.5 Influence of oxygen

In our experiments oxygen had no significant influence on opacity. The fact that the oxygen concentration had no influence on the sulfate formation also confirms the sulfur dioxide oxidation mechanism by the way of an aqueous phase mentioned in Chapter 3. The oxydation of sulfurous acid to sulfuric acid in the plume takes place in presence of entrained atmospheric oxygen.

7.6 Influence of ambient as well as exhaust gas humidity

The experiments showed that the ambient humidity as well as the exhaust gas moisture content did not have any relevant influence on plume opacity. As far as the sulfur dioxide oxidation is concerned, the presence of moisture in the exhaust gas is necessary, however the amount of water present in the exhaust gas is not important. Only the fact that this water has to be present in form of dispersed small water droplets (steam plume) is important.

One aspect that has to be considered is that at very high exhaust gas moisture contents (more than $200 \text{ g H}_2\text{O}/\text{m}_{n,dry}^3$ at 8.5°C) opacity due to ammonium chloride formation could possibly be increased as these salts are very hygroscopic. This threshold value can be explained by the fact that below this concentration the distance between water droplets and aerosols is quite large and that the steam plume dissipates very quickly.

7.7 Influence of dust

In our experiments the amount of dust was extremely small so that no influence of dust on plume opacity formation by the way of a heterogeneous nucleation could be studied. However dust should at least have a proportional influence on plume opacity as dust would scatter light

just as do aerosols.

7.8 Relevance for industry

Different inorganic aspects of the opacity phenomena have been studied in several experiments. With the results of the present work a few guidelines, as far as in-process as well as end-of-pipe technologies (for instance scrubbers) are concerned for reducing plume opacity, are given.

- **Temperature:** Temperature had a big influence on opacity. When using scrubbers for eliminating some precursor substances leading to opacity it has to be noticed that the exhaust gas temperature will be decreased. However a decrease of the exhaust gas temperature increases opacity. In case that not enough hydrogen chloride or ammonia for instance can be removed, opacity must not necessarily decrease. In fact the small positive effect of an opacity reduction by the removal of components could be annuled by a much bigger increase of opacity due to the temperature decrease of the exhaust gas. Unfortunately as far as the ambient temperature is concerned nothing can be done about this.

Heating up the gases after the scrubber by injecting hot air into the gas exhaust stream could be an additional measure to be taken in order to try meeting regulations on plume opacity. On one hand the gas exhaust components' concentrations could be reduced furthermore (the exhaust gas volume increases) on the other hand the formation of ammonium chloride could be reduced due to smaller reaction rates (the higher the temperature, the more the reaction equilibrium is located on the side of the gaseous species, i. e. hydrogen chloride and ammonia).

- **Active components:** Experiments showed that at normal exhaust gas concentrations hydrogen chloride had a much bigger impact on opacity as did sulfur dioxide. For plants having both sulfur dioxide as well as hydrogen chloride emissions it could be

interesting to concentrate on the reduction of hydrogen chloride rather than of sulfur dioxide, as ammonium chloride has a higher impact on opacity than have ammonium sulfates. In fact it was shown that by decreasing the HCl concentration from 204 to 81.6 mg/m³_{n,dry} opacity could be reduced from 20 to 10 % whereas opacity was only decreased from 15 to 7 % by reducing the sulfur dioxide concentration from 3571 to 1000 mg/m³_{n,dry} (see Figure 6.13). In case a plant has serious sulfur dioxide emission problems it is better to concentrate on the reduction of sulfur dioxide rather than on ammonia. In the presence of small quantities of ammonia the oxidation of sulfur dioxide to sulfates is still possible at low ambient temperatures. In this case, once sulfuric acid is formed a bimolecular nucleation with water droplets can take place in order to form the acid mist which also absorbs visible light. This is not the case for ammonia.

- **Moisture content:** Variation of moisture contents of both the ambient air as well as the exhaust gas showed to have no significant influence on opacity. However the addition of moisture to the exhaust gas while using scrubbers could increase opacity because in this case the addition of water is excessive. In this case, acid mist could be formed when sulfur dioxides are present. Special attention should be paid to this phenomenon while designing scrubbers.

Hydrocarbons

Although within this project no influence of organic matter on plume opacity was studied, the role of hydrocarbons should be discussed briefly as hydrocarbons can represent a serious problem as far as opacity phenomena are concerned. Hydrocarbons react readily with NO_x and UV - light (see Figure 3.2). At the same time ozone is formed which can oxidize for instance sulfur dioxide (as well as many other components; see Table 3.2), so that the problem related to sulfates becomes more obvious. Often hydrocarbons themselves have the potential to ab-

sorb visible light. In order to avoid such reactions, the hydrocarbons' concentration should be reduced (by the way of thermal treatment of the exhaust gases, scrubbers). A supplementary measure that could be taken is the effective NO_x reduction by the way of ammonia injection in to the furnace at temperatures around 1000°C . However the dosing of the ammonia has to be done carefully as otherwise additional ammonia would be added to the exhaust gas.

Design considerations

Increasing the exhaust gas velocity leads to enhanced entrainment (see Equation 4.1) and hence to a faster dilution of the exhaust gas components with ambient air. The exhaust gas velocity could be increased by reducing the stack diameter. In addition opacity would decrease due to the fact that a plume with a smaller diameter absorbs or scatters light less than a plume of exactly the same particle (aerosol) concentration but with a larger diameter. The plume temperature would decrease faster as a consequence of the fast dilution of the plume. However the opacity of a cooler exhaust gas is higher as it has been shown in Chapter 6. The interaction of the two opposite influences (cooling vs. dilution) has not been studied so far, however the dilution effect should be more important than the cooling effect so that smaller exits of the stacks are justified.

Moreover as higher exhaust gas temperatures lead to a decrease in opacity, hot air could be added to the exhaust gas. This measure would have 3 consequences:

1. The concentration of different exhaust gas components is decreased \implies opacity decreases
2. At constant stack diameter the increase of the exhaust gas volume leads to an increase of the exhaust gas velocity \implies increased entrainment velocity of ambient air and probably decreased opacity.
3. Finally the exhaust gas temperature is increased \implies opacity decreases.

Chapter 8

Outlook

In the present work an experimental equipment for simulating the formation of secondary plumes under different exhaust gas as well as atmospheric conditions has been designed, constructed and is fully operational. With the help of this equipment the influence of different variables was studied. The results concerning the influence of hydrogen chloride compared to sulfur dioxide, of the exhaust gas temperature as well as of the exhaust gas moisture content are of importance for the design and lay-out of in-process and end-of-pipe technologies in order to meet present opacity standards.

Within this project only the influences of inorganic precursor substances leading to plume opacity were studied. Therefore it would be very interesting to study the effect of organic compounds on plume opacity.

Moreover the modelling of secondary plume formation could be very interesting. One critical point of this modelling is the nucleation process (homogeneous as well as heterogeneous). In fact it has to be taken into account that the classical nucleation theory (Wilemski, 1984) is not anymore considered as being suitable for describing the nucleation process of a multicomponent vapour. From the thermodynamical point of view it is even incorrect (Viisanen et al., 1997). In fact in this theory the critical cluster size was determined numerically by using the Gibbs free energy of a liquid cluster at the saddle point. This method accounts not for surface adsorption and is equivalent to the theory presented by

Doyle (Doyle, 1961) which contains an extra surface tension derivative term. A new theory has been presented (Viisanen et al. 1997) which does not use this extra surface tension derivative term but considers surface adsorption phenomena and hence does not overpredict the nucleation rate. Moreover a device for determining the particle size distribution (for example a condensation nuclei counter (CNC)) should be added to the equipment in order to determine particle size distributions experimentally in order to compare them with the values given by the model.

Other authors have used the classical nucleation theory introducing however semi-empirical correction or tuning factors (Raes et al., 1992; Russell et al., 1994; Pandis et al., 1994).

A further possibility could be the determination of exact threshold values for the hydrogen chloride and ammonia concentrations and the correlation of experimental opacity values with real field opacity values. Therefore as well as for deeper insight in the scale-up, also experiments should be carried out at a plant and the same experiments should be reproduced in lab-scale.

Besides it could be interesting to study in lab-scale other influences on plume opacity in the future: for example influence of stack geometry (height, diameter), exhaust gas velocity or colour of the tunnel walls (which stands for the colour of the sky and is essential for the determination of opacity-dispersion correlation) on plume opacity.

Symbols, Abbreviations and Subscripts

8.1 Abbreviations

CAA	Clean Air Act
CEMS	continuous emission monitoring system
CNC	condensation nuclei counter
coeff	fractional factorial design coefficients
DAQ	data acquisition
EPA	Environmental Protection Agency
ESP	electrostatic precipitator
FFD	fractional factorial design
IR-light	infrared light
MIO	multipurpose Input/Output
PC	personal computer
ref	photometer reference measurement value
RM	Rauchgasmeßgerät
SCNR	selective catalytic nitrogen oxide reduction
UV-light	ultraviolet light
VDC	voltage direct current

8.2 Symbols

8.2.1 Latin symbols

A	attenuation coefficient	(m ² /g)
b	plume radius	(m)
b	FFD parameter	(-)
b _i	stack radius	(m)
C	species concentration	(mol/m ³)
C _m	dust mass concentration	(g/m ³)
Fr	densimetric Froude number ($= \frac{u_i}{\sqrt{g\Delta_i b_i}}$)	(-)
g	gravitational acceleration constant	(m/s ²)
K	equilibrium constant	(-)
L	path length	(m)
M _a	relative humidity of the ambient air	(%)
M _g	exhaust gas moisture content	(g water/m ³)
MW	average molecular weight	(g/mol)
\mathcal{R}	dimensionless speed ratio ($= \frac{u_i}{v}$)	(-)
R	effective plume radius	(m)
Re	Reynolds number ($= \frac{2u_i b_i}{\nu}$)	(-)
Ri	Richardson number ($= \frac{1}{Fr^2}$)	(-)
s	plume coordinate along plume axis	(m)
t	time	(s)
T	temperature	(K)
u	plume velocity	(m/s)
U	average plume velocity	(m/s)
u _i	exhaust gas velocity	(m/s)
V _a	ambient wind velocity	(m/s)
V _e	entrainment velocity	(m/s)
x	horizontal distance downwind of the stack exit	(m)
x _i	fractional factorial design variable	
y	response function (photometer value)	(-)
\bar{y}	mean photometer value	(-)
z	vertical distance above the stack exit	(m)

8.2.2 Greek symbols

α	empirical entrainment constant	(-)
Δ_i	excess temperature ratio at the stack exit $\frac{T_i - T_1}{T_1}$	(-)
ν	kinematic viscosity of the ambient flow	(m ² /s)
Θ_i	weighting factor of the FFD variable	(-)
Θ	plume inclination angle	(°)
Θ	light scattering angle	(°)
ρ	density	(g/m ³)

8.3 Subscripts

a	of the ambient air
e	of the entrained air
field	field data
g	gaseous
i	at the stack exit
i	number of variables, components
\boxed{i}	dispersion photometer sampling location
lab	under laboratory conditions
m	mass, particulate matter
p	of the plume
s	solid
1	of the ambient air at the stack height

References

- Box, G., Hunter, J. (1986) *Statistics for experiments*. John Wiley & Sons, New-York, ISBN 0-471-09315-7.
- Briggs G. (1965) *A plume rise model compared with observations*. J. Air Pollut. Control Assoc., 15(9), 433-438.
- Briggs G. (1975) *Lectures on air pollution and environmental impact analyses*. workshop Boston - Mass., American Meteorological Society, 29 September-3 October.
- Caluori, A. G. (1995), *Personal communication*. BCU, Untervaz.
- Carbolite (1997) *Reference manual*. Carbolite Furnaces Ltd., Sheffield, England.
- Chadbourne, J. F., Baker, B. A., Brown, R. L. (1980) *Reactive plumes - sampling and opacity concerns for cement kilns*. Annual APCA Meeting, Montreal, Quebec, June 22-27.
- Chadbourne, J. F. (1994) *Dynamic plumes hazardous air pollutants and the community right to know*. Annual APCA Meeting, Montreal, Quebec, June 22-27.
- Cheney, J. L., Conner, W. D., Benett, R.L., Luke, D. L., Walters, C. L., Knapp, K. T. (1983) *Formation of a detached plume from a cement plant*. Report No. EPA-600/3-83-102. Environmental Sciences Research Laboratory, Research Triangle Park, North Carolina.
- Cheney, J. L., Knapp, K. T. (1986) *Investigation of the formation of a Portland cement plant detached plume*. Report No. EPA-600/3-

- 86-029, Atmospheric Sciences Research Laboratory, Research Triangle Park, North Carolina.
- Cheney, J. L., Knapp K. T. (1987) *A study of ammonia source at a Portland cement production plant*. JAPCA, 37(11), 1298-1302.
- Collombier, D. (1996) *Plans d'expérience factoriels*. Mathématiques et applications 21, Springer, Paris.
- Countess, R. J., Heicklen, J. (1973) *Kinetics of particle growth. II. Kinetics of the reaction of ammonia with hydrogen chloride and the growth of particulate ammonium chloride*. J. Chem. Phys., 77(4), 444-447.
- CTL Project 050702 (1995) *Hydrogen chloride: Formation, Scrubbing and Emission Status report*. March 1995.
- Dahlin, R. S., Su, Ja-An, Peters, L. K. (1981) *Aerosol formation in reacting gases: Theory and application to the anhydrous NH₃-HCl system*. AIChE Journal, 27(3), 404-417.
- Damle, A. S., Ensor, D. S., Sparks, L. E. (1984) *Predictions of the opacity of detached plumes formed by condensation of vapors*. Atmos. Environ., 18, 435-444.
- Damle, A. S., Ensor, D. S., Sparks, L. E. (1987) *Options for controlling aerosols to meet opacity standards*. JAPCA, 37(8), 925-933.
- Danfoss (1993) *VLT Serie 3000 Produkthandbuch*. Danfoss, Dänemark.
- Davidson, G. A. (1989) *Simultaneous trajectory and dilution predictions from a simple integral plume model*. Atmos. Environ., 23, 341-349.
- Dellinger, B., Grotecloss, G., Fortune, C. R., Cheney, J. L., Homolya, J. B. (1980) *Sulfur dioxide oxidation and plume formation at cement kilns*. Environ. Sci. Technol., 14, 1244-1249.
- Dickinson, H. W., Jenkins, R. (1981) *James Watt and the Steam Engine: the memorial volume prepared for the Committee of the Watt*

- Centenary Commission at Birmingham 1919*. Ashbourne : Moorland, second edition, ISBN 0-903485-92-3.
- Doyle, G. J. (1961) *Self-nucleation in the sulfuric acid-water system*. J. Chem. Phys., 35(3), 795-799.
- Dubois, R., Flores, G. (1996) *Reporte cualitativo de las pruebas realizadas para eliminar la formación de la columna de vapores de Cloruro de Amonio en el proceso de producción de Clinker en la Planta de Tecomán, Colima*. Apasco Reporte No. GPR-R-96-09
- Environment Agency (1999) *Agency emerges from the smoke*. Environment information; environment action, issue 18, March 1999.
- EPA (1984) *Visible determination of the opacity of emissions from stationary sources*. EPA Research Triangle Park, EPA-600/4-77-027b, February 1984.
- EPA (1997A) *Notice of violation EPA-5-97-WI-17*.
- EPA (1997B) *Environmental News Release No. 97-OPA326*. December 1.
- EPA (1998A) *Environmental News Release No. 98-OPA015*. January 21.
- EPA (1998B) *Environmental News Release No. 98-OPA155*. March 31.
- EPA (1998C) *Environmental News Release No. 98-OPA306*. October 19.
- Ervin, E. (1996) *Personal communication*. Holnam Inc., Florence, CO.
- Fay, J. A., Escudier M., Hoult D.P. (1970) *A Correlation of Field Observations of Plume Rise*. J. Air Pollut. Control Assoc., 20(6), 391-397.
- Federal Register (1971) *Standards of performance for new stationary sources.*, 36(247), 24878-24895.

- Federal Register (1974) *Opacity provisions for new stationary sources promulgated and appendix A, Method 9-Visual determination of the opacity of emissions from stationary sources.*, 39(219), 39872-39876.
- Finlayson-Pitts, B. J., Pitts jr., J. N. (1986) *Atmospheric Chemistry: Fundamentals and Experimental Techniques*. John Wiley & Sons, New-York.
- Frankhauser, U. (1995) *Telex*. "Holderbank" Management und Beratung AG., June 13.
- Güemez-Garcia, R., Ganatra, C. P., Gore, W. L., and Associates (1994) *Elimination of emission problems at Cementos Guadalajara*. World Cement, 50-57.
- Grize, Y.L. (1999) *Versuchsplanung leicht gemacht mit STAVEX*. Workshop STAVEX, Mettler-Toledo (Schweiz) AG, Greifensee, April.
- Haury, G. (1976) *Untersuchungen zur katalytischen Oxidation von Schwefeldioxid an Aerosolen unter atmosphärischen Bedingungen.*, Dissertation Universität Heidelberg und KFK Bericht 2318UF.
- Haury G.(1979) *Das Ausmaß von katalytischen SO₂-Reaktionen in Rauchfahnen*. Staub Reinhalt. Luft, 39, 241-245.
- Hawks, R.L., Rose, T. (1995) *A proactive approach to minimizing opacity from cement kilns.*, IEEE-IAS, 0-7803-2456-0/95, 451-463.
- Heinsohn, R. J., Davis, J. W., Anderson, G. W. (1992) *Individual accuracy in estimating plume opacity*. JAPCA, 42(4), 443-447.
- Hess, T. (1993) *Potential for visible plume formation at a coal-fired boiler using ammonia injection for non-catalytic NO_x control*. Proc. Annual Meeting APCA, 86th(8), 93-RP-135.05.
- Hewett, T. A., Fay, J. A., Hoult, D. P. (1971) *Laboratory experiments of smokestack plumes in a stable atmosphere*. Atmos. Environ., 5, 767-789.

- Hoigné, J. (1992) *Environmental chemistry I*. Scriptum of the lecture at the chemical engineering department, ETH Zürich.
- Hoult, D. P., Fay, J. A., Forney, L. J. (1969) *A Theory of Plume Rise Compared with Field Observation*. J. Air Pollut. Control Assoc., 19(8), 585-590.
- Hoult, D. P., Weil, J. C. (1972) *Turbulent plume in a laminar cross-flow*. Atmos. Environ., 6, 513-531.
- Hung, R., Liaw, G. (1981) *Advection Fog Formation in a Polluted Atmosphere*. J. Air Pollut. Control Assoc., 31(1), 55-61. 55-61.
- Hungerbühler, K., Ranke J., Mettier, T. (1999) *Chemische Produkte und Prozesse; Grundkonzepte zum umweltorientierten Design*. Springer Verlag, Berlin.
- Ilmac 96 (1996) *Personal communications of different suppliers of devices for dosing powder* International trade fair and congress for chemical technology analytics and biotechnology, trade fair Basle, Switzerland, November 19-22, 1996.
- Kent, W. (1897), Engineering News, November 11.
- Kunsch, J.-P. (1996) *Personal communication*. Institut für Fluidodynamik, ETH, Zurich, Switzerland.
- Küpfer, M. (1999) *Personal communication*. Laboratory for Technical Chemistry, ETH, Zurich, Switzerland.
- Kutschera, P. (1999) *Personal communication*. "Holderbank" Management and Consulting Ltd., Holderbank, Switzerland.
- Lindau, L. (1991) *NO₂ effect on flue gas opacity*. JAPCA (note-book), 1098.
- Lou, J. C., Lee, M., Chen, K. S. (1997) *Correlation of plume opacity with particles and sulfates from boilers*. J. Environ. Eng., July 1997, 698-703.

- MacIver, D. Y., Yannone, M. A., Klemm, W. A., Adams, L. D. (1988) *Reaction products or pseudoparticulate issues in testing Portland cement plant emissions*. Annual APCA Meeting, Dallas, Texas, June 19-24.
- Mamane, Y., Gottlieb, J. (1989) *Heterogeneous reactions of minerals with sulfur and nitrogen oxides*. J. Aerosol Sci., 20(3), 303-311.
- McLean, R. A., Anderson, V. L. (1984) *Applied factorial and fractional designs*. Statistics textbooks and monographs, Vol 55, Marcel Dekker, Inc., New York.
- McMurry, P. H., Grosjean, D. (1985) *Photochemical formation of organic aerosols: growth laws and mechanisms*. Atmos. Environ., 9, 1445-1451.
- Netterville, D. D. J. (1990) *Plume rise, entrainment and dispersion in turbulent winds*. Atmos. Environ., 24A, 1061-1081.
- Oberholzer, B., (1992) *Untersuchungen über den Einfluß von anorganischen Spurenstoffen auf die Zusammensetzung des Niederschlages während winterlichen Feldmessungen an der Rigi (Zentralschweiz)*, Dissertation ETHZ Nr. 9854.
- Ooms G. (1972) *A new method for the calculation of the plume path of gases emitted by a stack*. Atmos. Environ., 6,899-909.
- Pandis, S. N., Russell, L. M., Seinfeld, J. H. (1994) *The relationship between DMS flux and CCN concentration in remote marine regions*. J. Geophys. Res., 99(D8), 16945-16957.
- Parker, J. M. (1995) *Continuous Emission Monitoring (CEM)*. Handbook of Air Pollution Control Engineering and Technology, edited by Mycock, J. C., McKenna, J. D., Theodore, L., ETSI, CRC Press Inc.
- Pilat, M. J. (1984) *Plume opacity*. Handbook of Air Pollution Technology, edited by Calvert S., Englund H. M., John Wiley & Sons, New-York., chapter 32.

- Pueschel, R. F. (1993) *Potential climatic effects of anthropogenic aerosols*. Aerosol effects on climate, edited by Jennings S. G., Univ. of Arizona Press, Arizona, chapter 3, 110-132.
- Raber, L. (1997) *Public unaware of air quality gains*. Chem. Eng. News, 75(19).
- Raes, F., Saltelli, A., van Dingenen, R. (1992) *Modelling formation and growth of H₂SO₄-H₂O aerosols: uncertainty analysis and experimental evaluation*. J. Aerosol Sci., 23(7), 759-771.
- Raj, P. E., Devara, P. C. S. (1989) *Some results of lidar aerosol measurements and their relationship with meteorological parameters*. Atmos. Environ., 23, 831-838.
- Richner, T. (1995) *Reduction of opacity in cement plants*. internal report Holderbank.
- Ringelmann, M. (1898) *Méthode d'estimation des fumées produites par les foyers industriels*. La revue technique et les annales des travaux publics et des chemins de fer, 12, 268.
- Rippin, D. W. T. (1992) *Mathematische & System-Methoden*. Skriptum zur Vorlesung, ETH Zürich.
- Römpp (1996) *CD Chemie Lexikon, A - Z*. Thieme Verlag, Stuttgart, 9. Auflage.
- Rose, T. H., Egsegian, R. (1991) *Cement facility out of stack opacity evaluation*. ETA report, Holnam Industries Dundee, Michigan, December 1991.
- Russell, L. M., Pandis, S. N., Seinfeld, J. H. (1994) *Aerosol production and growth in the marine boundary layer*. J. Geophys. Res., 99(D10), 20989-21003.
- Scheffler, E. (1997) *Statistische Versuchsplanung und -auswertung - Eine Einführung für Praktiker*. Deutscher Verlag für Grundstoffindustrie, Stuttgart.

- Seinfeld, J. H. (1986) *Atmospheric Chemistry and Physics of Air Pollution*. John Wiley & Sons, New-York.
- Setzer, A. W., Jacko, R. B., Hoffer, R. M. (1982) *The use of color-IR-photos for air pollution plumes*. J. Air Pollut. Control Assoc., 32(8), 837-838.
- Sick (1995A) *Betriebsanleitung zu MEPA-RM210 Menügeführte Parametrierung*. Sick AG, Reute, Germany.
- Sick (1995B) *RM210 Staubkonzentrations- und Rußzahlmeßgerät*. Sick AG, Reute, Germany.
- Sick(1996) *Electronic documentation system*. Environmental monitoring v. 1.0, Sick AG, Reute, Germany.
- Toro, R. F. (1984) *Source control-food*. Handbook of Air Pollution Technology, edited by Calvert S., Englund H. M., John Wiley & Sons, New-York., chapter 9, 376.
- VA-Datenbank-Blatt (1991) *Detached high opacity plumes*. VA-Dok. N15, "Holderbank" Management und Beratung AG., April 1991.
- Viisanen, Y., Kulmala, M., Laaksonen, A. (1997) *Experiments on gas-liquid nucleation of sulfuric acid and water*. J. Chem. Phys., 107(3), 920-926.
- Weir, A. Jr., Dale, J. J., Papey, L. T., Seymour C., Shiu Chow Yung (1976) *Factors influencing plume opacity*. Environ. Sci. Technol., 10(6), 539-544.
- Wilemski G. (1984) *Composition of the critical nucleus in multicomponent vapor nucleation*. J. Chem. Phys., 80(3), 1370-1372.
- WQA (1997) *WQA Glossary of terms*. Water Quality Association homepage, <http://www.wqa.org/WQIS/Glossary/opacity.htm>.

Appendix A

Opacity reading according to EPA Method 9

Out-of-stack opacity can be measured in several ways (for example lidar aerosol measurement (Raj et al., 1989) or color-IR-photos (Setzer et al., 1982)) but to comply with federal regulations the reading of plume opacity by certified smoke inspectors according to EPA Method 9 is the final arbiter. This method is described in (EPA, 1984).

A.1 Certification and training of observers

The field inspectors and observers are required to maintain their opacity evaluation skills by periodically participating in a rigorous certification program (semi annual).

section Procurement of apparatus and supplies

Method 9 describes in detail the procurement of apparatus and supplies as well as the preobservation operation which will not be discussed here. For the visible emission determination the following procedure has to be followed (EPA, 1984):

A.2 Preobservation operations

These preobservation operations include (among others) the establishing of an observation protocol (number of observers required, applicability of Method 9, etc.) as well as the performance of equipment checks for on-site use.

A.3 On-site field observations

Observer position

The main directives concerning the observer position are the following (Rose and Egsegian, 1991):

1. *The observer must stand at a distance that provides a clear view of the emissions with the sun oriented in the 140° sector to his/her back. If the observer faces the emission/viewing point and places the point of a pencil on the sun location line such that the shadow crosses the observers position, the sun location (pencil) must be within the 140° sector of the line (see Figure A.1).*
2. *When possible, the observer should make observations from a position in which the line of vision is approximately perpendicular to the plume direction.*
3. *The observer must stand at a distance that provides total perspective and a good view.*
4. *In order to comply with the sun angle requirements it is recommended that the observer should try to avoid the noon hours (11:00 a. m. to 1:00 p. m.) in the summertime.*
5. *The reading location should be safe for the observer.*

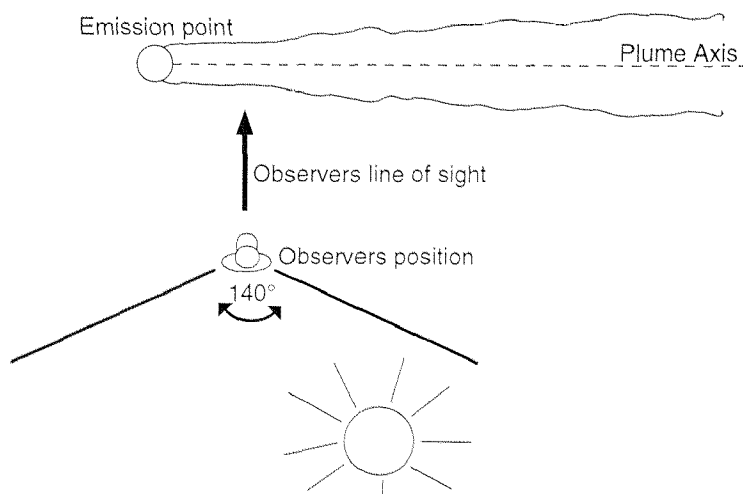


Figure A.1: Source layout sketch

A.3.1 Opacity observations

Some directives concerning the opacity readings are (Rose and Egsegian, 1991):

1. *Opacity observations must be made at the point of greatest opacity in that portion of the plume where condensed water vapor is not present.*
2. *The observer must not look continuously at the plume but should observe the plume momentarily at 15-s intervals*
3. *Location where opacity has to be read for attached plumes (see Section 2.1.2).*
4. *Location where opacity has to be read for detached plumes (see Section 2.1.2).*
5. *Reading must be made to the nearest 5 percent opacity. A minimum of 24 observations must be recorded.*
6. *A clearly visible background of contrasting colour is best for greatest reading accuracy.*

7. *The best viewing spot is usually within one stack diameter above the stack exit, where the plume is densest and the plume width is approximately equal to the stack's diameter.*

A.3.2 Field data: the "Visible Emission Observation Form"

The 1977 revision of EPA Method 9 specifies the recording of certain information in the field documentation of a visible emission observation. The required information includes the name of the plant, the emission location, the type of facility, the observer's name and affiliation, the date and time, the estimated distance to the emission location, the approximate wind direction, the estimated wind speed, a description of the sky conditions and the plume background. Therefore a form was developed that includes not only the data required by Method 9 but also the information necessary for maximum legal acceptability.

A.4 Postobservation operations

The postobservation operations include the establishing of a data summary and a report as well as the data validation and the equipment check.

A.5 Calculations

At the end three different types of calculations can be carried out: the calculation of average opacity, the calculation of path length through the plume and the prediction of steam plume formation.

A.6 Auditing procedures

An audit is an independent assessment of data quality. Observers and analysts other than the original observer or analyst can guarantee this independence.

Appendix B

Solving of fluid dynamical problems

B.1 Initial wind tunnel

In the beginning the tunnel consisted of a box (7m x 1m x 2m) with a rectangular ambient air inlet (0.34m x 0.80m) at a tunnel height of 1.35m and a circular air outlet (diameter 0.35m) at a tunnel height of 0.85m (see Figure B.1). The maximum volume flow rate of the fan was 1800 m³/h. The stack was located near the inlet of the tunnel in order to have a maximum travel distance of the plume in the tunnel. The average wind velocity inside the tunnel was rather low (0.26 m/s).

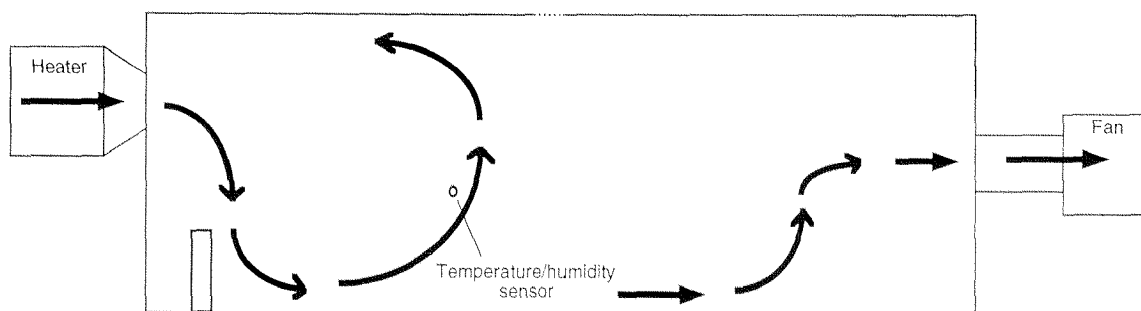


Figure B.1: Initial lay-out scheme of the wind tunnel before modifications

It could be noticed during a first check of the flow that the air flow inside the tunnel was far from being uniform. The air flow inside the wind tunnel was not straight forward but there existed a strong recirculation at the tunnel inlet (this zone extents to 3m from the in-

let). The temperature/humidity sensor was located in this zone so that the actual temperature and humidity of the incoming air could be measured. These values however were not representative for the temperature/humidity values in the test sections to be considered for the analysis of the plume.

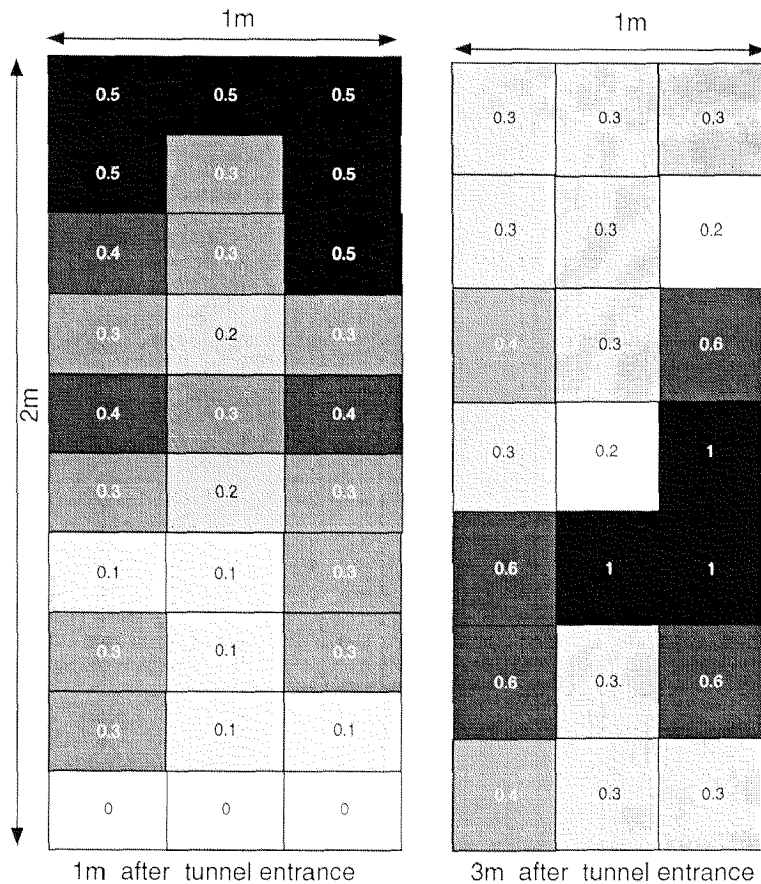


Figure B.2: Distribution of the air flow velocity (indicated in m/s) over the entire tunnel cross section at 1m and 3m after the tunnel's entrance; $T_{Lab} = 26^{\circ}C$, $T_{a,setting} = 20^{\circ}C$, $velocity_{setting} = 0.25$ m/s

In order to be able to interpret the air flow, it was measured over the entire wind tunnel cross section (1m resp. 3m after the tunnel inlet) with the help of an anemometer. The results of these measurements can be seen in Figure B.2. The results lead to the conclusion that there should be a strong recirculation zone near the inlet. The fact that the anemometer indicates positive velocities only, independently of the air flow direction, makes the interpretation of the results difficult. After a distance of 3m from the inlet it can be shown by estimating the volume

flow rate that the tunnel is not completely tight. The underpressure in the tunnel generated by suction of the fan at the tunnel exit was responsible for an increased volume flow rate at the tunnel exit.

The jet which entered the tunnel, moved downwards due to its high density or low temperature. It was felt that a correct analysis of the plume dispersion was not possible with a configuration where the incoming air flow impinged on the floor at the location of the stack.

The velocity distribution obtained by means of a traverse of the test section further downstream was far from being homogeneous too. Several attempts were made to alleviate the stratification effects due to the strong vertical temperature gradient:

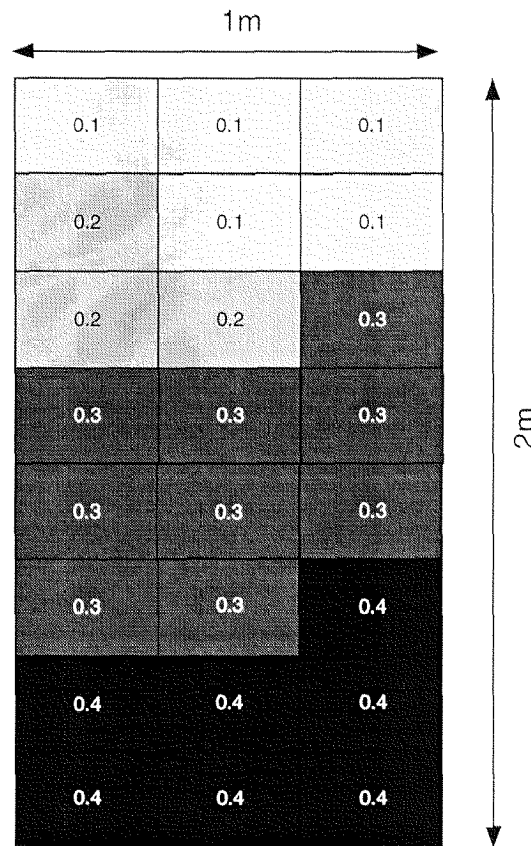


Figure B.3: Distribution of the air flow velocity (indicated in m/s) over the entire tunnel cross section at 3.9 m after the tunnel's entrance; $T_{Lab} = 26^{\circ}C$, $T_{a,setting} = 20^{\circ}C$, $velocity_{setting} = 0.25$ m/s

- The tunnel had to be sealed completely.

- The stack had to be moved from the tunnel inlet to a zone where the air flow had become more uniform and more stable (i. e. 4m after the tunnel entrance).
- The tunnel outlet had to be changed. The outlet tube was replaced by a cone section of the channel in order to obtain a better flow homogeneity over the whole cross section.
- The fan had to be replaced by a more powerful one in order to increase the volumetric flow rate (max 3600 m³/h possible) and hence the air flow velocity.

B.2 Situation after the first modifications

B.2.1 Wind tunnel

A scheme of the wind tunnel, after the modifications were made, can be found in Figure B.4.

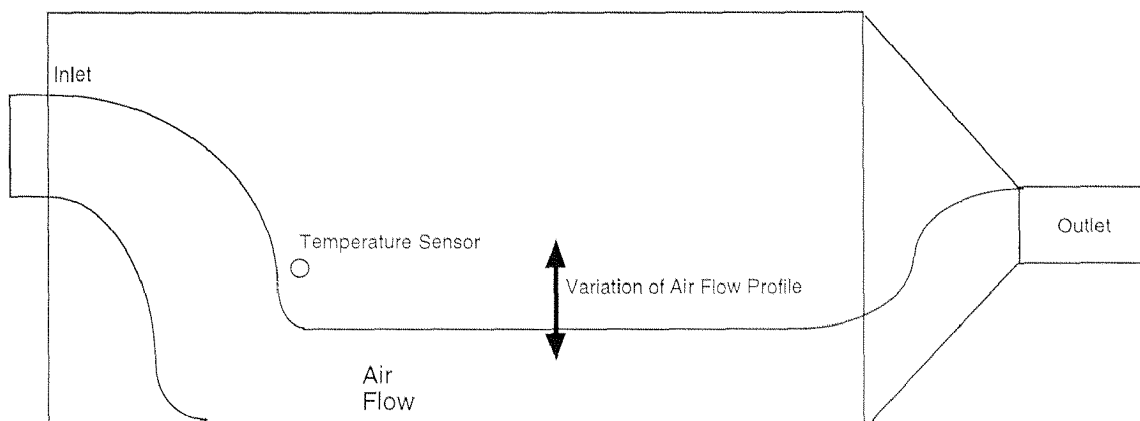


Figure B.4: Scheme of the wind tunnel after the modifications

Unfortunately it turned out, that after the tunnel modifications had been made, the air flow profile inside the wind tunnel was still far from being uniform. Several tests confirmed this observation (see Figure B.5).

The centerline of the air jet dropped drastically at the tunnel inlet (see Figure B.4). The temperature of the incoming air, which was

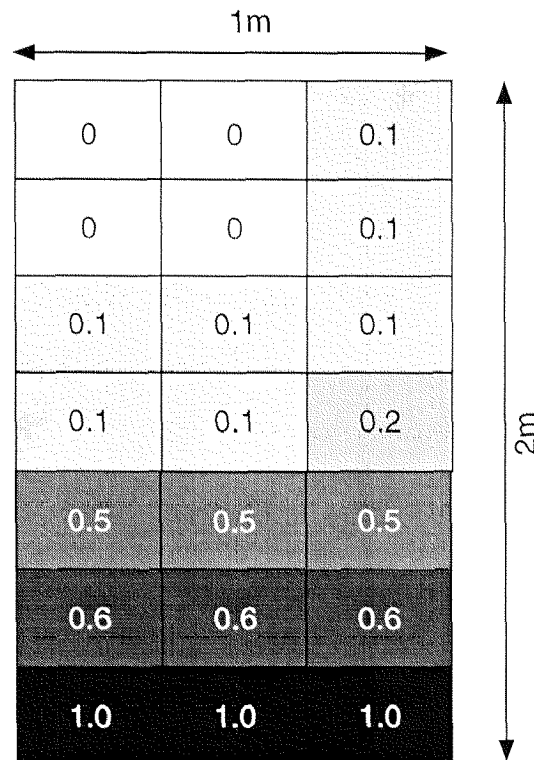


Figure B.5: Distribution of the air flow velocities (indicated in m/s) over the tunnel cross section at 3m after the tunnel entrance; $T_{Lab} = 12^{\circ}C$, $T_{a,setting} = 8^{\circ}C$, $velocity_{setting} = 0.30$ m/s

much lower than that of the air inside the tunnel, was the reason for this phenomenon, called stratification. The centerline of the jet rose or sank to a certain extent (± 30 cm) depending on the incoming air temperature (density). This temperature was controlled by the air conditioner. However the actual value needed for the temperature control was measured 2 m downwind close to the tunnel wall at a height of 80 cm. As a consequence of the oscillation of the plume centerline, the temperature recorded by the sensor was not always representative of the actual value of the temperature of the incoming air flow. However this value was used as an input value for the temperature controller. The corresponding unstable and periodic temperature oscillation was responsible for the oscillation of the temperature and velocity in the tunnel (see Figure B.6).

As the relative humidity is correlated to the temperature, it also varies with the temperature. The air-conditioner controller reduced the coolant

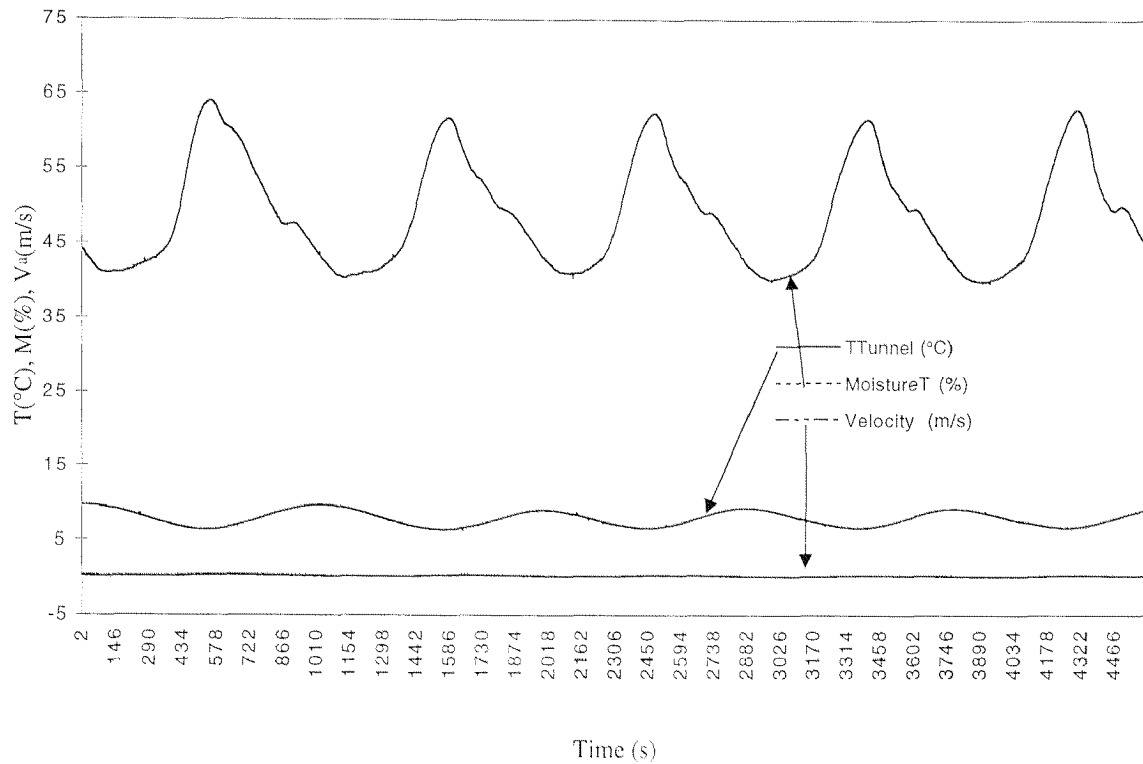


Figure B.6: Record of the tunnel temperature $TT_{\text{Tunnel}}(^{\circ}\text{C})$, the tunnel relative humidity $MoistureT$ (%) and the flow velocity V_a (m/s) after tunnel outlet modifications; $T_{\text{Lab}} = 12^{\circ}\text{C}$, $T_{a,\text{setting}} = 9^{\circ}\text{C}$, $M_{a,\text{setting}} = 56\%$, $velocity_{\text{setting}} = 0.30$ m/s

temperature too much, because the sensor was not always able to capture the real temperature in the air flow, due to its position. Another difficulty is that the relative humidity varies with the temperature. As a consequence the water, that condensed inside the air-conditioner, froze. After 2 hours some of this ice broke off. As the heating bars follow the condenser, this ice was vapourized completely. This led to a humidity 'runaway' inside the tunnel. The humidity could not be controlled any more and the equipment had to be shut down.

An analysis of the problem led to the following conclusions:

- The velocity profile in front of the model stack was far from being realistic or uniform.
- The installed controllers could not handle the problem in a proper way. The control led to an unstable flow.

It was aimed at a better uniformization of the incoming air flow and an improvement or replacement of the control.

B.2.2 Mixing problem

In order to improve the mixing over the entire tunnel cross-section, some modifications were made at the tunnel inlet. The modifications as far as the mixing is concerned have already been discussed in Section 5.3.2. A scheme of the modified tunnel inlet can be found in Figure 5.7.

B.2.3 Controller problem

The second problem was that the two controllers were not suitable for a stable tunnel operation. Therefore the appropriate controllers were chosen and installed ((Ero Electronic 4-digit temperature controller input: 1xPt-100, 1x0-10 VDC; output 0-20 mA)(Ero Electronic temperature controller SMART, input 0-10 VDC; output 0-20 mA)).

In addition the temperature/relative humidity sensor was moved to a location immediately behind the punched plate in the middle of the tunnel at a distance of 50 cm from the floor. A recording of the actual temperature as well as the relative humidity value was made possible with this position of the sensor. Moreover the system consisted of three controllers. When the air entered the air-conditioner, it was first cooled down in order to remove the water of the ambient air (drying the air by condensation). This step was controlled by the first controller. Another temperature sensor was installed after the cooling unit in order to collect the actual air temperature value for this first controller. After this, the air was heated up to the desired temperature (second controller). Afterwards, water vapour could be added if needed in order to reach the desired humidity (controller 3). By splitting up the controlling of the heating up and cooling down of the ambient air (in the initial setup only one controller was used), the control circuit became much more stable (see Table B.1 and Figure B.7). Temper-

ature deviations did not amplify humidity deviations any more (and vice versa).

Table B.1: Accuracy of the old and new control system for the modified wind tunnel (outlet cone)

control system	accuracy (temperature)	accuracy (relative humidity)
old (2 controllers)	$\pm 3^\circ\text{C}$	$\pm 10\%$
new (3 controllers)	$\pm 0.3^\circ\text{C}$	$\pm 2\%$

The accuracy of the new control system was even better when the extreme sensitivity of the air flow to small temperature changes was considered which again were influencing the temperature control.

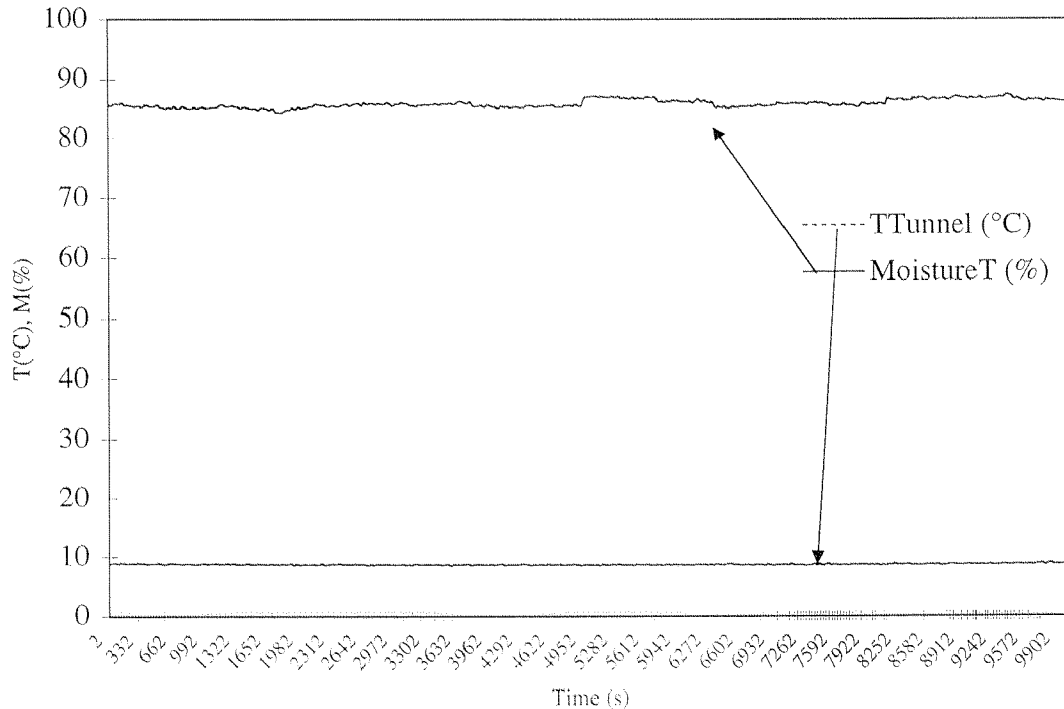


Figure B.7: Record of the tunnel temperature $TT_{\text{Tunnel}}(^{\circ}\text{C})$, the tunnel relative humidity $MoistureT$ (%) and the flow velocity V_a (m/s) after controller and tunnel inlet modifications; $T_{\text{Lab}} = 12^{\circ}\text{C}$, $T_{a,\text{setting}} = 9^{\circ}\text{C}$, $M_{a,\text{setting}} = 85\%$, $velocity_{\text{setting}} = 0.35$ m/s

Moreover the air flow inside the wind tunnel was quite laminar after all these modifications have been made. This has been tested with the determination of the air flow velocities over the wind tunnel cross section 3m after the punched plate (which corresponds to the stack

location (see figure B.8). With the exception of the zone 15 cm beneath the tunnel ceiling (where the photometer crane moving unit is located) where the air flow was close to zero, the velocity distribution over the rest of the tunnel's cross section was quite uniform and the mean value was around 0.30 m/s.

Afterwards the experiments were carried out with wind velocities of 0.35 m/s. However the air-flow tests were made at velocities around 0.30 m/s because under this condition, a uniform velocity distribution is more difficult to obtain than at higher velocities. At wind velocities of 0.35 m/s the velocity distribution was as good as in the case of 0.30 m/s (see Figure B.7).

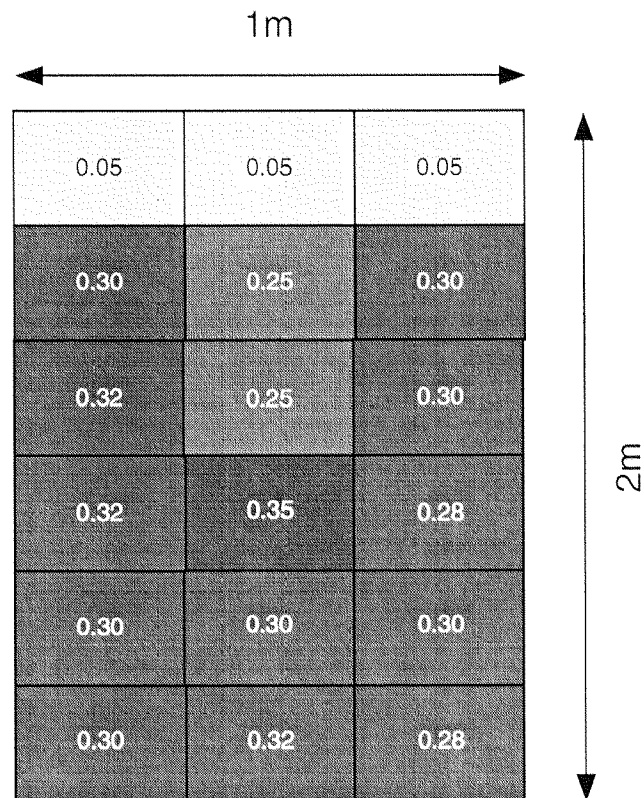


Figure B.8: Distribution of the air flow velocity over the entire tunnel cross section at 3m after the tunnel's entrance after all the modifications have been made; $T_{Lab} = 12^{\circ}C$, $T_{a,setting} = 9^{\circ}C$, $velocity_{setting} = 0.30$ m/s

Appendix C

LabView programs

In this section the program for controlling the crane for moving the photometer in three directions inside the wind tunnel is described. Similar programs have been written for controlling other devices (dispersion photometer, balance, etc.) as well as for data acquisition.

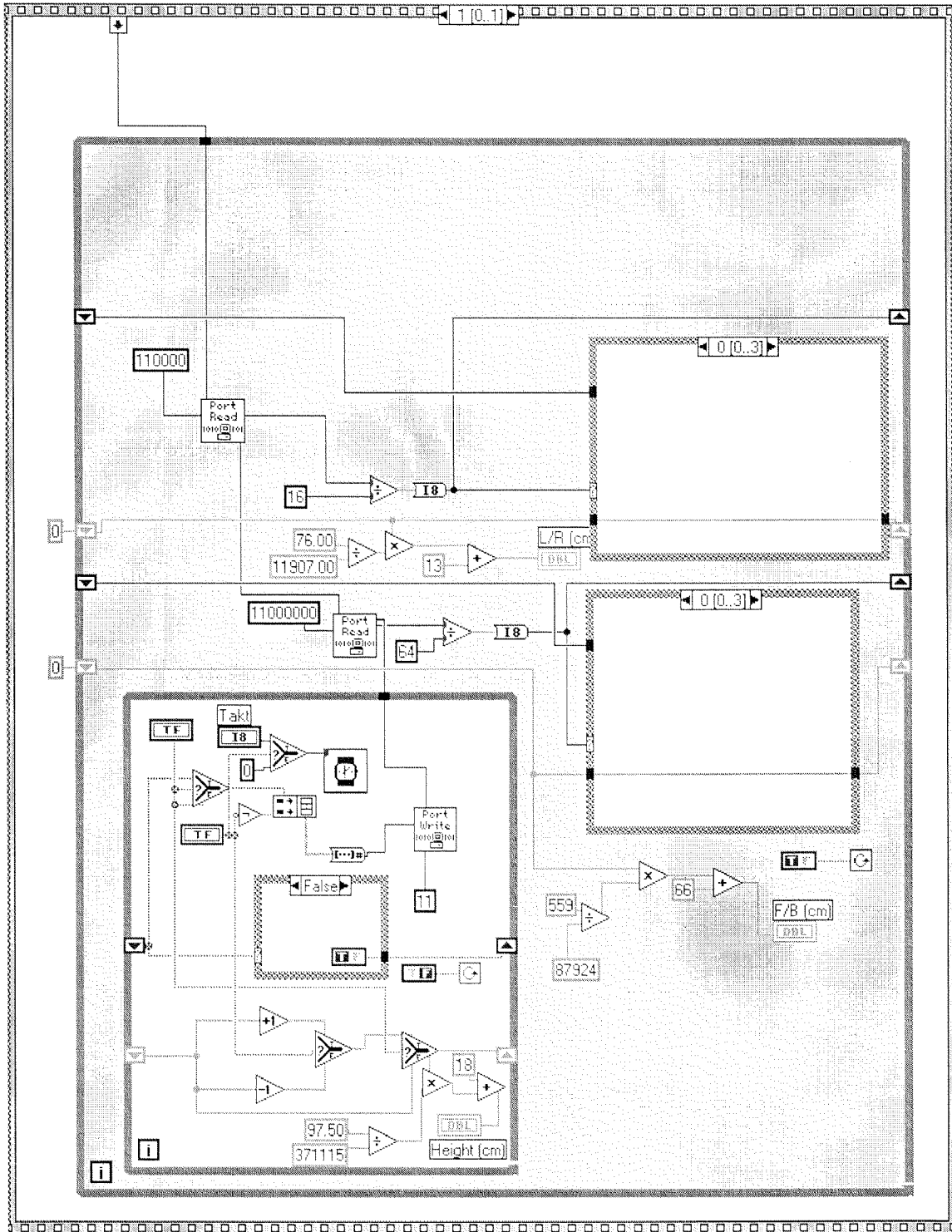


Figure C.1: Example of the LabView program for controlling the moving of the photometer (part 1)

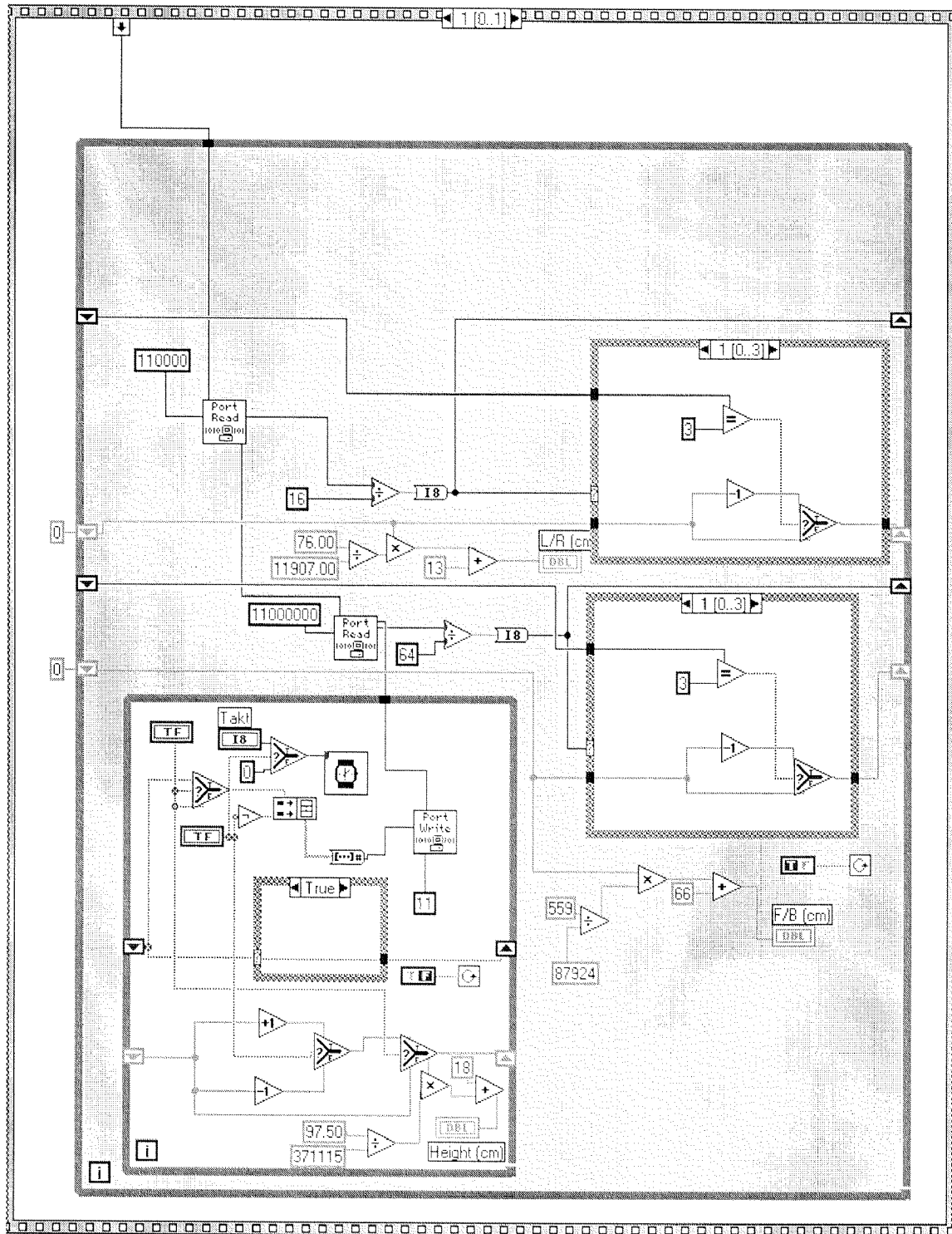


Figure C.2: Example of the LabView program for controlling the moving of the photometer (part 2)

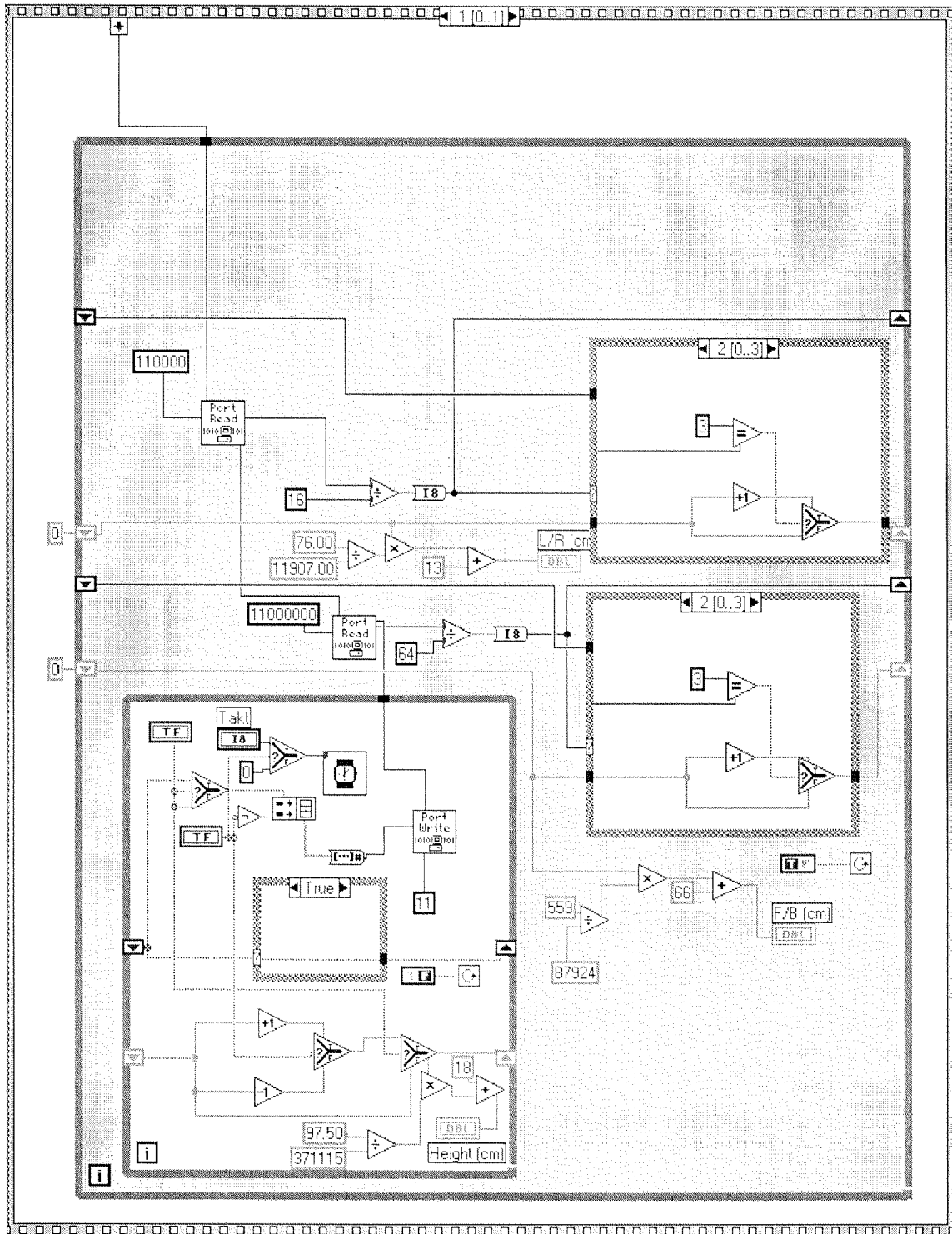


Figure C.3: Example of the LabView program for controlling the moving of the photometer (part 3)

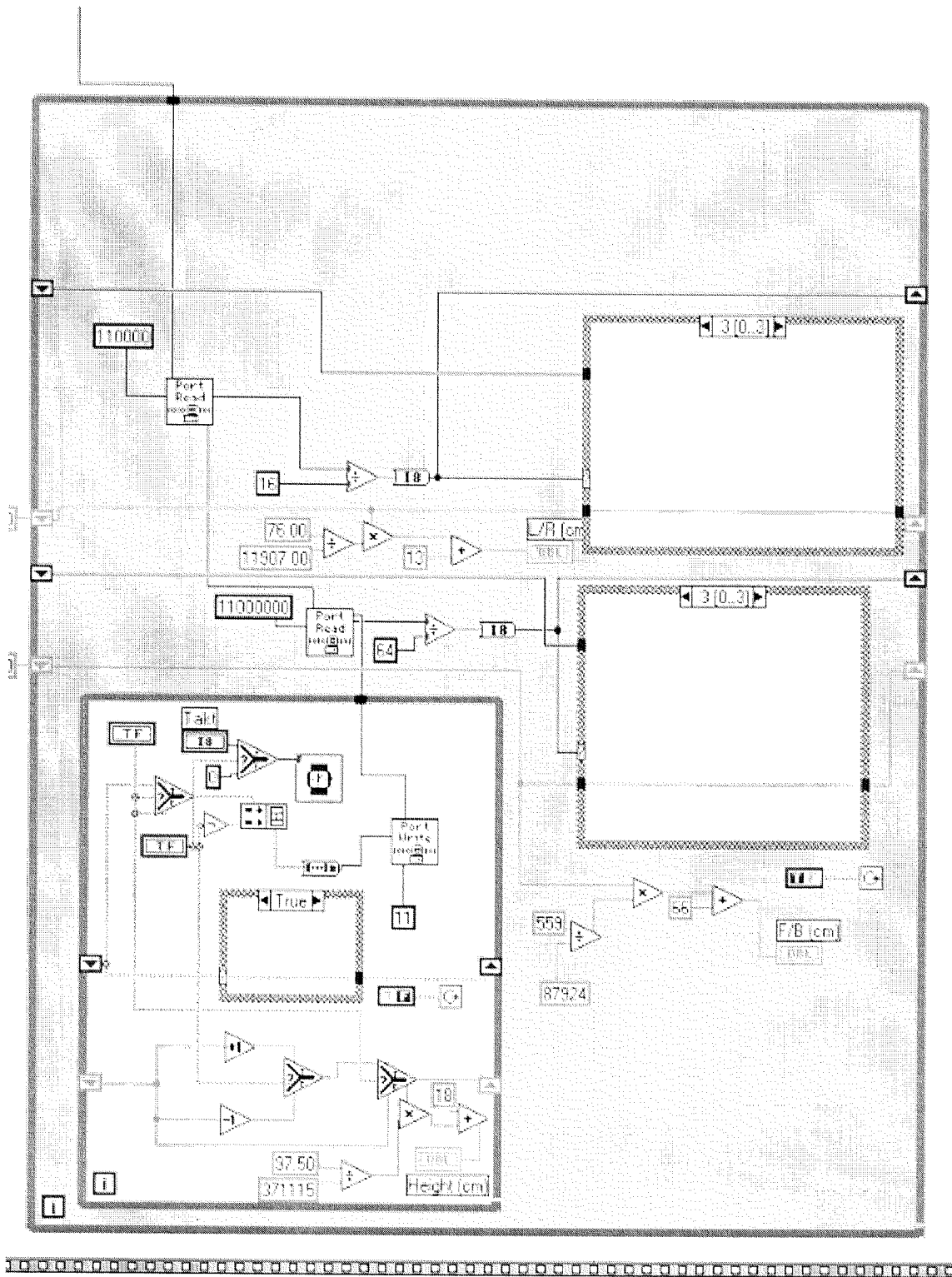


Figure C.4: Example of the LabView program for controlling the moving of the photometer (part 4)

Curriculum Vitae

Name	Laurent Seyler
Date of birth	September 06, 1971
Place of birth	Luxembourg
Nationality	luxembourgish

Education

1977 - 1983	Primary school, Beckerich, Luxembourg
1983 - 1990	High school, Lycée Classique Diekirch, Luxembourg scientific-mathematical degree

Studies

1990 - 1995	Studies in chemical engineering at the Swiss Federal Institute of Technology (ETHZ), Zurich, Switzerland Diploma as Dipl. Chem.-Ing. ETH. Diploma work in the group of Prof. A. Baiker: " <i>Katalytische heterogene Flüssigphasen-oxidation von sekundären Alkoholen</i> "
1996 - 1999	PhD studies at the Chemical Engineering Department in the group of Prof. K. Hungerbühler, Swiss Federal Institute of Technology (ETH), Zurich. Title of the project: " <i>Investigation of Plume Opacity Formation at Cement Kiln Stacks</i> "
1997 - 1998	Post-graduate studies in business management at AKAD, Zurich. Diploma as "Wirtschaftsingenieur STV". Title of the masters thesis: " <i>Die Terminplanung von Projekten unter Unsicherheit - Ein Fallbeispiel aus der Forschung</i> "

Employment

spring 1992	Industrial training at DuPont de Nemours, Contern, Luxembourg
1996 - 1999	Teaching assistant in the group of Prof. K. Hungerbühler